UNIVERSITY OF BERGAMO

School of Doctoral Studies

Doctoral Degree in Engineer and Applied Science

XXX Cycle

SSD: ICAR/09

Joint PhD program with Italcementi – Heidelberg cement group

Mechanical performance of sulfo-based rapid hardening concrete systems focusing on blends with Portland cement

Advisor

Chiar.mo Prof. Paolo Riva

Co-Advisor

Maurizio Marchi

Doctoral Thesis

Davide Sirtoli

Student ID 005642

Academic year 2017/18

TABLE OF CONTENTS

LIST OF FIGURES

LIST OF TABLES

1 INTRODUCTION

1.1 Research significance

One of the most important material used in structures since long time ago is cement. Nowadays Portland cement (PC) represents the most used material in the World from human beings beside water. Its production was around 4.3 billion tons (cembureau 2014) in the year 2014. It is a multiphase material which initially looks like a powder which becomes liquid when mixed with water, hardening in time until it is completely solid. During this last phase it develops a microstructure which gives it strength and durability skills. All of these properties are really useful in the construction field, allowing the realization of elements with any kind of geometry which can resist to high stresses, even in an environment with severe conditions. However, besides its performance, there is a huge environmental impact due to the CO_2 emitted during its production process [1], which has become an issue in the last years. Some of the possible solutions proposed are the use of supplementary cementitious materials blended with PC [2] or the use of alternative fuels in the cement kiln [3]. As about 60% of the CO2 emission in Portland cement production come from the calcination of limestone, another alternative is to modify the cement chemistry, in particular towards cements that contain less CaO [1]. One of these possible solutions is represented by calcium sulfoaluminate cement (CSA), which emits less CO_2 compared to PC thanks to the use of raw materials containing less limestone and the lower temperature of clinkerization [4]. Besides to a lower carbon footprint, even its performance has contributed to its growing interest. The key-component of this material is the ye'elimite ($C_4A_3\bar{S}$) which reacts with lime and sulphates during the hydration to form ettringite (Aft). The precipitation of this last element during the hydration is the main responsible for the characteristic material properties, such as rapid setting and early-age strength development [5] and compensate shrinkage [5], [6], performance which Portland reaches only with the use of admixtures. Due to the high cost of the CSA raw materials, blends with PC are gaining more importance. The correlation between their hydration reaction is still under investigation; however, seems that CSA cement governs the first week reactions while PC is completely involved just after the first 7 days. The bigger campaign done on these systems was carried out by the People's Republic of China between the 70s and the 90s, resulting in the production of several

standards and indications [7] which put in evidence that the key feature of CSA based systems was the rapid hardening behaviour and the subsequent fast development of performance. This campaign remains the only example of a complete investigation on these systems, involving both research and real scale applications. Nowadays, due to the high cost of the raw material and the lack of knowledge of CSA concrete application, systems based on CSA are mainly used as expansive agent to compensate shrinkage of PC concrete [8]–[10] and, in few cases, in the production of self-levelling screeds [11]–[13] and sealing mortar for road works [14].

1.2 Research objective

This research program has the aim to cover the gap between structural application of CSA based concretes and the required knowledge to do so. The first step was defining a mix design for each investigated system which was useful for practical applications, highlighting, at the same time, CSA fast reaction. Three mixtures were defined, representing a pure CSA system, a reference Portland limestone system and a blend of the two at a CSA/PC ratio of 50/50 with the same 28th days strength class. Afterwards, their main aspects were identified and evidenced by a vast campaign on mortar scale. Once defined their main properties, a campaign on concrete scale was developed, underlining their principal mechanical aspects. Eventually, in order to define formulas which summarize the CSA investigated aspects, a comparison with Portland constitutive laws reported in the main technical documents was proposed. That last step was fundamental because gives designers references for the CSA utilization in structures calculation.

1.2.1 STEP I: MIX DESIGN

As the aim of the research is the mechanical characterization of CSA based concretes to be used for structural applications, the mix design was defined mainly on concrete aspects, adapting it on mortars later on. The key parameter on which the mix design was based was the concrete compressive strength class at 24 hours, so as to underline their rapid hardening behavior. The target was fixed at a C30/37 class for the blend system. The class was chosen because it represents a typical strength class at 28 days for a common structure. The blend was considered because was the system with major possibilities to be used in practical field. The other two systems were defined with the same 28th days strength class in order to highlight their early age differences. For practical reasons, also the concrete workability class at 45 minutes in the Abrams' cone was considered as a key parameter, in order to let the matrix harden after the transport to the construction place. To respect these key parameters, variables as w/c ratio, total amount of binders and amount and type of admixtures were considered. These last added in a minimum amount.

1.2.2 STEP II: MORTAR CAMPAIGN

Before the mechanical characterization campaign on concrete scale the main aspects of the defined mixtures were investigated on mortar scale. In this way, mixtures were easier to manage and lower in total volume involved, allowing the investigation of more aspects, under more condition and in less time. Particular attention was put on the rapid hardening behavior and on the dimensional stability. For the strength investigation, aspects as compressive strength, flexural strength, modulus of elasticity and Poisson's ratio were studied from the first moment after setting until 28 days, paying particular attention on the early age. Similarly, in the dimensional stability campaign the full shrinkage evolution from the very first time in which a solid microstructure was formed until 182 days was defined, investigating different possible environmental conditions. Moreover, the effect of the load on the deformative evolution was analysed by creep tests in both autogenous and drying conditions. Other particular aspects analysed on mortar scale were the identification of the setting time, the heat evolution during hydration from the very first time in which water was added until one week and the inner relative humidity evolution from the setting time on. The set-ups for the heat evolution, relative humidity, dynamic modulus of elasticity, EMM-ARM and autogenous shrinkage from the moment of setting (corrugated tube) were not available for concrete scale test. Beside it, early age strength investigations were really complex to handle with concrete mixtures, while in mortar the procedure was easier, faster and manageable from only one person.

1.2.3 STEP III: CONCRETE CAMPAIGN

If in the mortar campaign the aim was purely scientific, thus, there was no perspective to really apply the designed mixtures, in concrete scale the correlation with the practical field is required and fundamental. The investigations were based on the assumption defined in the mortar campaign and optimized for their future practical application. Results were collected in both early and later age. In secondary tests, the considered deadlines were 24 hours and 28 days. The first representing the early age properties and the second the "normal" properties (reference deadline for the main technical documents). Compressive strength and drying shrinkage were the two main investigation done. Other tests were flexural and splitting tensile strength, dynamic and static modulus of elasticity, stress-strain diagrams in compression, autogenous shrinkage and creep in both

autogenous and drying conditions. For the two main tests of compressive strength and drying shrinkage the investigation started from an hypothetical demolding time, earlier for CSA based concretes, until a maximum of one year. For these tests, three more mixtures were defined: two blends, one at a PC/CSA ratio of 50/50 and the other of 60/40, and one pure CSA. They were characterized by different 24 hours strength class, also between the original mixtures. In this way the number of CSA based system increased and the comparison with PC become more accurate. The six mixtures defined so far were investigated even for flexural and splitting tensile strength, dynamic and static modulus of elasticity in order to use the collected results in the last stage.

1.2.4 FINAL STAGE: CONSTITUTIVE LAWS EVALUATION

Results collected so far in concrete campaign were useful for scientific evaluation; however, no practical connection was still evidenced. Thus, the last step was defined in order to give designers formulas which represent CSA based concrete constitutive laws to use in structural projects. As the definition of a precise constitutive law based on a mechanical aspect of these new system is time-consuming (because of the high number of data required to create a valid statistical trend), a first validation was done comparing the already well-known Portland constitutive laws with the data collected for these new systems. A good agreement between these results allows the use of PC constitutive laws for CSA based mixtures. As a reference mixture was defined (PC), this comparison was done on all systems, even the one that was supposed to be described by these laws. In this way two different comparison can be done: one on the relation between CSA based system results and the considered constitutive law and the other directly between CSA based systems and PC results.

1.3 Notations

1.3.1 CEMENT CHEMISTRY NOTIFICATIONS

A	Al_2O_3
C	CaO
F	Fe_2O_3
H	H_2O
S	SiO_2
$\overline{S}$	SO_3
M	MgO

1.3.2 OTHER ACRONIMS

C_2S	Dicalcium Silicate
C_3A	Tricalcium aluminate
C_3S	Tricalcium Silicate
C_4AF	Tetracalcium Aluminoferrite
$C_4A_3\overline{S}$	Ye'elimite
$C\overline{S}$	Calcium Sulfate
CH	Calcium Hydroxide
CSA	Calcium Sulfoaluminate
CSAB	Calcium Sulfoaluminate-Belite
CSH	Calcium Silicate Hydrate
HPC	High Performance Concrete
MIP	Mercury Intrusion Porosimetry
PC	Portland Cement
RH	Relative Humidity
SAB	Sulfoaluminate-Belite
w/c	Water to cement

2 BACKGROUND AND LITERATURE REVIEW

2.1 Portland cement

2.1.1 BACKGROUND

Portland cement is the most used binder in the World thanks to the low cost of the raw materials and their availability, to the mechanical and durability properties it develops after hydration and to the easy applicability in several different conditions. It represents an evolution of binders already used by Egyptians and Romans, improved in time by the contribution of Palladio with his *calce nigra* and the presence of clay impurity, Jhon Smeaton and the study of the chemical analysis, James Parker's roman cement and the hydraulic studies of Vicat. The name Portland comes just in 1824 with Jhon Aspdin's patent. However, the composition of the original Portland cement is not that similar to the one used nowadays. The improvements in the production process, in the quality control and in the production technic changed deeply its features.

2.1.2 COMPOSITION

Portland cement is produced by mixing limestone, clay, sand and pyrite ash in precise proportions, calcining and burning them in a rotary kiln at 1450°C obtaining spheres of a material called clinker which is grinded and mixed with gypsum to obtain the final binder. Gypsum is added as a setting time regulator. The main phases composing Portland cement are tricalcium silicate (C_3S), dicalcium silicate (C_2S), tricalcium aluminate (C_3A), and tetracalcium aluminoferrite (C_4AF), known as "alite", "belite", aluminate and ferrite respectively. Other minerals can be added to the base cement to give it some particular properties. For instance, minerals with pozzolanic behaviour are used commonly as a partial replacement from 6 to 95% of Portland cement. Fly ash, silica fume and blast furnace are examples of these minerals. Their use increases the strength, the durability and the workability of concrete and reduce the fuel consumption and the CO_2 emission. The composition of Portland cement is presented in several standards like the European UNI EN 197-1 [15]. Other materials known as admixtures can be added to the mixture to change its properties. These materials represent the next frontier of cement because, depending on their composition and preparation, they can modify a particular aspect of

the mixture. Thus, several different admixtures are in commerce; is a decision of the mix designer which one and how much use.

2.1.3 HYDRATION

As said before, cement is a material which is initially presented as a powder. To obtain the final hard solid material, water is required. The reaction that water triggers when in contact with cement leading to the final hard state is called hydration. It is characterized by three main phases in which the microstructure of the matrix undergoes several changes. The first regards the time at which water touches the cement creating a viscous fluid mixture. The heat of hydration is initially high, evidencing the amount of reactions happening, followed quickly by a dormant period. When the heat restarts to grow, so does the hydration reactions, the mixture sets and a solid skeleton begins to form. This is the moment in which some stress can be sustained by the mixture and is identified as the setting time. The mixture no longer looks like liquid but plastic. As the hydration continues, the microstructure becomes more connected until it creates a solid element which can sustains bigger stress. This moment is identified as the hardening time, when the mixture is completely solid and the hydration reaction slows down.

The phases making up Portland cement react differently, in the way and in the moment, creating a series of hydration reactions.

Tricalcium silicate (C_3S) are the most important clinker constituent. They represent from 75 to 80% of the solid constituents in clinker and they are responsible for the mechanical performance of the cement paste. Tricalcium silicate is the responsible of the early age properties, reacting already in the first days with water producing calcium silicate hydrate C-S-H, its main hydration product, and calcium hydroxide. C-S-H confers strength to the matrix and is the responsible for the hygral shrinkage and the viscoelastic properties of Portland cement paste.

Dicalcium silicate (C_2S) is the other silicate present in the Portland solid constituents. It is slower than C_3S and is the responsible for the later age mechanical properties. Compared to the tricalcium silicate, C_2S produces more ettringite and less calcium hydroxide considering a full hydration state on the same amount of material.

Tricalcium aluminate (C_3A), although it represents from 1 to 13% of the clinker, strongly influences the early hydration reaction. Its reactivity, the highest of the four, is enhanced

by the presence of lime. Gypsum is added to the mixture in order to slow down the cement reaction and delay the setting time. During this reaction, ettringite is formed in the first hours, leading the early age setting process.
Tetracalcium aluminoferrite (C_4AF) represents from 8 to 13% of the clinker solid constituents. Its reaction is assumed to be equivalent to that of C_3A with a lower speed.

2.1.4 PERFORMANCE

When the cement paste becomes solid the first mechanical properties begin to develop. The forming hardened microstructure due to the ongoing cement hydration is the responsible for the mechanical properties, e.g. strength in compression and in tension, the stiffness, the shrinkage and creep, and the durability properties, e.g. sulfate resistance, carbonation and chloride ingress. Depending on the design request, variations on the mix design can be made in order to obtain a particular performance. The type of binder is the first aspect to define since the entire chemistry of the reactions depends on it. Afterwards, other important aspects in the mix design influencing the cement properties are the ratio between water and cement, the total amount of cement, the amount/type/dimension of the aggregates and the kind/amount of admixtures. The mix design represents the potential to obtain a good material. To assure the designed performance also a correct application and maturation has to be respected.

2.2 Calcium sulfoaluminate cement

2.2.1 BACKGROUND

Calcium sulfoaluminate cement represents an eco-friendly alternative to Portland cement thanks to its low CO_2 emission during production. Its main component is the ye'elimite ($C_4A_3\bar{S}$) which is present in an amount that varies from 30 to 70%. This element was found by Alexander Klein in 1966 and initially used as an expansive or shrinkage compensating addition to cementitious binders [16]. These binders were known with several acronyms, depending on their main compounds: calcium sulfoaluminate cement (CSA), which is the one at which we refer, sulfoaluminate-belite cement (SAB) or calcium sulfoaluminate-belite cement (CSAB). Between the 70s and the 90s, a large research and production effort targeted at both calcium sulfoaluminate and calcium sulfoaluminate belite cements took place in the People's Republic of China, resulting in several Chinese standards. It represents the first industrial production for these new binders, known as "third cement series" [17]. This series included sulfoaluminate and ferroaluminate cement, which have the same basic components ($C_4A_3\bar{S}$, C_2S, C_4AF and calcium sulfate) only with different proportions depending on the application. According to a summary about this period [7], calcium sulfoaluminate cement found specialized application in small/medium precast concrete shapes, heavy pre-stressed concrete elements, casting in cold environment, high performance concrete, mass and impermeable concrete, glass-fiber reinforced concrete and as an expansive admixture. The key feature in all these applications was the rapid hardening behaviour and the subsequent fast development of performance in concrete made with CSA cement. Another field in which CSA cement found some application is in the hazardous waste encapsulation [18], [19]. It became suitable for this kind of application thanks to its low pH, its low porosity and the ability of ettringite to bind heavy metal. Despite this increasing interest for these new binders, industrial scale production and usage are still limited to China [20]. The lack of bauxite deposits, required for the alumina extraction, and the consecutive increasing cost of the CSA raw material led to a loss of interest for such systems. However, the new millennium brought the environmental impact at the top of the issues for human being to be solved or, at least, limited. Nowadays, thanks to its low carbon footprint compared to Portland cement, CSA based system are receiving increasing attention. While alite release 0.578g CO_2 per g of the cementing phase when

made from calcite and silica, CSA clinker releases only 0.216g CO_2 per g of cementing phase when made from limestone, alumina and anhydrite [20]. During CSA clinker production, the firing temperature reaches 1250°C which is around 200°C less than that used for Portland cement clinker. In addition, thanks to the higher porosity of CSA clinker, the energy required to grind it is lower [21]. Nowadays, due to the high cost of the CSA raw materials and the insufficient characterization of CSA concrete for structural application, CSA cement is used as expansive agent to compensate shrinkage of PC concrete [8]–[10] and, in few cases, in the production of self-levelling screeds [11], [12], sealing mortar for road works [14] and high performance concrete at early age [12], [22]. Though, several more field of application are already analysed and defined [23].

2.2.2 COMPOSITION

As said before, the key-component of this material is the ye'elimite ($C_4A_3\bar{S}$) which is present in combination with other characteristic phases in relation to the raw materials used. These materials are limestone, bauxite and calcium sulfate. Due to the high cost of bauxite extraction, several industrial by-products and waste materials (fly ash, blast furnace slag, baghouse dust or scrubber sludge) are explored for the manufacture of CSA clinkers [24], [25]. Other characteristic phases which can be found in CSA clinker are belite (C_2S), ferrite (C_4AF), mayenite ($C_{12}A_7$), anhydrite or free lime, calcium aluminates or gehlenite [26]. Usually, around 20 wt.% of calcium sulphate is interground with the clinker to regulate the setting time, the strength development and the volume stability of the matrix [21], creating a binary system. Depending on the kind and amount of the added sulfate, the hydration kinetic and the phase assemblage can vary [27], [28]. Another potential way to use CSA is in combination with other cementitious material such as Portland cement, defining a ternary system which can improve the strength development or anticipate the setting/hardening time [29]–[31].

2.2.3 HYDRATION

The hydration reaction of pure ye'elimite is influenced by the presence of calcium sulfate or calcium hydroxide [32]. With water alone, ye'elimite forms monosulfate (AFm) and aluminum hydroxide (AH_3) according to the Eq. (I), which contributes to the early-age property development. The addition of sulfate sources like gypsum or anhydrite improves

the speed of this reaction, leading to the formation of ettringite (Aft) and aluminum hydroxide instead of monosulfate according to Eq. (II). The calcium sulfate addition is of relevant importance for the hydration kinetics [6], [33]. If the sulfate sources are completely consumed, the reaction produces monosulfate following Eq. (I). The ratio between ye'elimite and calcium sulfate determines the ratio between ettringite and monosulfate in the final product. Above a value of 2, just Eq (II) occurs. The reaction changes when calcium hydroxide is added. Ye'elimite reacts rapidly to form C_4AH_x while the combination of calcium hydroxide and calcium sulfate leads to the rapid formation of ettringite according to Eq. (III). The calcium hydroxide of Eq (III) can be derived from the belite reaction with water as shown in Eq (IV).

$$C_4A_3\bar{S} + 18H \rightarrow C_3A \cdot C\bar{S} \cdot 12H + 2AH_3 \quad \text{(I)}$$

$$C_4A_3\bar{S} + 2C\bar{S}H_2 + 34H \rightarrow C_3A \cdot 3C\bar{S} \cdot 32H + 2AH_3 \quad \text{(II)}$$

$$C_4A_3\bar{S} + C\bar{S}H_2 + CH + 74H \rightarrow 3C_3A \cdot 3C\bar{S} \cdot 32H \quad \text{(III)}$$

$$C_2S + 2H \rightarrow CH + CSH \quad \text{(IV)}$$

Similar reactions occur in CSA cements, even if they usually contain several other hydraulic phases. Ye'elimite is more reactive than the other accessory phases, thus it dominates the reaction compared to C_2S, C_4AF or CA [34], [35]. Depending on the clinker composition, other hydration products such as C-S-H, strätlingite (C_2ASH_8) or hydrogarnet can be formed [36]. For instance, calcium sulfoaluminate belite cement contains C_2S which react with water to form CH, which increases the calcium hydroxide resources, and C-S-H, which contributes to the long-term property development. The water-cement ratio required to fully hydrate the cement depends on the amount of calcium sulfate added, and it is at a maximum around 30% [21], [27]. Considering the full hydration of the pure ye'elimite reacting with 2 molar equivalents of anhydrite, the stoichiometric w/c ratio is around 0.78 [37] or around 0.6 for technical cements [21], which are higher than that of Portland (around 0.40-0.42). Compared to Portland cement, CSA reacts faster and most of the hydration heat evolution occurs between 2 and 24 h of hydration [6]. As in the pure ye'elimite, also in CSA cements the hydration reaction depends mainly on the type and amount of the added calcium sulfate [21], [27], [32], [34].

A formula for the calculation of the optimum sulfate level to obtain the different types of CSA cements was developed in China [23] and is reported in Eq (1).

$$C_T = 0.13 \cdot M \cdot \frac{A}{\bar{S}} \quad (1)$$

where C_T is the ratio gypsum/clinker, A the mass % of ye'elimite in the clinker, $\bar{S}$ the mass % of SO_3 in the gypsum, M the molar ratio gypsum/ye'elimite, and the value 0.13 is a stoichiometric factor containing all the conversions between mass and molar units. The value M represents the type of CSA cement that will form. From 0 to 1.5 yields to a rapid hardening or high strength cement. Higher values lead to expansive cement (1.5-2.5) and self-stressing cement (2.5-6). According to Eq (1), the properties of the CSA cements are directly related to the formation kinetics and to the total amount of the voluminous ettringite phase in the hardened system.

Considering the blended system of CSA/PC [29], [30], [38], it was observed that the precipitation of Aft during the hydration process of CSA is the main responsible for the material properties, such as rapid setting and early-age strength development [5] and compensates shrinkage [5], [6]. Moreover, PC seems to be involved in the hydration process after the first 7 days. Some other factors were also found to influence the expansive behaviour of CSA-based material [39] such as the type and amount of calcium sulphate [27], [28] and the PC quantity [30].

2.2.4 PORE STRUCTURE

Due to the rapid hydration reaction that occurs in CSA systems the pore development is different between Portland cement [40]. By mercury intrusion porosimetry (MIP) it was found that a bimodal pore structure is fast developed (after 2 hours of hydration) by CSA cement [37] due to the fast formation of ettringite which quickly reduces the internal spaces. The bimodal distribution is related with a disconnected and denser internal structure which is reached by Portland only after 7 days of hydration. During the investigated period of 28 days, CSA system remains bimodal but it changes the pore dimension distribution. The prevalence in the first hours is on the bigger pores which changes to the smaller after 12 hours of hydration. The fast hydration reaction quickly produces products which reduce and isolate the inner space, creating a region of prevailing lower porosity. As the hydration reaction slow down quickly, the evolution of

porosity proceeds very slowly for later age. Due to the slower hydration reaction, Portland cement initially produces a unimodal pore distribution, prevailing zones of bigger pores, which evolves in a bimodal with time. Nevertheless, the strong effect of calcium sulfate on the early age properties influences also the pore structure evolution of CSA systems. In fact, by a different formulation with lower ye'elimite content, a coarser pore structure and higher porosity than for a Portland Cement was found for a CSA system at 90 days [41]. However, the 15 wt.% addition of a Portland CEM I 42.5 to the CSA have a positive role in its pore structure, leading to a distribution similar to that of Portland mixtures [31].

2.2.5 STRENGTH DEVELOPMENT

As for the other properties, even the strength is influenced by the cement composition. Firstly, by the hydration of ye'elimite in CSA ettringite is produced. This is the most important hydration product for the properties evolution The addition of gypsum in the range of 10-20 wt.% optimize the early age properties [42], regulating the reactivity and increasing the compressive strength. The addition of a less reactive anhydrite leads to a delay in the ettringite formation causing a lack of sulfate ions in the pore solution which slow down the dissolution of the CSA clinker particles and their reaction to ettringite, affecting the strength development [27]. In the case of CSAB or in ternary systems with Portland cement, calcium hydroxide is provided to the system. It is involved in the hydration reaction with ye'elimite and calcium sulfate to produce ettringite only in a higher amount than that without CH. This reaction leads to greater strength [27], [43] although the fast set lead to complications in its utilization.

Thus, depending on the amount of $C_4A_3\bar{S}$, $C\bar{S}$, C_2S and C_4AF several different systems can be produced; e.g. fast setting, high early age performance, long term performance system or a combination of them [4], [22], [44], [45].

2.2.6 DIMENSIONAL STABILITY

The formation of ettringite from the hydration reaction of CSA cement can be expansive if it is formed after setting in a reasonable amount [1], [46], [47]. It was reported that expansion increases with the gypsum content [21], [39].By the hydration reaction showed in Eq. (2) it is possible to see the importance of the sulfate source in the formation of ettringite. If calcium hydroxide is also present, the hydration reaction of Eq. (3) happens

instead, forming even more ettringite. Thus, it can lead to expansion if it reacts before setting [27]. The phase assemblage is not the only factor which influences the expansion behavior of CSA cement; the already mentioned pore structure has also a big influence on it, determining the available space in which ettringite can form. If a dense microstructure is developed by the matrix during hydration, an expansive behavior is expected since ettringite formation has no space in which forms [44]. On the contrary, a coarser pore structure with high porosity leads to a non-expansive CSA matrix [41]. There are several other factors which influence the expansive behavior of CSA cements like the water to cement ratio, the sulfate content, the free lime content, the alkali hydroxide content and the particle fineness. However, these factors just affect the two main aspects of the total amount of ettringite produced in time and the mechanical aspect of the matrix pore structure [48].

Even if the factors which influence the CSA cement expansion are well known, a wide accepted theory on the expansion mechanism is not yet defined [5], [39], [48]–[55].

2.3 Mechanical performance

2.3.1 STRENGTH

The main parameter which characterizes the mechanical performance of a concrete is its strength. In the most commonly used international standards, different classes are defined based on the mechanical performance. The aspect that was chosen to realize this classification was the compressive strength. As said in the Eurocode 2, "*The compressive strength of concrete is denoted by concrete strength classes which relate to the characteristic (5%) cylinder strength f_{ck}, or the cube strength $f_{ck,cube}$…"*. To the concrete compressive strength classes are refereed the major part of the other mechanical aspects, like the tensile strength, the modulus of elasticity, the flexural strength etc. Thus, differences in the compressive strength lead to differences also in the other aspects. Moreover, the compressive strength is the parameter used to compare the performance of the realized structure with the one designed. In the last fifty years, an evolution of this parameter was observed in concrete systems, leading to the creation of new systems that reached higher performance than in the previous years. In the 70s the need to build higher structures lead to the first design of a "high-strength" concrete. This new concrete class was thereafter widely studied, leading to a new concrete system called High Performance Concrete (HPC) [56]. Their formulation was not aimed at the strength increase only, but even several durability aspects were improved. A similar situation happened in the 80s, when the concrete strength overpaseds 150 MPa. A new concrete class was defined, known as Ultra High Performance Concrete (UHPC) [57]. These new systems were suitable for a wide variety of structures and situations thanks to their high compressive and tensile strength, which allowed the optimization of structural elements, and their discontinuous pore structure, which reduced liquid ingress increasing their durability. These systems are based on four principles: the use of a very low w/c ratio (around 0.20-0.25) in order to obtain a very dense structure, a high packing density of the fine grains in order to reduce the water demand, the high use of superplasticizers to adjust the workability and, depending on the needs, the use of fibers to increase the ductility of these otherwise brittle materials. In terms of strength, another binder showed interesting performance. Calcium sulfoaluminate cements were produced since the 70s in China because of their natural rapid hardening behaviour reaching high strength in the early age comparable to a 28 days HSC. They were used in the formulation of HSC mixtures for

structural application, e.g. 103 m high building of Shenyang Long Distance Telecommunication Hub in 1993 or the 100 m high-rise building of Liaoning Products Building in 1994 [23]. Thanks to these rapid hardening properties and to a high heat production, CSA cement were often used for concrete products and in winter construction [7], [23]. However, due to their different chemistry, CSA systems require specific studies to close the gap between the scientific knowledge and their widespread application by the realization of technical regulations.

2.3.2 SHRINKAGE

Due to the hydration, cement based systems are subjected to internal structure variations in time. Once a solid skeleton is formed, loads can be sustained. On one hand, these loads are related to the strength evolution of the matrix; on the other hand, the internal consumption of water due to the ongoing hydration or to the external evaporation of water result in a stress formation inside the matrix. This stress leads to a deformation which is called "shrinkage" [58]. If the tensile strength developed from the matrix during hydration is lower than the stress produced by the shrinkage, cracks are formed [59], [60]. These cracks are detrimental for the matrix performance, in terms of both strength and durability. Shrinkage cracks can appear at any time, from the first moment in which a solid skeleton is formed [61] until 1-2 years, time in which shrinkage exhausted its potential. Depending on the moment in which happen and on what activates the driving forces, shrinkage can be divided into four categories: chemical [36], plastic [62], autogenous [63] and drying [58]. The first represents the deformation due to the hydration reaction and the different volume between reactants and products. The major part of this deformation happens when the matrix is still liquid, thus is generally not a problem for practical use. Differently, plastic shrinkage represents the deformation which happens in between the time when concrete is placed and the time when it sets, thus the time in which the mixture is plastic. The evaporation of water creates menisci on the evaporating surface which cause both the settlement of the concrete and the tensile stress development, which is the responsible of cracks formation.

Autogenous shrinkage represents a deformation of an already rigid structure due to the hydration reaction of cement. As reported by Jensen and Hansen [64], autogenous deformation is defined as "*the bulk deformation of a closed, isothermal, cementitious*

material system not subjected to external forces". It is related with the pore pressure produced by the menisci formed in the microstructure due to the water consumption during hydration which generates a drop of the internal RH (self-desiccation). These menisci and the corresponding capillary pressure are the responsible of the separation between chemical and autogenous shrinkage [65]. When the amount of mix water is enough to completely hydrate the paste no stress is produced, otherwise some menisci start to form and capillary pressure grows. This represents the main driving force for autogenous shrinkage. The separation between chemical and autogenous shrinkage represents the initial set, e.g. the moment in which a solid structure begun to form. Thus, the global evaluation of the autogenous shrinkage requires the exact identification of the setting point [66], [67]. This mechanism was known but not investigated before the 70s because at that age the typical concrete used in the structures was a normal strength concrete. These systems were characterized by a w/c ratio higher than the stoichiometric, leading to a fully hydrated matrix which not self-desiccate. However, with the widespread diffusion of HPC systems, this aspect became an issue because of their characteristic low w/c ratio [68]. Considering technical CSA cement, it is characterized by a stoichiometric w/c ratio of about 0.60 [1]. Such ratio is not necessary to achieve high performance, neither an acceptable workability for practical use [69]; on the contrary, a low w/c ratio is required to reach high performance; thus, a low w/c ratio is more representative for real applications considering HPC systems. A lower value than the stoichiometric causes a drop in the internal relative humidity (RH) of the cement paste in sealed condition (self-desiccation), which leads to a higher autogenous shrinkage.

Different is the situation when concrete is exposed to drying condition. A RH gradient is formed between sample inner condition and external environment. If the external RH is lower than the one inside the sample, water tends to migrate outside, evaporating. This process changes the microstructure condition, consuming the water from the bigger pores, forming menisci in the smaller one. These menisci are responsible for the capillary force generated during this process, which is, as in the autogenous shrinkage, the main driving force for drying shrinkage [70]. Figure 1 reports the typical relation between drying and autogenous shrinkage for a normal and a high-strength concrete. If in autogenous condition the amount of shrinkage depends on the only hydration process (mainly on the water amount related to the binder chemistry), in drying condition these variables are

strongly related to the time at which the material is exposed to drying (especially in the early age, when the structure is not yet well formed) and to the RH gradient between sample material and external environment.

Usually in concrete structures autogenous condition is typical in elements not yet demolded or in structures with large cross-section, in which the outer layer dry out, while the inner part, far away from the drying front, undergoes self-desiccation. While drying shrinkage becomes important after demolding, when the element is exposed to the external environment, and its full development could take months or even years, autogenous shrinkage typically develops in a matter of days to weeks even when the concrete is sealed. As reported by many authors (e.g.,[68], [71], [72]) autogenous shrinkage in concrete must be limited because it may induce microcracking or macrocracking and compromise the durability. An effective technique which limits autogenous deformation is the "internal curing" [73]. By the addition of cells or gels in the mixtures, which act as a sort of water store, water can be provided to the cement paste in later age. Wet lightweight aggregate were also used for internal curing [74]. This technique became particularly relevant with the increased use of HPC systems [75]. Other examples of possible solution in reducing the autogenous shrinkage are the addition of an expansive agent, of a shrinkage-reducing admixture or a combination of the two [8], [10], [76]. Precautions are required even for cracks appearance due to drying shrinkage. Eventually, as the cracks are the results of a stress state in the matrix, fundamental is the correlation between strain at different levels, from the outer layer to the deepest part of the structure, and the corresponding stress generated, which is compared with the tensile strength already matured.

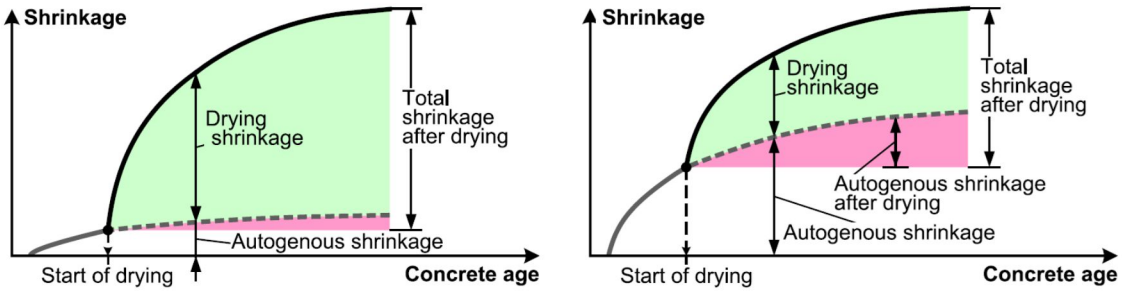

Figure 1 – Shrinkage strain components in normal (left) and high-strength (right) concrete [60]

2.3.3 CREEP

An aspect that was firstly evaluated and studied at the beginning of the last century and still not fully understood nowadays is the deformation of concrete under load, or the so-called “creep”. Several authors tried to define the basic mechanisms on which is based [77] in order to define solid mathematical models to predict it [78]. However, despite the definition and clarification of the major part of the phenomenon involved in its process, researchers are still debating on which theory is the most valuable, improving the quality and the knowledge on the basic processes [79].

Creep represents the deformation of concrete only due to the applied load; thus, from a mechanical point of view, its evaluation involves strength and shrinkage aspects. The strength is considered at the moment of loading, when the element elastically deforms. This deformation is related with the concrete stiffness, thus to its modulus of elasticity. After the application of load, the concrete element evolves a deformation which includes the “unloaded” part, known as shrinkage. The final evolution represents the structure tendency to deform in time under a certain load, which can be considered as some kind of relaxation. For instance, creep is fundamental for bridges, where a relaxation of the structure can lead to a non-linearity on the upper road. Not only for the efficiency of the entire structure but also for the effective use of the non-structural components which sometimes can be damaged by a highly deformable structure. Therefore, it is really important for designers to know how strong is the creep effect in a structure in order to predict a total deformation in service for the entire building.

Another element in which creep is important is in reinforced concrete, especially in pre-stressed structures [60]. When concrete is casted in molds, no adherence is exerted with the reinforcement because concrete is still fluid. After setting, the concrete matrix starts to produce adherence forces on the reinforcement. At the same time, the matrix starts to shrink overall; however, in the zones around the reinforcement, this deformation is hindered by the steel which is not deforming because of its higher stiffness. In this situation, if the tensile strength evolved is not enough, cracks can form. However, as the creep is seen as a relaxation of the material under a certain load, even if the stress is generated by a hindered deformation, creep is involved. Thus, this stress due to shrinkage is lowered by the creep; the higher the creep, the more the relaxation, the smaller the

stress on the concrete in contact with the reinforcement. A summary of this aspect is reported in Figure 2.

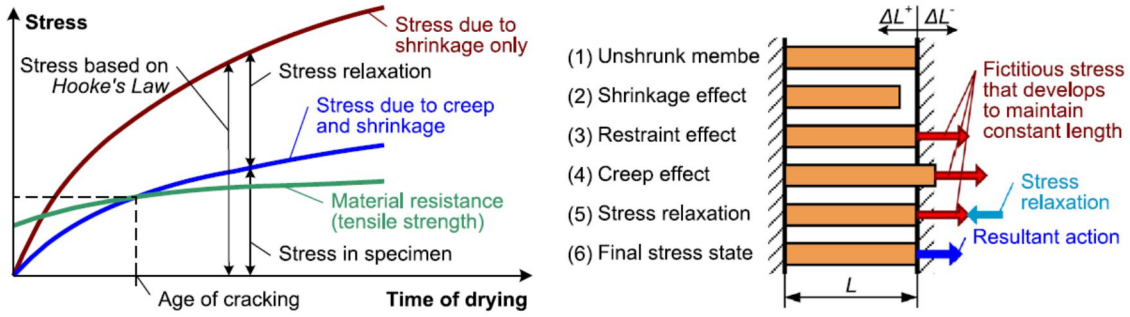

Figure 2 – Restrained shrinkage-induced stresses in concrete: stress development (a) and conceptual description of relaxation (b) [60]

3 MATERIALS AND METHODS

Two different cements were used for concrete composition. A CEM II-LL 42.5R (according to EN 197-1) as Portland cement and a commercial CSA cement (i.tech ALICEM® by Italcementi). For all concrete mixtures, siliceous coarse aggregate and river sand conforming to EN 12620 standard were used. They were considered in saturated surface dry (SSD) condition. The admixtures used in the mix design were a polycarboxylate as superplasticizer, citric acid as retarder and lithium carbonate as set inductor. They were added in different amounts to achieve the mix design aims.

For the entire mechanical characterization campaign, three mixtures were considered, each one representing a particular binder class. A pure CSA, a Portland limestone and a blend of the two (50/50 ratio) labeled hereafter as CSA, PC and MIX, respectively. The Portland limestone cement was chosen for the stabilization effect of the calcium carbonate present in limestone on the ettringite that will form during hydration. These mixtures were chosen because of their 28 days strength class which was the same C50/60 while the 24 hours strength class was different. In this way the mechanical performance can be compared and the differences in the early age underlined.

3.1 Material conditioning

Each material composing the final mixture was used during the mixing operation in a well-defined state. Aggregates were initially dried in an oven for 1 day at 50°C and then stored in a room with 50% RH - 20°C conditions until their use. The dry state allows the water calculation to obtain an SSD condition during the mixing operation. Due to its propensity to react with water, cement was stored in a room with 36% RH – 20°C conditions inside its pack covered by a plastic bag in order to avoid any contact with water. Admixtures were left in sealed plastic bottles in a typical conditioned room at around 20°C not directly under the sunlight to avoid any reaction that can affect the admixture effect. In mortar mixtures, deionized water was used.

3.2 Mixing procedure

As the focus of the present research is basically on concrete mixture, the mixing procedure followed for the material preparation was optimized for concrete scale and adapted to mortars. Mixing operation were carried out in controlled laboratory conditions (20°C – 50% RH), casting in molds conforming to EN 12390-1 quality according to EN 12390-02 procedure. 1/3 of the mixing water was used to wet the dry aggregates and left adsorbing for 2 min. In the mixing water was considered also the slight amount required to saturate the aggregates, not modifying the w/c ratio. Afterwards, the cement was added and the mixing operation started, while the remaining water was gradually poured. Admixtures were added after 120, 180 and 210 seconds for superplasticizer, retarder and set inductor respectively in concrete mixture, while in mortar after 90, 135 and 180. After 270 seconds for concrete and 210 seconds for mortar, the mixing operation was stopped to manually mix and restart mechanically for other 30 seconds. In total, the mixing operation required five and four minutes for concrete and mortar mixtures, respectively.

3.3 Mortar

Table 1: Mortar mixtures design [kg/m^3]

	MIX	CSA	PC
CEM II A-LL 42.5R	288	-	660
ALICEM	288	542	-
Sand 0-1	829	829	829
Sand 1-2	658	658	658
SP (% on binder)	1	0.4	1.4
Retarder (% on binder)	0.5	0.4	-
Accelerator (% on binder)	0.2	0.1	-
Water	259	271	231
w/b	0.45	0.5	0.35

As the behaviour of the chosen mixtures was not known and the number of researches on this topic is too low to predict a possible trend, an initial research was scheduled at the mortar scale. This first step allowed a wider investigation on several aspects. By this way, an initial general knowledge on these mixtures was obtained and used to organize the second and more important investigation campaign on concrete

Mortar mix design differs from the one defined for concrete by the total amount of aggregates (maximum particles size of 2 mm) which was fixed at 55% of the total volume for workability reasons. A higher percentage led to the impossibility of filling the molds with the mixture. This amount was kept constant between the three mixtures in order to emphasize the binder reaction independently from other effects. While the admixtures dosage for the retarder and the accelerator were not modified, the amount of superplasticizer was increased in PC to improve its workability, which was the lowest of the three. Eventually, the amount of cement was corrected in order to respect the w/c ratio. The mixtures proportions are reported in Table 1.

The following investigation focused mainly on the deformative behaviour and on the early age properties evolution. The main mechanical aspects were monitored initially and then extended with other special tests to confirm or extend their trend. Deformations in terms of shrinkage and creep, considering both autogenous and drying shrinkage, were investigated in both early and later ages, monitoring the evolution in time of their internal RH.

3.3.1 COMPRESSIVE STRENGTH, FLEXURAL STRENGTH AND STATIC MODULUS OF ELASTICITY

Measurements of static modulus of elasticity, compressive strength and flexural strength were performed in two steps. In the first step, the general trend was analysed, measuring the properties at 1, 3, 7 and 28 days. The second step focused on the early age evolution, starting the investigation immediately after setting, collecting as much data as possible for the first hours, slowing down with time. The tests were performed following the EN 196 standard for compressive and flexural strength and the EN 12390-13:2013 for the static modulus of elasticity. Measurements were carried out on three prismatic samples of dimensions 4×4×16 mm^3. The samples were produced filling the mold in two times and vibrating for 10 seconds after each pour. Once the upper surface was rectified, the samples were stored in a chamber at 20°C and 95%RH for 24 hours covered with a glass plate to prevent moisture loss. After this initial period, the samples were demolded, sealed with plastic sheet and stored in a chamber at 20%C and 95%RH until the day of testing. A single sample was initially tested to determin the flexural and compressive strengths, obtaining results that were used to calibrate the modulus of elasticity test. An example of the used set-up is presented in Figure 3. Then, first the modulus of elasticity was measured on the two remaining samples and, afterwards, also the flexural and the compressive strength was determined. Following this procedure, each batch of three samples yielded two repeated measurements of the modulus of elasticity and three repeated measurements of the compressive and flexural strengths.

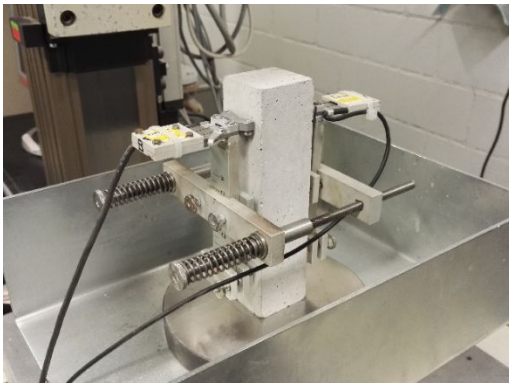

Figure 3 – Mortar elastic modulus of elasticity set-up

3.3.2 DYNAMIC MEASUREMENTS

Dynamic measurements were carried out with single mode resonant ultrasound spectroscopy (SIMORUS) (Figure 4a). This method represents a non-destructive technique which measures the frequency spectrum of a sample. It is obtained by exciting the sample with a sinusoidal vibration, recording the amplitude of the output signal at different frequencies. Depending on the position of the source and receiver piezoelectric transducers, a particular vibration eigenmode is excited, and its eigenfrequency is determined (Figure 4b). Two set-ups were organized according to [80], one to obtain mainly the longitudinal spectrum and the other for the torsional spectrum. According to analytical equations present in the reference standard [80], the elastic modulus *E* and the shear modulus *G* of the sample can be calculated. An accurate measurement on the sample geometry and mass is required for the calculations. The same standard presents another equation which combines elastic and shear modulus in order to obtain an evaluation of the dynamic Poisson's ratio. These rules are based on the elastic rods theory; hence, the sample geometry needs to be longer in one direction compared to the other. More accurate information about this set-up are available in [81].

The investigation follows the same steps as the static modulus of elasticity campaign (general trend plus early age). Even the number of sample tested at each deadline, their geometry, the maturation and the storage details are the same.

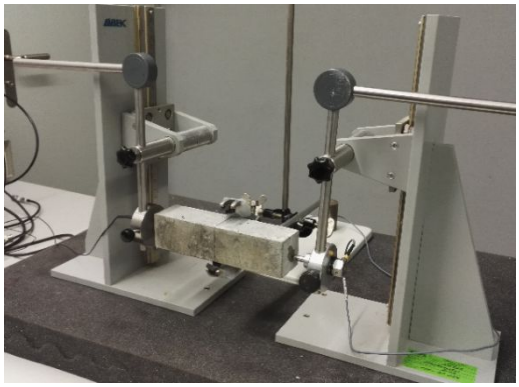

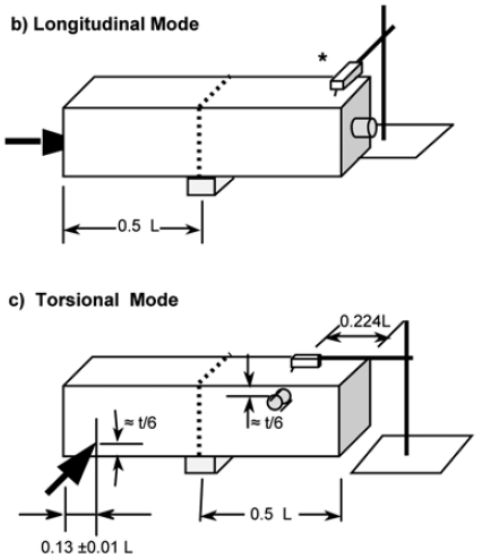

(a) (b)

Figure 4 – Mortar dynamic modulus of elasticity set-up (a); ASTMC215 sensors disposition (b)

3.3.3 DYNAMIC POISSON'S RATIO

Acquired by the set-up described in paragraph 3.3.2, its evolution was obtained from an elaboration carried out on the longitudinal and torsional vibration modes. These two aspects were collected on the same sample, with the same testing machine but with different set-ups; thus, a 5 minutes time-laps was created between longitudinal and torsional investigation. As the Poisson's ratio is obtained by dividing the longitudinal mode by the torsional [82], an error occurs on its final evaluation due to this gradient, e.g. considering, for instance, the 120 minutes deadline, the longitudinal will represents the 120 minutes value while the torsional the 125 minutes value This effect is negligible at later ages; however, it is detrimental for the very early age evaluation (Figure 5). To solve it, the longitudinal and torsional evolution curves in time were drawn point by point from the test results. They were, subsequently, described by mathematical functions following the rule of the "best fit". The advantage was the possibility to investigate these curves at each time point. Thus, the final values considered in the composition of the dynamic Poisson's ratio were collected from these mathematical functions which describe the torsional and longitudinal curves obtained from the test (Figure 6). As the mathematical function is not described by its tolerance, even the final dynamic Poisson's ratio curve was described without any standard deviation.

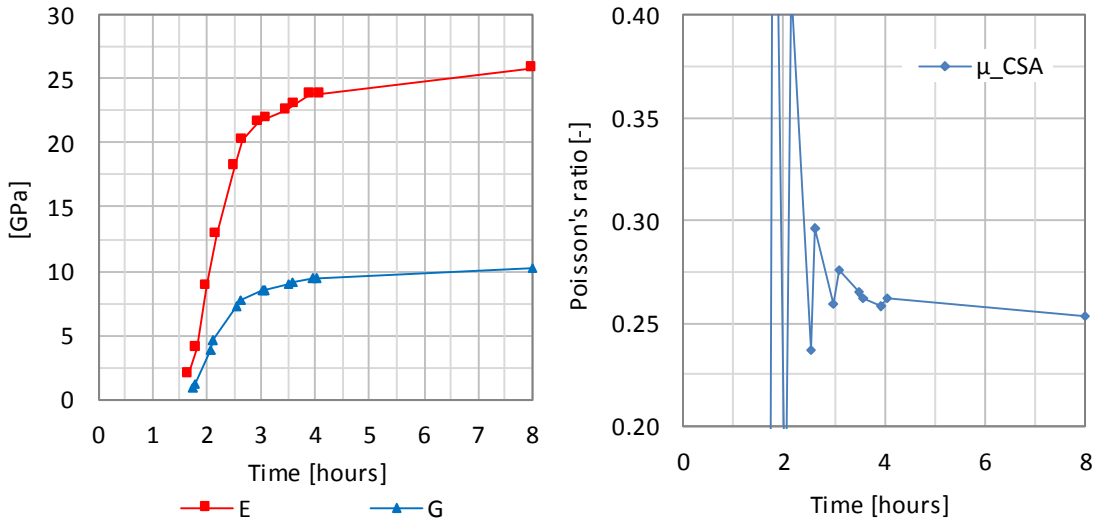

Figure 5 – Dynamic Poisson's ratio evaluation from direct calculation

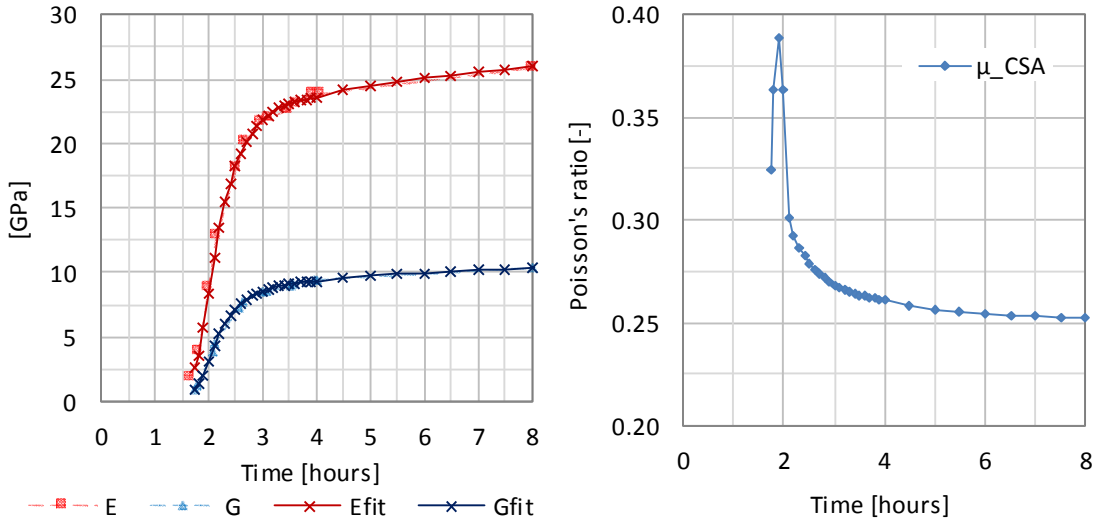

Figure 6 – Dynamic Poisson's ratio evaluation after the fitting procedure

3.3.4 EMM ARM

A special technique that was used in the present research was the E-Modulus Measurement through Ambient Response Method (EMM-ARM). It is a resonant frequency method which allows the automatic and continuous evaluation of the modulus of elasticity in time. The main differences with the other resonant frequency methods are that the sample is not demolded before testing and the exiting vibration comes from the ambient and not from an external device. In this way, measurements can start when the mixture is still fluid, without interfering with its early age weak surface. That leads to the possibility of acquiring data when the material is going to set.

The configuration reported below and represented in Figure 7a-b is typical for cement paste and mortars. For concrete mixtures, a bigger set-up is available but was not used in this research program.

An acrylic tube of 550 mm length and a circular section with internal and external diameter of 16 and 20 mm respectively is used as mold for the mixture. One of its edge is capped with a rigid plastic sheet by applying a layer of glue. When the glue hardens, the mixture is slowly poured inside, avoiding the formation of bubbles, until it fills the entire mold. An aluminum sheet is used to close the second edge. The material filling the tube needs to be homogeneous in order to distribute equally the mass. In this stage, a cantilever structure is created by clamping the pipe at one edge, leaving a cantilever of 450 mm length on the other side. An accelerometer is placed on the free edge of the structure to record the frequencies. Measurements are collected by a data logger which

elaborates them and gives back directly the value in time of the modulus of elasticity. The data logger collects frequency data for 285 seconds at a sampling rate of 200 Hz, elaborates them for 15 seconds and then givese the modulus of elasticity result, which means one result each 5 minutes. Before starting the data collection, the program requires the details of the materials composing the cantilever structure in terms of mass in order to define the stiffness. A more detailed procedure and set-up description is present in [83]. Each result is formed by the mean of two pipes, which are prepared and tested simultaneously, starting before setting continuing until seven days. Each mixture has at least one result. For CSA based mixture a second test was performed. To increase the ambient noise, a fan coil is placed in front of the set-up and turned on during the measurements. The test is performed in a room with 20±0.1°C - 70±3% RH conditions. Figure 8 reports an example on how EMM-ARM results looks like.

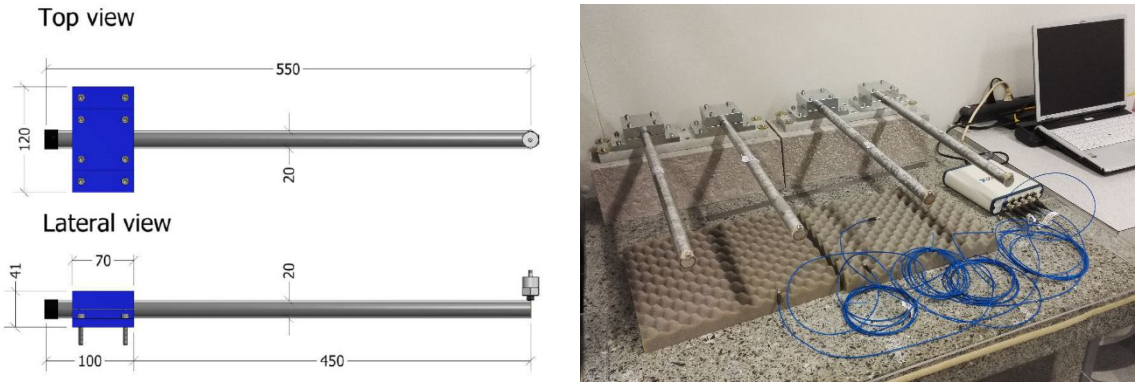

(a) (b)

Figure 7 – EMM-ARM set-up geometry (a) and disposition (b)

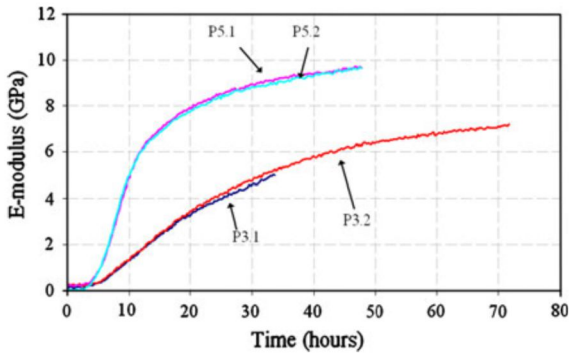

Figure 8 – E-modulus evolution collected by EMM-ARM set-up in [83]

3.3.5 ISOTHERMAL CALORIMETRY

A conduction calorimeter (Thermometric TAM Air), reported in Figure 9, was used to determine the rate heat liberation due to cement hydration during the first week. After the normal mixing procedure, 9.00 grams of mortar were weighed into a flask that was then capped and placed into the calorimeter. Data were plotted after normalizing for the cement mass in the sample. Due to the external mixing, the very early thermal response (first peak upon water addition) of the samples could not be measured. The total heat of hydration after one week was determined by integration of the heat flow curve between the first minimum, after the initial peak, and seven days.

Figure 9 – Thermometric TAM Air conduction calorimeter

3.3.6 RELATIVE HUMIDITY

The fresh mortar was poured into hermetic plastic containers just after mixing, cupped and stored in a chamber at 20°C and 95%RH. Just before the moment of setting the sample was enclosed into hermetic measuring chamber and the test started. The RH evolution was measured with AW-DIO and HC2-AW water activity stations by Rotronic. The accuracy of the sensors was 1.0 and 0.8% RH, respectively. However, the quality of the results was improved by means of calibrating the sensors before and after each measurement with 4 saturated salt solutions with equilibrium RH in the range of 75-98%. The temperature of the measuring chamber was maintained at 20±0.05°C by means of water circulating in the casing of the measuring chambers, whose temperature was controlled by a water bath. The readings were logged at 1 min intervals. The presented results are the average from 2 samples measured at the same time in two different stations.

The development of the RH in the samples and the temperature were continuously measured at least for 1 week after mixing.

3.3.7 SETTING TIME

Initial and final set were determined with the Vicat needle test (Figure 10) and the final set results were used for zeroing the autogenous shrinkage measurements. Results are reported as the average of three test. The needle was released at intervals of 5 minutes. The final set was considered as the moment in which the needle could not penetrate anymore into the mortar. Usually this method is applied to cement paste; however, in this case it was assumed that the penetration of the needle was not influenced by the aggregates due to their small dimension and the bigger needle used instead of the traditional. The test was carried out in a chamber at 20±0.1°C and moisture conditions were controlled applying a stretched food-wrap atop the specimens, guaranteeing sealed condition during the test. The sample had the form of a truncated cone with 75 and 85 mm diameters and 40 mm height enclosed in PVC molds.

Figure 10 – Particular of the covered upper surface of the investigated sample in the Vicat set-up

3.3.8 AUTOGENOUS SHRINKAGE – MANUAL MEASUREMENTS

Depending on the investigated period, two types of measurements were performed. For the early age shrinkage, an automatic set-up was chosen, while, after 24 hours, manual measurements were started and continued until 182 days. Manual measurements of autogenous deformation were carried out on three prismatic samples of 4×4×16 mm^3 produced following the same procedure of the compressive strength samples. After demolding, they were sealed with adhesive aluminum tape and measured in a metallic

frame (Figure 11) equipped with a digital deformation transducer in a chamber at 20°C. During the data acquisition, samples were always placed in the same position on the frame so as to avoid scatter due to the different conditions. Samples were placed horizontally in the frame and the distance between the two upper and lower sides were used as the base of measure. Not only the shrinkage but also the mass was measured at each deadline. Automatic and manual measurements were combined together in order to obtain a complete description of the autogenous shrinkage after setting. A superposition of both measurements from 24 hours to 7 days allowed to confirm the reliability of these methods.

Figure 11 – Measuring device for prismatic samples used for drying and autogenous shrinkage for manual measurements

3.3.9 AUTOGENOUS SHRINKAGE – AUTOMATIC MEASUREMENTS

As said in the previous paragraph, for the early age shrinkage, an automatic set-up was chosen (Figure 12a), which acquires data with 1 minute intervals by LVDTs (Figure 12b). Specimens were cast into corrugated polyethylene molds [84] with a length-to-diameter of approximately 425 to 30 mm applying vibration. At approximately 40 minutes after water addition, they were closed by plastic plugs and placed on a rigid stainless-steel frame, capable of accommodating six specimens at a time, immersed in an oil bath maintained at 19.8±0.1°C and data acquisition was started. Measurements were zeroed to the time of final set obtained by Vicat. Results are expressed as the average of two samples. More accurate information about this automatic set-up are available here [85].

(a) (b)

Figure 12 – Corrugated tube set-up; automatic and manual devices (a); LVDT particular (b)

3.3.10 DRYING SHRINKAGE

Samples used in these measurements are of the same kind of the one used for manual autogenous investigation, including curing, initial storage and measuring set-up (Figure 11). After 24 hours from water addition, they were demolded and placed in four distinct chambers with constant temperature of 20±0.1°C and different RH: 36, 57, 70 and 90% (all ±3% RH). These RH levels were chosen to underline the effect of the external water conditions on the evolution of the microstructure by means of shrinkage and mass loss. The acquired data were used in combination with the automatic autogenous shrinkage results measured with the corrugated tube from the time of setting until the beginning of drying in order to have a complete shrinkage profile with different moisture conditions. These conditions simulate concrete in real application in which the demolding operation are done after 24 hours, exposing the structure to the environment after that. As a simulation, there are differences from the reality and the test, like the small sample size for the mortars, the temperature effects and the change in temperature and RH with time. The results reported are the average of three samples with a measuring accuracy of ±10μm/m.

3.3.11 CREEP

Creep test was used to investigate the deformative evolution during time under a certain load. The procedure described in this paragraph is based on the one used for concrete and reported in paragraph 3.4.6. Four prismatic samples of the same dimension of the one used in the shrinkage test were produced for each condition following the same rules. To investigate the early age properties of the mixtures, samples based on calcium

sulfoaluminate cement were loaded after 8 and 24 hours, while PC after 1 and 3 days with a load corresponding to a stress of 1/3 of the compressive strength at the age of loading. At each step, the load was increased directly on the loaded samples, without removing the previous load. A further loading step after 28 days was considered for MIX and PC in order to investigate the evolution at later age. The pure CSA mixture was not considered in this investigation because of its stability already reached before 28 days, which was considered as its final deadline. In the other mixtures, the test was stopped after 182 days. Once the samples reached the first deadline (8 and 24 hours for MIX-CSA and PC respectively) they were demolded and provided by metallic pins in order to allow their investigation. The pins were placed on two opposite longitudinal sides at a distance of 100 mm avoiding the casting surface. Samples were covered by adhesive aluminum tape as described in the manual autogenous shrinkage test. In this case the pins were glued directly to the sample surface by cutting the aluminum tape which will be covered by the glue. In this way, the pins are influenced only by the sample deformation and the integrity of the aluminum tape is restored by the glue so as to avoid any moisture loss in time. After their preparation, samples were placed in a room at 20±0.5°C and 57±3% RH. Of each batch of four samples, two were used to measure shrinkage (Figure 13a) and two were placed in the creep machine one over the other to measure the deformation under load (Figure 13b). In this way both self and load deformation were investigated on samples treated equally; thus, the shrinkage measured on the un-loaded samples can be assumed to be similar to that occurred in the loaded samples and subtracted from the total deformation with the elastic deformation in order to isolate the part due to the load. Figure 14 reports the evolution of each single creep aspect and a reference on the evidence of the shrinkage and creep coupling.

The results from the creep test were presented as a coefficient calculated as:

$$\varphi = \frac{\varepsilon_{tot} - \varepsilon_{shr} - \varepsilon_{el}}{\varepsilon_{el}} \quad (2)$$

where: φ = creep coefficient [-];

ε_{tot} = total deformation calculated from the creep test [$\mu m/m$];

ε_{shr} = deformation calculated from the shrinkage test [$\mu m/m$];

ε_{el} = elastic deformation at the moment of loading [$\mu m/m$].

Another possible solution to express the creep results was by the creep compliance:

$$J = \frac{\varepsilon_{tot} - \varepsilon_{shr} - \varepsilon_{el}}{\sigma} \quad (3)$$

where: J = creep compliance $[\mu\varepsilon/MPa]$;

σ = compressive stress applied to the sample $[MPa]$.

All data shown in the graphs in the results section represents the average of two samples and are plotted with their standard deviation.

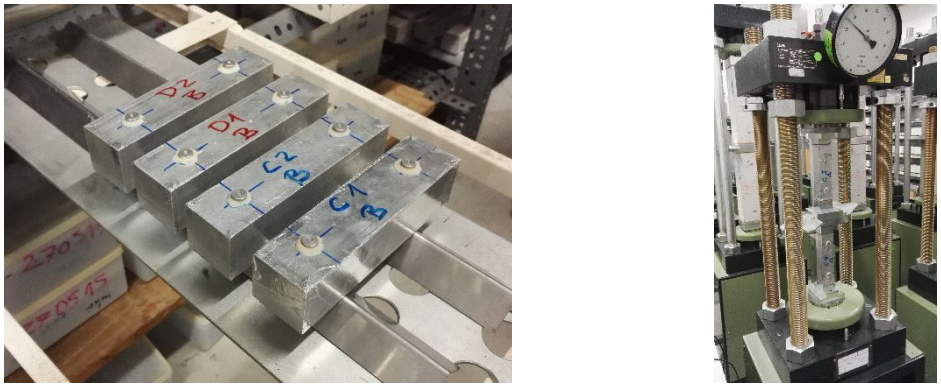

(a) (b)

Figure 13 – Specimens disposition for the shrinkage (a) and the creep (b) deformation measurements

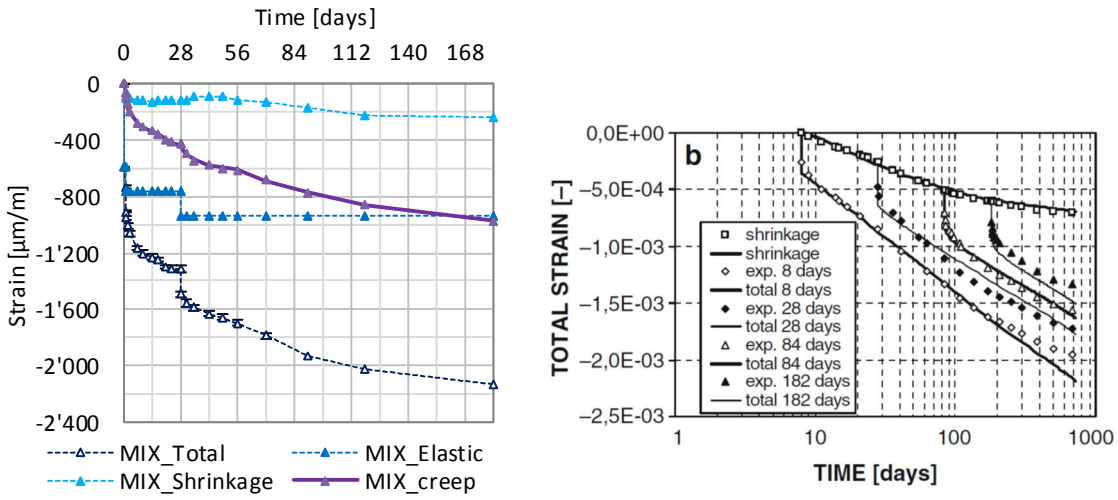

(a) (b)

Figure 14 – Shrinkage and creep coupling; total strain components identification (a) and literature evidence of the phenomenon (b) [86]

3.4 Concrete

Table 2 – Concrete mixtures design [kg/m^3]

	PC	CSA	MIX	CSA I	MIX I	MIX II
CEM II-LL 42.5R	450	-	200	-	210	175
ALICEM	-	350	200	400	140	175
Sand 0.20-0.35	258	265	255	256	264	264
Sand 0.6-1.0	197	202	195	196	201	201
Sand 1.5-2.5	262	270	260	261	268	268
Gravel 3-4	142	146	141	141	145	145
Gravel 6-10	335	344	331	333	343	343
Gravel 10-20	584	600	578	580	597	597
SP (% on binder)	1.0	0.3	0.5	0.5	1	1
Retarder (% on binder)	-	0.4	0.5	0.4	0.5	0.5
Accelerator (% on binder)	-	0.1	0.2	0.2	0.1	0.2
Water	157.5	175	180	180	175	175
w/b	0.35	0.5	0.45	0.45	0.5	0.5

Table 3 – Concrete mixtures key factors

	PC	CSA	MIX	CSA I	MIX I	MIX II
Strength class at 24 hours	C25/30	C35/45	C32/40	C45/55	C20/25	C30/37
Strength class at 28 days	C50/60	C50/60	C50/60	C55/67	C35/45	C45/55
Abrams cone drop at 45 minutes [mm]	180	180	180	205	190	160

As already mentioned in the introduction to this chapter, the main aim of the present research is to study the possibility to use calcium sulfoaluminate cement based material for structural applications. Thus, the focus of the whole program is at the concrete scale. For concrete mixtures, a Bolomey curve was followed in order to set the particle size distribution of the aggregates. A first campaign was organized on the investigation of the main properties in terms of deformative behaviour and mechanical performances of the three chosen mixtures. For the compressive strength and the deformative evolution, both early and later age were analysed, while the other investigated aspects were defined just in two stages: 24 hours and 28 days. The first represents the early age material properties while the second was used in accordance with the international standard, which refers generally to the 28 days performance to describe the material properties. In order to make the use of these material practical, their trend needs to be described with constitutive laws

that engineers can use to design structures. Instead of create new rules for concrete based on calcium sulfoaluminate cement, Portland constitutive laws reported in the main standards were used [87]–[89] and validated. The collected results for the chosen mixtures were used in these constitutive laws, making a comparison between the real and the predicted value. For this last step, three other concrete mixtures were defined to increase the extension of the applicability of the research conclusions. The rules on which these mixtures are designed are the same followed for the first campaign. One pure CSA and two blends (50/50 and 60/40 PC/CSA ratio) are used, named CSA I, MIX I and MIX II respectively, defining them in terms of strength class at 24 hours. The mixture proportion are reported in Table 2 while the key-factor values are reported in Table 3.

3.4.1 COMPRESSIVE STRENGTH

Measurements of compressive strength were performed up to one year following the EN 12390-3 standard. The measurements were carried out on ten cubic samples (edge 100 mm) for each deadline in order to have a reasonable number of data to make a statistical evaluation of the strength characteristic value. The samples were produced by pouring the molds in two layers and vibrating for 5 seconds after each pouring. Once the upper surfaces were rectified, the samples in the molds were stored in a climatic room at 20±2°C and RH > 95%, while covered with plastic sheets. The samples were demolded at 24 hours of age and stored in the same climatic room until they were tested, except for those used for the early age tests at 4, 8 and 16 hours.

The value obtained from the test represents the average compressive strength on cubic samples of 100 mm edge ${R_{cm}}^{100}$. As reported in [90] a conversion factor of 0.968 was used to obtain the correspondent compressive strength on cubic samples of 150 mm edge ${R_{cm}}^{150}$ (4). Then, the characteristic compressive strength R_{ck} was calculated according to the relation (5).

$${R_{ck}}^{200} = 0.95 \cdot {R_{ck}}^{150} = 0.92 \cdot {R_{ck}}^{100} \quad [N/mm^2] \tag{4}$$

$${R_{ck}}^{150} = {R_{cm}}^{150} - k \cdot s_n \quad [N/mm^2] \tag{5}$$

where

k is a factor representing the n percentile of the Gaussian distribution (for the 5th is 1.64);

s_n is the standard deviation.

The characteristic cylindrical compressive strength was calculated from this value with the typical formula present in the most common standards $f_{ck} = 0.83 \cdot R_{ck}$ from which the cylindrical average compressive strength can be back-calculated.

3.4.2 FLEXURAL STRENGTH

One of the method used to investigate the tensile strength indirectly was the flexural strength test. It was performed following EN 12390-5 standard on three prismatic samples (100×100×400 mm^3). The set-up details are reported in Figure 15. Two deadlines were investigated; one after 24 hours, which represents the early age material performance, and the other after 28 days, which characterize the material in the later age and is used as a reference with the standards. The operations followed to produce and store the samples are the same as the one described in paragraph 3.4.1. The results gathered from this test were transformed into a tensile strength by the following formula, taken by the Model code 2010:

$$f_{ctm} = \alpha_{fl} \cdot f_{ctm,fl} \tag{6}$$

where: f_{ctm} = mean tensile strength [MPa]

$f_{ctm,fl}$ = mean flexural tensile strength [MPa]

$\alpha_{fl} = \frac{0.06 \cdot {h_b}^{0.7}}{1 + 0.06 \cdot {h_b}^{0.7}}$

h_b = beam depth [mm]

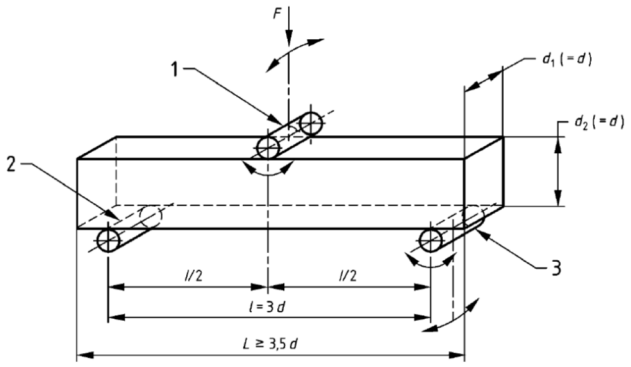

Figure 15 – Flexural strength test set-up details as reported in EN 12390-5

3.4.3 SPLITTING TENSILE STRENGTH

Another indirect method used for the tensile strength investigation was the splitting tensile strength test. It was performed on cylindrical samples of 100 mm diameter and 200 mm length, following EN 12390-6 standard. Details on the loading system used in this test are reported in Figure 16. The deadlines followed in this test were the same as the flexural strength test. Also the operations for producing and storing the samples are the same as in the paragraph 3.4.1. The collected results were transformed into tensile strength by the following formula, taken from the Model code 2010 [89]:

$$f_{ctm} = \alpha_{sp} \cdot f_{ctm,sp} \tag{7}$$

where: $f_{ctm,sp}$ = mean splitting tensile strength [MPa]

$$\alpha_{sp} = 2.2 \cdot (f_{cm})^{(-0.18)}$$

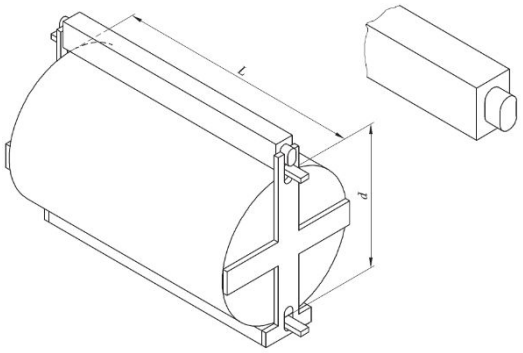

Figure 16 – Loading system for the indirect tensile strength test

3.4.4 STATIC MODULUS OF ELASTICITY

Another important aspect for the mechanical characterization of concrete is the stiffness of the matrix which is identified by the modulus of elasticity. In particular, the static modulus of elasticity, or Young's modulus, is defined as the ratio between the applied stress and the resulting strain within the elastic limit. It especially characterizes the material stiffness in real field, e.g. when they are under exercise condition. Two cylindrical samples of 150 mm diameter and 300 mm length were used for the test. The standard EN 12390-13 was followed to perform the test. To cast and store the samples the same procedure as in paragraph 3.4.1 was followed. Two deadline were considered in order to investigate the early and later age properties as said in paragraph 3.4.2.

3.4.5 DYNAMIC MODULUS OF ELASTICITY

Another way to measure concrete stiffness is by dynamic methods. The one used in this campaign was based on the propagation of ultrasound in the matrix, performed following UNI 9771 standard. Unlike the static investigation method, the dynamic test did not affect the structure during the test. However, for structural application an evaluation conditioned by an applied load is more realistic and more interesting to know for designers.

Two prismatic samples (100×100×400 mm^3) were considered at each deadline. The casting and storing procedure are the same as in paragraph 3.4.1, while the two considered deadlines follow the considerations of paragraph 3.4.2.

3.4.6 SHRINKAGE AND CREEP

Three different campaign were carried out on these aspects. The first focused on the drying shrinkage evolution following UNI 11307 standard on all the six considered mixtures until 364 days. The specimens were provided with surface pins that were glued after 6, 16 and 24 hours for pure CSA, blends and Portland mixtures respectively. The prisms were then stored in a 50% RH - 20° C chamber, their length measured with a calibrated deformometer and their mass weighted.

The second campaign added the autogenous investigation on the two main calcium sulfoaluminate based mixtures CSA and MIX. Following the same procedure described for the first campaign, six prismatic samples were produced for each mixture; three were used for the drying investigation as in the first campaign and the other three were used for the autogenous investigation. Sealed conditions were assured by covering completely the samples with adhesive aluminum tape just after demolding, in order to avoid moisture loss in time. Unlike the first campaign, samples were demolded and firstly measured after 8 hours, which was considered as the moment in which structures in practice will be demolded using this material in order to obtain a real advantage in terms of time and performance. The test ended after 182 days, providing the relation between samples cured in sealed and drying condition. The third and last campaign introduced the creep investigation on all the three main mixtures CSA, MIX and PC. In order to obtain the creep deformation, even the classic shrinkage investigation on samples produced with the same batch is required. They were measured under autogenous and drying condition according to the Swiss standard SIA 262/1:2013 F until 364 days. In the case of creep, only MIX was measured until this deadline, while the measurements on the other mixtures

were stopped after 182 days because their rate of creep had slowed down by this age, especially when compared to MIX. The specimens were 120×120×360 mm^3 prisms cast in steel molds and stored in a climatic room at 20±0.5°C and RH > 95%, while covered with plastic sheets. The samples were demolded at 24 h of age, which was the time when the test started. Two samples were prepared for each test and condition. To each sample, two measuring pins were glued at a distance of 250 mm on two opposite sides of the sample, avoiding the cast surface. In this way, two length measurements on each of two samples were performed. For the drying condition, all the surfaces of the sample were exposed to a 20±0.5°C and 57±3% RH environment, while the sealed conditions were assured as in the second campaign by aluminium tape. While the shrinkage samples were stored horizontally on two thin blade supports (Figure 17a), to allow drying from all their surfaces, the creep samples were placed vertically one over the other, with a metallic plate in between (Figure 17b). Three loading steps at 1, 7 and 28 days were applied to the samples in order to investigate the initial creep evolution, which is particularly important for the rapid-hardening behavior of CSA cement. Generally, the applied load corresponded to a stress of 1/3 of the compressive strength at the age of loading. However, due to reaching the capacity of the creep setups, some samples needed to be loaded instead to 25% of the compressive strength. Nevertheless, when considering the specific creep coefficient this difference in loading level becomes negligible, especially because in the range between 25 to 30% of the compressive strength creep is expected to vary linearly with the applied stress [78]. Results for the shrinkage tests were expressed in terms of µm/m and were calculated based on the following formula:

$$\varepsilon = \frac{l_i - l_0}{l_0} \tag{8}$$

where: ε = shrinkage, either autogenous or drying [$\mu m/m$];

l_i = length at time i [μm];

l_0 = initial length between the measuring pins, equal to 250 mm.

Units for shrinkage are known also as microstrain and are represented by [µε].

The results from the creep test were presented in the same way of mortar samples using Eq (2) and Eq (3).

$$\varphi = \frac{\varepsilon_{tot} - \varepsilon_{shr} - \varepsilon_{el}}{\varepsilon_{el}} \quad (2)$$

where: φ = creep coefficient [-];

ε_{tot} = total deformation calculated from the creep test [$\mu m/m$];

ε_{shr} = deformation calculated from the shrinkage test [$\mu m/m$];

ε_{el} = elastic deformation at the moment of loading [$\mu m/m$].

$$J = \frac{\varepsilon_{tot} - \varepsilon_{shr} - \varepsilon_{el}}{\sigma} \quad (3)$$

where: J = creep compliance [$\mu\varepsilon/MPa$];

σ = compressive stress applied to the sample [MPa].

All data shown in the graphs in the results section represents the average of two samples and is plotted with its standard deviation.

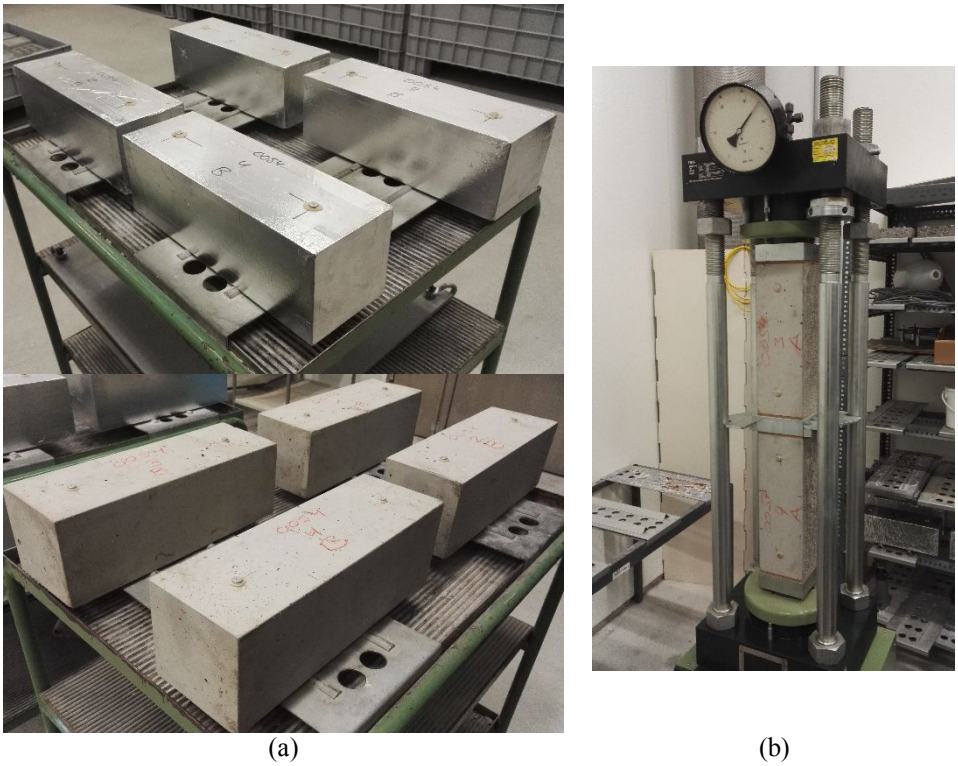

(a) (b)

Figure 17 – Shrinkage (a) and creep (b) samples position during the test in the third campaign

3.4.7 STRESS – STRAIN DIAGRAMS IN COMPRESSION

The stress-strain behaviour (in compression) was determined according to an internal procedure at 28 days on two cylindrical samples of 150 mm diameter and 300 mm length.

The early age investigation was avoided because of the difficulties encountered preparing the samples. The two circular surfaces were rectified before starting the test in order to have a planar area on which apply the load, which requires to be centred and equally distributed. The general procedure consists in applying a load which increments in time and measuring the deformation due to this load on three different vertical lines on the lateral surface of the cylinder. The mean of these three lines represents the final strain used to create the stress-strain graph. Each test on each investigated mixture was combined with a compressive strength test on two cubic samples treated and tested in the same way as in paragraph 3.4.1 in order to calibrate the set-up. Due to the different stress and strain reached for each mixture at the peak point, data were also expressed after normalization. This procedure consists in drawing the stress data in terms of f'_c/f_c where f'_c and f_c represent the peak and the general stress respectively. The same procedure was followed to normalize the strain $\left(\varepsilon'_c/\varepsilon_c\right)$. The obtained graph helps to compare the behaviour between mixtures and underline their differences. Moreover, the area underneath the curve drawn in that way represents the dissipative capacity of the material, an aspect that is fundamental for real applications.

3.4.8 CONSTITUTIVE LAWS EVALUATION

The aim of the present research program is to characterize mechanically materials based on calcium sulfoaluminate cement in order to evaluate their applicability to real structure. During the structure design formulas which simulate the material mechanical aspects are used. These constitutive laws are reported in the major technical documents and are the results of several investigations. Typical cement based materials standards were developed with researches on Portland, which means that for calcium sulfoaluminate cement there are no references. Instead of creating new one for this new material, which requires a lot of resources, the collected results in the tests previously described are used inside the Portland standards and the results are compared to the reference mixture PC in order to have a range of accuracy. This range can say if the standards already used for Portland are suitable even for calcium sulfoaluminate cement and, if they are not, can underlines where are the main differences.

Two main standard collections and one international reference were considered: the Italian NTC 08, the European EN and the international Model code 2010 [87]–[89]. More in details, the chapter 11.2.10 "concrete characteristics" of the NTC 08, the section 3.1 "concrete" of the eurocode 2 and the chapter 5.1 "concrete" of the model code 2010. These references describe the mechanical aspects of concrete by formulas which usually use as the main variable the characteristic compressive strength. In our case, we directly have the mean of the compressive strength f_{cm}. By a direct comparison between the formulas and the values obtained in the tests a first evaluation was done. Moreover, by inverse analysis the coefficient used in the standards were back-calculated.
A summary of the considered formulas is reported in Table 4.

Table 4 – Standardized formulas for the mechanical characterization of the material

	NTC 08	**Eurocode 2**	**Model code**
Compressive strength	$f_{cm} = f_{ck} + 8\ MPa$ $R_{ck} = 0.83 \cdot f_{ck}$		
Tensile strength	$f_{ctm} = 0.30 \cdot {f_{ck}}^{2/3}$ for classes ≤ C50/60 $f_{ctm} = 2.12 \cdot ln\left[1 + \frac{f_{cm}}{10}\right]$ for classes > C50/60 $f_{ctm,5} = 0.7 \cdot f_{ctm}$ $f_{ctm,95} = 1.3 \cdot f_{ctm}$		
From flexural strength	$f_{cfm} = 1.2 \cdot f_{ctm}$	$f_{ctm,fl} = max\left[\left(1.6 - \frac{h}{1000}\right) \cdot f_{ctm}; f_{ctm}\right]$	$f_{ctm} = \frac{0.06 \cdot {h_b}^{0.7}}{1 + 0.06 \cdot {h_b}^{0.7}} \cdot f_{ctm,fl}$
From splitting	-	$f_{ct} = 0.9 \cdot f_{ct,sp}$	$f_{ctm} = 2.08 \cdot (f_{cm})^{-0.16} \cdot f_{ctm,sp}$
Dynamic modulus of elasticity	-	-	$E_{ci} = 21500 \cdot 1 \cdot \left(\frac{f_{cm}}{10}\right)^{1/3}$
Static modulus of elasticity	$E_{cm} = 22000 \cdot \left[\frac{f_{cm}}{10}\right]^{0.3}$		$E_c = \left(0.8 + 0.2 \cdot \frac{f_{cm}}{88}\right) \cdot E_{ci}$

A qualitative study on the tensile strength formulas accuracy was done, comparing standard curves with campaign test results. The theoretical curves of the standardized tensile strength were used as a reliability limit for the campaign results. The two curves

$f_{ctm,5}$ and $f_{ctm,95}$ were used as the upper and lower results boundaries. Model code 2010 formulas of the flexural and splitting tensile strength were used to translate the campaign results into tensile strength values. These values are inserted in the same graph of the two curves and their relation evaluated.

Another qualitative study was done on the modulus of elasticity results. At first, the standard formula used in the Model code 2010 for both static and dynamic measurements was plotted and related with the test results. Afterwards, the coefficient used in the standard to translate dynamic results to static one was directly checked with the test results.

Moreover, a study which did not involve any standard but widespread accepted researches was done on the stress-strain relation in compression. Some different models were considered [91]–[95] in order to define their suitability with CSA based concrete and which one of them was the best in fitting their general trend. Also in this case a qualitative evaluation was carried out.

4 RESULTS AND DISCUSSION

This chapter is divided into three main section. The first one reports the results obtained during the mortar campaign, while the second shows the results collected in the concrete campaign. Both are organized in two paragraphs representing the strength and the dimensional stability investigations. While the first section is characterized by a more scientific analysis of the different aspects, the second focus on the practical application of the results collected, reporting examples and indications. Eventually, the third section reports an analysis of the results collected in the concrete campaign in terms of constitutive laws. The major technical documents and the most valuable researches were considered in order to compare their formulas (describing a specific mechanical aspect) with the concrete results collected during this research.

4.1 Mortar

4.1.1 STRENGTH CHARACTERIZATION

4.1.1.1 *Isothermal calorimetry*

The results of conduction calorimetry are given in Figure 18. No dormant period was evident for the pure calcium sulfoaluminate mixture, where the acceleration period started just after 1 hour from water addition. The main peak was reached after 2 hours, followed by a rapid decrease of the rate of heat liberation until the end of the test. In the CSA/Portland cement blend, the acceleration period started at about the same time as the CSA but the rate of heat liberation was lower. Different peaks were recorded in the first 6 hours, due to the influence of the admixtures on the hydration reactions. The main peak is reached after 4 hours and is three times smaller than the CSA. After about 6 hours, the rate of heat liberation gradually decreases. The Portland-based mixture showed a completely different evolution in time. After the first initial peak, there is a dormant period until 8 hours followed by an acceleration period between 8 and 18 hours, when the main peak is reached. Compared to the CSA, the Portland cement peak is about ten times smaller; however, the total amount of heat produced in time is higher in PC: 280 J/g in 7 days compared to the 270 J/g and 250 J/g of CSA and MIX respectively.

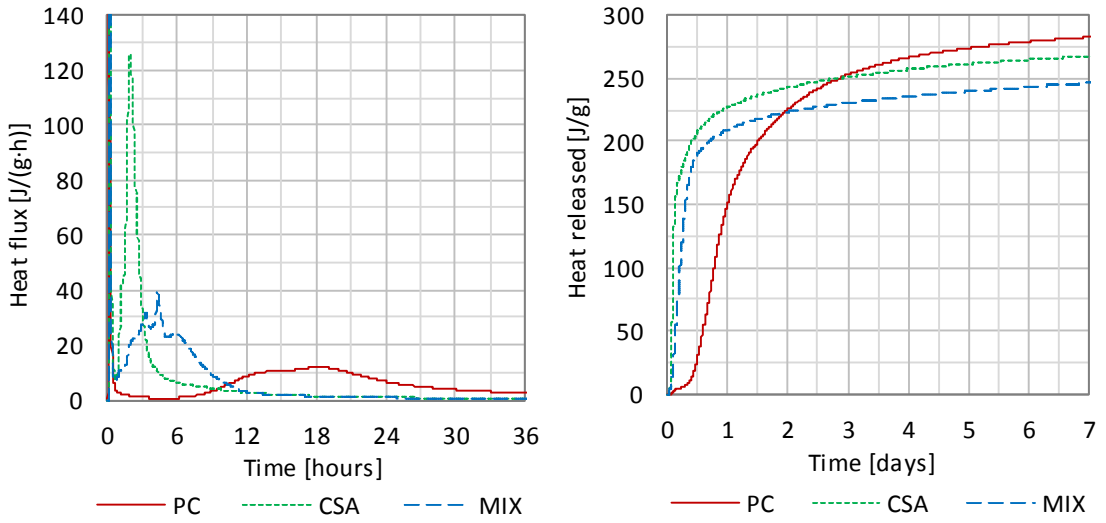

Figure 18 – Isothermal conduction calorimetry for the three investigated mixtures; Heat flow in the first 36 hours (a) and cumulative heat until 7 days (b)

The reported conduction calorimetry results are representative of the CSA cement faster reaction compared to Portland. The initial sharp peak in CSA is connected with the high temperature reached by the material (height of the peak point) and the rapidity of the hydration products formation (nearly vertical curve slope). The tight base of the peak is related, instead, with the short duration of the reaction. In the case of PC, the two close smaller peaks expressed later than CSA are typical of a slower reaction connected with a lower perceived material temperature. However, the large base indicates a long reaction, which depletes its potential later on, in longer time than CSA. Despite the smaller peak reached by PC, the total heat released in time is higher than CSA, evidencing the higher amount of hydration products formed. The blend system is characterized by a fast initial reaction which last later than CSA. However, its total heat released in time is the smallest before 7 days; though, after this deadline some reaction in this system can happen due to the presence of Portland cement. Comparisons with other research results are difficult because of the high number of variables present in the studied mixtures. The composition of the used CSA (already mixed with gypsum), the CSA/OPC ratio in the blend and the use of three different admixtures are examples of the aspects which can influence the final results.

4.1.1.2 *Compressive and flexural strength*

Figure 19 represents the compressive and flexural strength evolution until 28 days for the three investigated mixtures, with a focus on the very early age evolution. Both aspects underline the rapid hardening behaviour of CSA and MIX compared to PC. However, after this initial period, CSA based mixtures slow down their evolution, reaching at 28 days 67.95, 63.00 and 70.58 MPa for CSA, MIX and PC respectively in compression while in flexion was 9.00, 7.27 and 10.00 MPa. Mixture CSA slow down gradually after the first 24 hours, while MIX showed a stand-by around 1-3 days. In the compressive strength test the evolution restarted to increase at 7 days while in flexural strength a plateau was reached until 28 days. A focus on the very early age properties evolution is represented in Figure 20. Mixture CSA was the fastest, showing some performance already after 2 hours, immediately followed by MIX while PC had a 9 hours delay from them. After 4 hours CSA started to slow down while MIX evolution continued to increase at a higher ratio, becoming the most performant after 8 hours. Portland mixture PC started

to react when CSA and MIX had already around 35 and 40 MPa in compression and around 6 and 7 MPa in flexion. In both tests, for the early age evolution, the general trend and the relation between mixtures is comparable, thus not influenced by the investigated aspect.

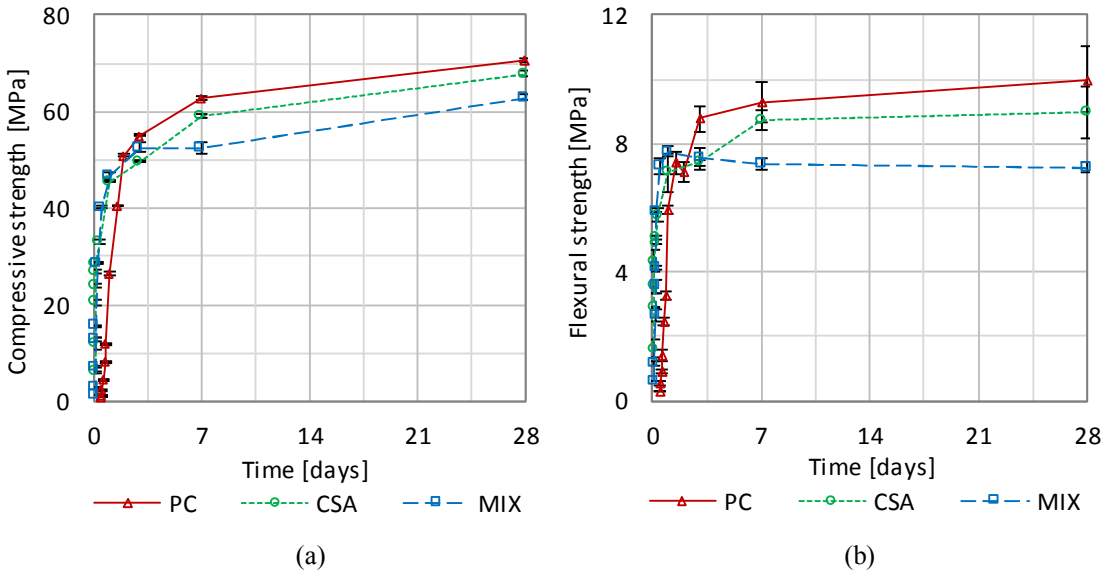

Figure 19 – Compressive (a) and flexural (b) strength evolution until 28 days

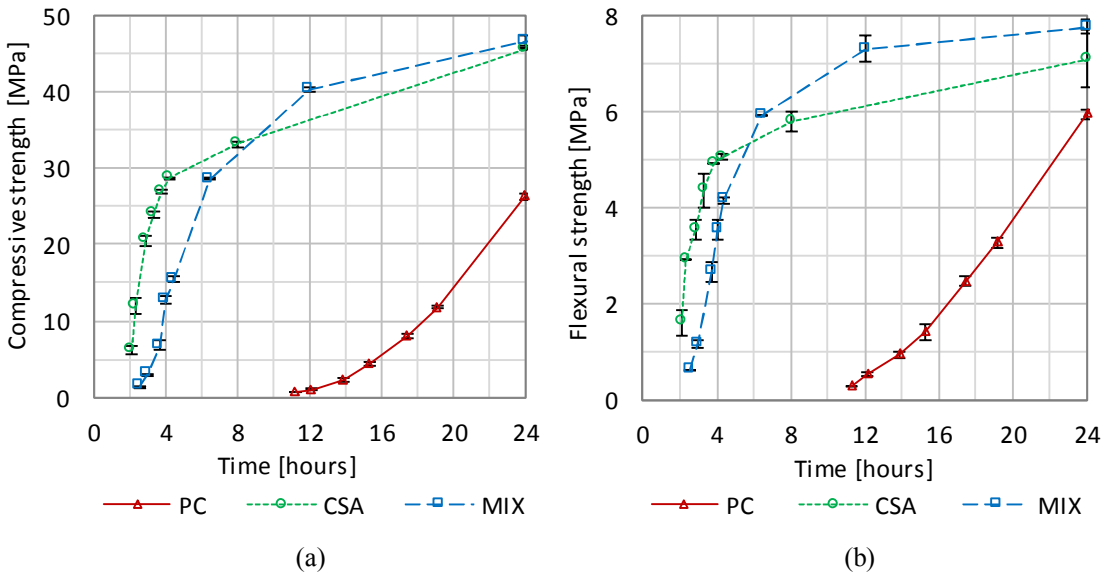

Figure 20 – Early age compressive (a) and flexural (b) strength

The early age investigation attests the rapid hardening behavior of CSA based systems. In both compressive and flexural strength test high performance are reached quickly.

Portland based system recover the initial gap after around 3 days, reaching thereafter higher values. The blend system strongly slows down after 1 days in both test. While compressive strength just showed a short break, flexural strength interrupts the evolution until the end of the investigated period of 28 days. A similar decrease in flexural strength was found by Pelletier et al [96]. In their CSA mortar samples blended with gypsum and limestone/quartz filler the flexural strength evolution showed a decrease between 7 and 28 days. Also Zhang [23] reported in his findings the loss of flexural strength in between 3 and 28 days. He related this phenomenon to binary CSA-gypsum systems without explaining the reasons why it happened. However, intergrinding clinker with limestone and gypsum prevents this occurring. Quilling reported results on a CSAB system attesting an increasing compressive strength in later age [22]. He supposed that this ongoing strength development was due to the hydration of the slow reacting belite component. A similar delayed reaction could happen in MIX with the Portland contained in the mixture. The fast reacting CSA cement dominates the early age reactions while Portland cement get involved in the hydration process later on, with a plausible combination of the two in between. In order to better understand the effect of this interaction on the mortar performance, later age investigations should be done.

4.1.1.3 *Static and dynamic modulus of elasticity*

The modulus of elasticity evolution in both static and dynamic condition until 28 days is represented in Figure 21. A focus on the very early age evolution was done. As seen in paragraph 4.1.1.2, also the modulus of elasticity investigations underlined the faster reaction of CSA and MIX and the higher performance of PC at later age. After 28 days, the static modulus of elasticity was 31.10, 26.55 and 31.55 GPa for CSA, MIX and PC respectively, while the dynamic was 34.57, 32.81 and 36.96 GPa. The very early age evolution is presented in Figure 22. Like what happened in the compressive and flexural strength, CSA reacted firstly after 2 hours, followed immediately by MIX and after a delay of 9 hours from PC. At the moment in which PC started to show some performance, CSA and MIX already had around 22 and 23.5 GPa in static set-up and both around 26.5 GPa in the dynamic.

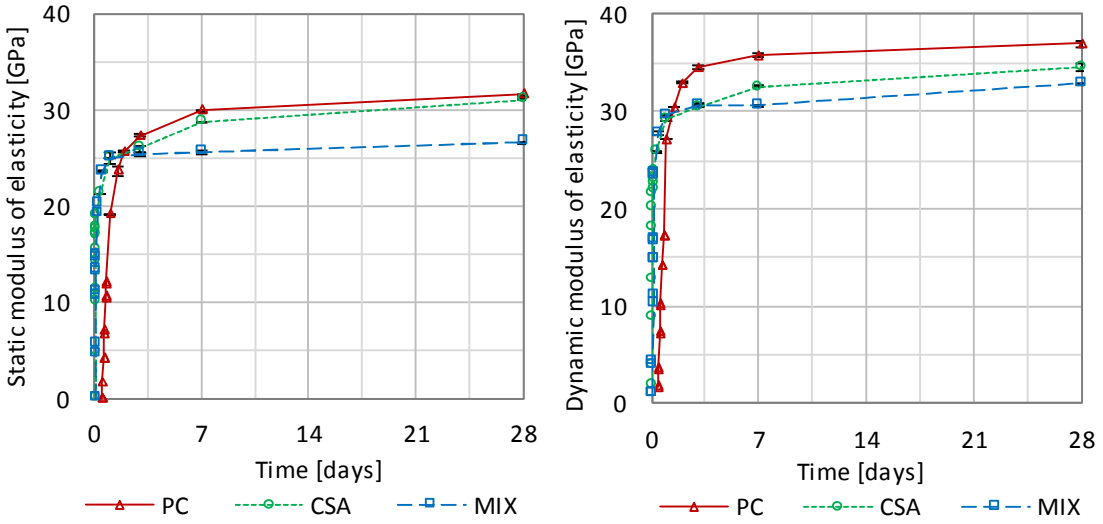

Figure 21 – Static (a) and dynamic (b) modulus of elasticity evolution until 28 days

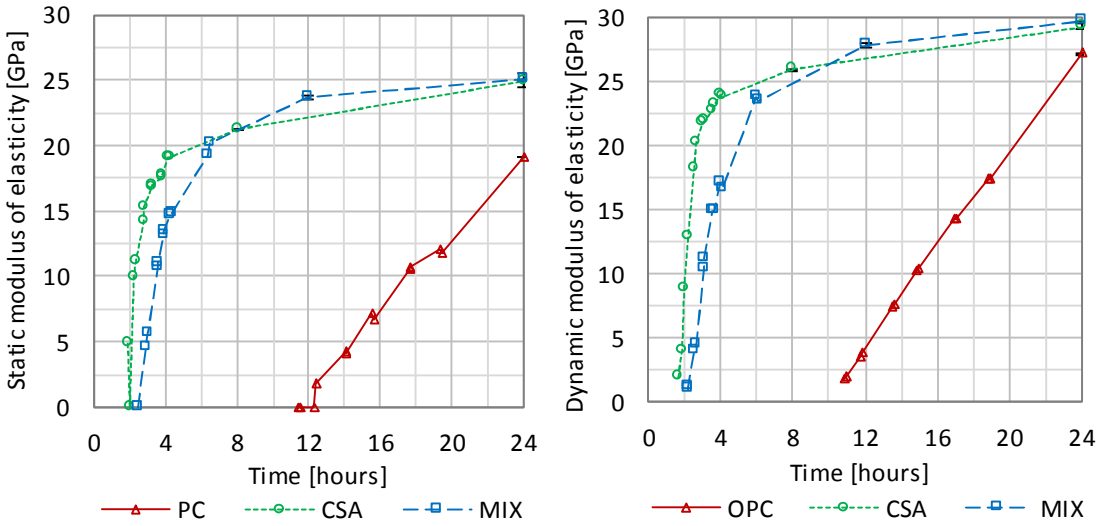

Figure 22 – Early age static (a) and dynamic (b) modulus of elasticity

Comparing the two methods, no differences are evidenced in the general trend; the dynamic values are always higher than the static and the range of difference is similar between mixtures. Thus, the microstructure developed by CSA based mixture is physically comparable with that of PC. Moreover, these results confirm the quality of the data collected in paragraph 4.1.1.2 on the early age compressive and flexural strength and the assumption done on the CSA based material, like their fast reaction and the peculiar hydration reaction after 1 day in MIX. As reported by Zhang [7], the elastic modulus,

splitting strength and flexural strength increase in step with compressive strength for CSA concrete; thus, a correspondence between trends from different investigations was expected. The fast development of a stiff microstructure for CSA based systems seems not to be detrimental for the long term performance. However, a longer investigation period is required in order to check the stability of blend system after 28 days.

4.1.1.4 *EMM ARM*

Results from EMM ARM are reported in Figure 23, from the early age (a) until 7 days (b). As expected, the early age was characterized by the faster CSA reaction compared to MIX, though it slowed down before and at a higher ratio, reaching smaller values after 12 hours. PC showed the first evolution after 9 hours, increasing slowly, reaching at 12 hours 5.05 GPa compared to the 25.52 and 27.45 GPa of CSA and MIX respectively. The initial vertical lines represent the moment in which data were acquired for the first time and were not yet set. After the first 12 hours, MIX modulus of elasticity evolution showed just a little increase until 3 days being nearly constant afterwards. Conversely, CSA, which decelerated before, evolved with a higher ratio, reaching MIX values around 7 days. In the case of Portland mixture, it was slower than the other two but it evolved higher stiffness in time. After 30 and 40 hours its evolution crossed CSA and MIX respectively, continuing to increase thereafter. At 7 days the modulus of elasticity was 34.4, 29.35 and 29.1 GPa for PC, CSA and MIX respectively. Moreover, by the evaluation of the moment in which the curves shifted from the initial white noise, the final set can be defined. Results obtained from this evaluation were 6.8, 1.1 and 1.4 hours for PC, CSA and MIX respectively.

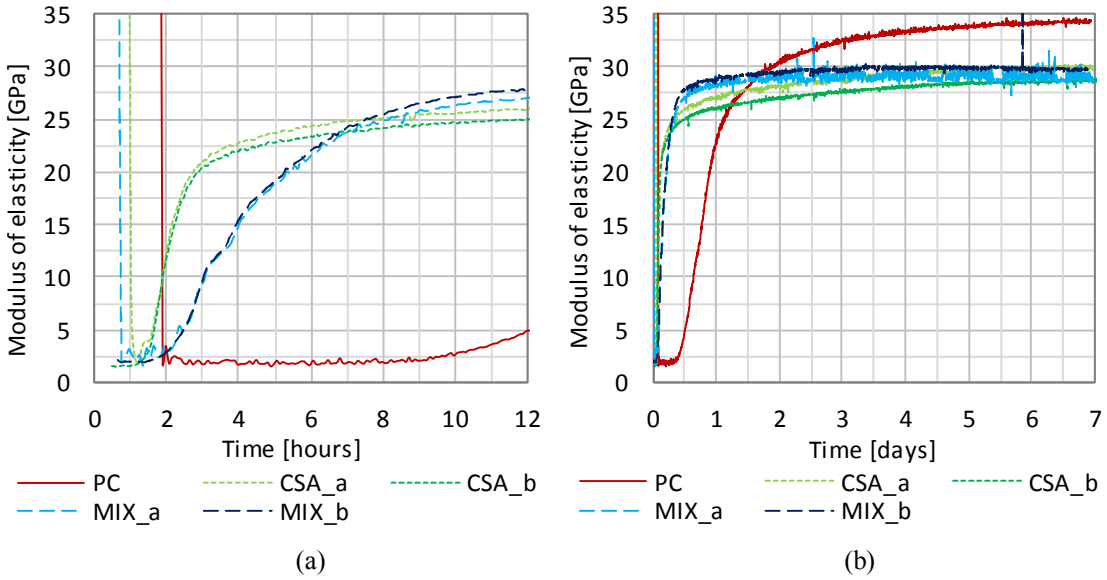

Figure 23 – Modulus of elasticity evolution measured by EMM ARM technique in the first 12 hours (a) and until 7 days (b)

4.1.1.5 *Modulus of elasticity relation*

Figure 24 reports the relation between modulus of elasticity evolution defined by the three different techniques described in paragraphs 3.3.1, 3.3.2 and 3.3.4. It is already known that static and dynamic investigation lead to different values, although there is some relation between the two [97]. This difference can be related with the real aspects investigated by the tests. In the dynamic case the structure is not influenced by external load, thus it represents the un-conditioned evolution due to the only hydration progression. In the static case, the microstructure is subjected to a stress due to an external load which produces a deformation within the elastic range. Thus, the investigation is carried out on a conditioned structure by the load. The results collected in the present research confirmed the existence of a relation between the static and dynamic investigation, extending this assumption to CSA based system. Moreover, the gap between these two techniques seemed to follow the modulus of elasticity evolution; it was at its minimum in the initial stage, increasing with the ongoing modulus of elasticity evolution, attesting on a nearly constant value when the modulus of elasticity slowed down. This evolution followed the hydration reaction progression, evidencing a strong correlation with the microstructure formation.

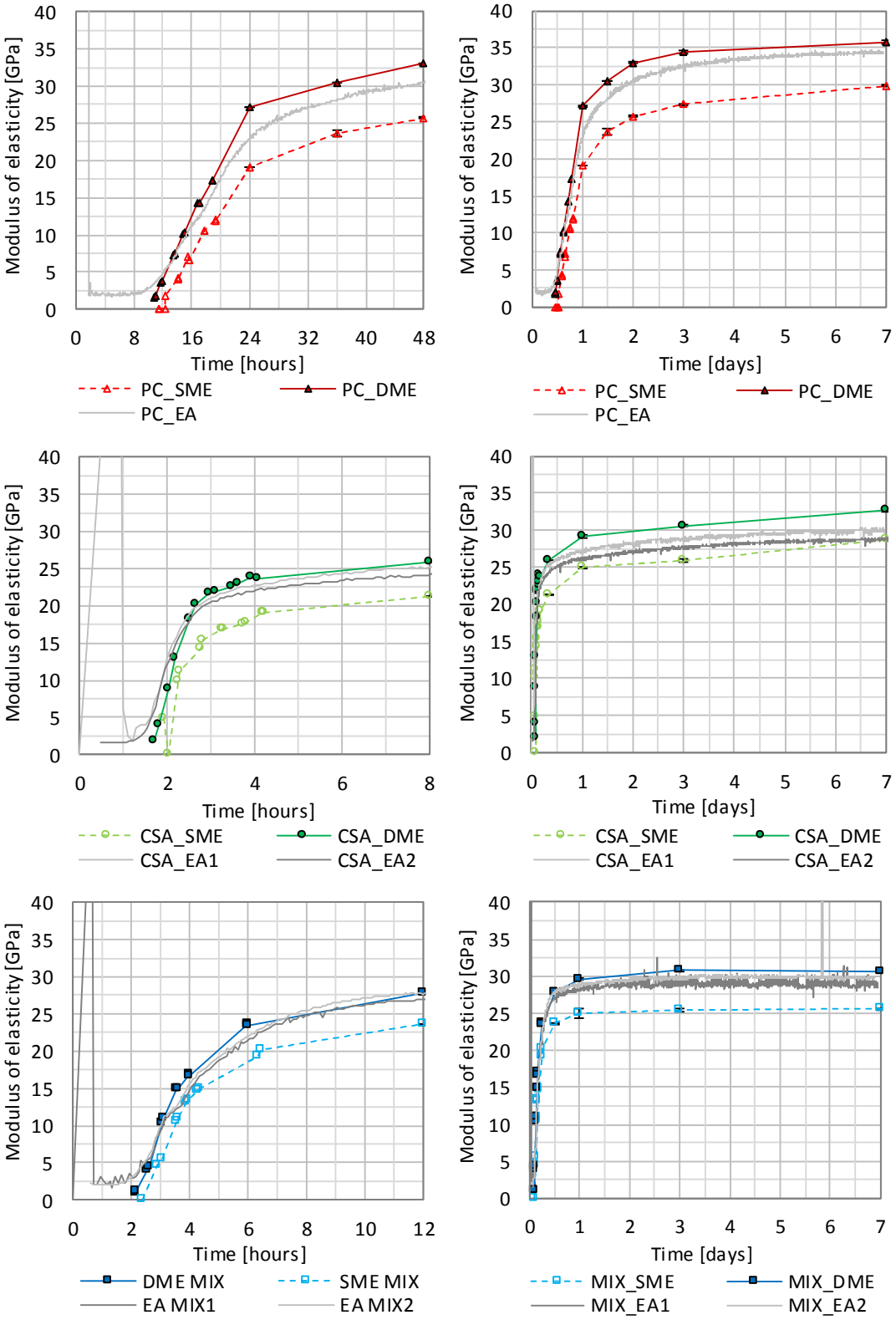

Figure 24 – Interrelation between static and dynamic modulus of elasticity evolution compared to the EMM ARM technique.

The curve representing the modulus of elasticity evolution with the new EMM-ARM technique laid in between the static and dynamic methods, closer to the latter. This technique allowed to investigate the material in the very early age in a continuous manner, evidencing a plausible final set point. For materials with a rapid hardening behavior, like calcium sulfoaluminate based systems, this technique is fundamental for the early age analysis. Inasmuch, results reported below showed an immediate reaction in the EMM-ARM curve to the microstructure formation compared to the other methods. That is due to the sample management during test [98]. The static set-up required a solid sample to load, while the dynamic test a semi-solid structure on which place the sensors. In EMM-ARM the sample evolved inside the mold, which was itself the set-up machine; thus, no particular problems were evidenced for its investigation. In all the considered mixtures, EMM-ARM curves respected the dynamic modulus of elasticity evolution. However, in CSA it slowed down before than the dynamic, attesting its values closer to the static. This was probably due to set-up details, like the initial white noise, which are still under optimization. Nevertheless, the general trend was respected and the modulus of elasticity values were rational, even in the new calcium sulfoaluminate based system investigated. Eventually, the quality of a new modulus of elasticity investigation technique (EMM-ARM) was proven, especially for rapid hardening systems; moreover, the relation between static and dynamic values was confirmed also for CSA based systems, underlining the similitudes between their microstructure with that of Portland.

4.1.1.6 *Dynamic Poisson's ratio*

Results from the dynamic Poisson's ratio investigation are reported in Figure 25 until 7 days (b) with a focus on the early age (a). Graphs are reported up to a Poisson's ratio value of 0.50 as it represents the liquid state. Over that range the conditions are not rational for cementitious systems. Each mixture is supposed to have an initial stage, before setting, in which has this value. Due to the rapid hardening behavior of CSA and MIX, this complete initial stage was not possible to record. However, their initial branch is enough to see a descending trend which is the typical evolution during the hardening of the matrix. On the contrary, the slower PC allowed the investigation of more points during the initial hardening, describing better this initial branch. Each mixture had a nearly constant value after 3 days, with CSA and MIX already stable after 1 and 2 days

respectively. After 7 days, time in which the investigation was stopped, the dynamic Poisson's ratio was 0.239, 0.253 and 0.222 for PC, CSA and MIX respectively.

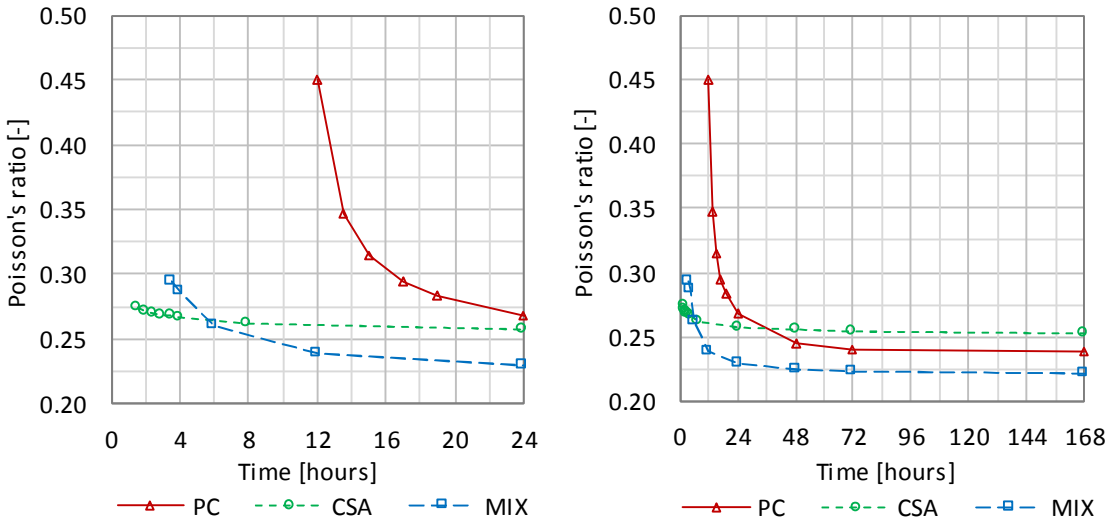

(a) (b)

Figure 25 – Dynamic Poisson's ratio evolution in the first 24 hour (a) until 7 days (b)

Early age results underline the initial fast reaction of CSA based systems, quickly developing a well-connected microstructure which stands deformations and stress. The stable later age Poisson's ratio results evidenced, instead, the higher CSA tendency to deform in the opposite direction of the force direction and the lower of MIX.

4.1.2 DIMENSIONAL STABILITY

4.1.2.1 *Internal RH*

Figure 26 shows the relative humidity evolution in time in autogenous condition for the three investigated mortars. Usually this test lasts up to a couple of weeks, however, in order to take into account the entire evolution of the blend mortar, longer periods were considered in the systems based on calcium sulfoaluminate cement. The Portland system did not show any strong tendency to self-desiccate, reaching 92% RH after 14 days; on the contrary, pure calcium sulfoaluminate mortar showed a strong initial drop to 84% RH just after 24 hours. The blend mortar behaved differently from both previous systems. After a RH drop in the first twelve hours which follows the pure calcium sulfoaluminate mortar trend, the evolution slowed down reaching 95% RH after 3 days. At that moment, a slight increase was recorded, getting to 96% RH after 14 days from water addition, restarting to go down afterwards. That multi-phase evolution for the blend system underlines the need of a longer period of investigation, where not only the absolute value but even the trend during time is important to understand the material behavior. This test represents an important investigation because it analyzes a parameter which is fundamental for the performance evolution and it lasts later than the usual 28 days. Indeed, a strong correlation between RH and the previous investigated aspects is highlighted. Considering MIX, assuming the variation in RH as an index of the reactivity of the matrix, the early age performance evidenced in paragraphs 4.1.1.2 and 4.1.1.3 are in good accordance with the initial fast drop in RH. Moreover, the point in which performance evolution slowed down fits with the RH stable period. Furthermore, the RH evolution restarted to drop after around 21 days, reaching its maximum slope after 28 days which matches with the plateau until 28 days found in flexural strength evolution. In this sense, flexural strength could restart to grow after the investigated 28 days. Thus, in order to describe MIX properties, a longer investigation period is required as for the early age since its evolution its characterized by a multi-phase trend.

Figure 26a reports peaks in which the RH seems to initially increase. These peaks are due to the water present on the upper surface of the mortar which is still fresh at the moment in which the test starts. This water can condense on the sensor varying the initial measurements [99]. The duration of the adjustment depends on the mortar reactivity.

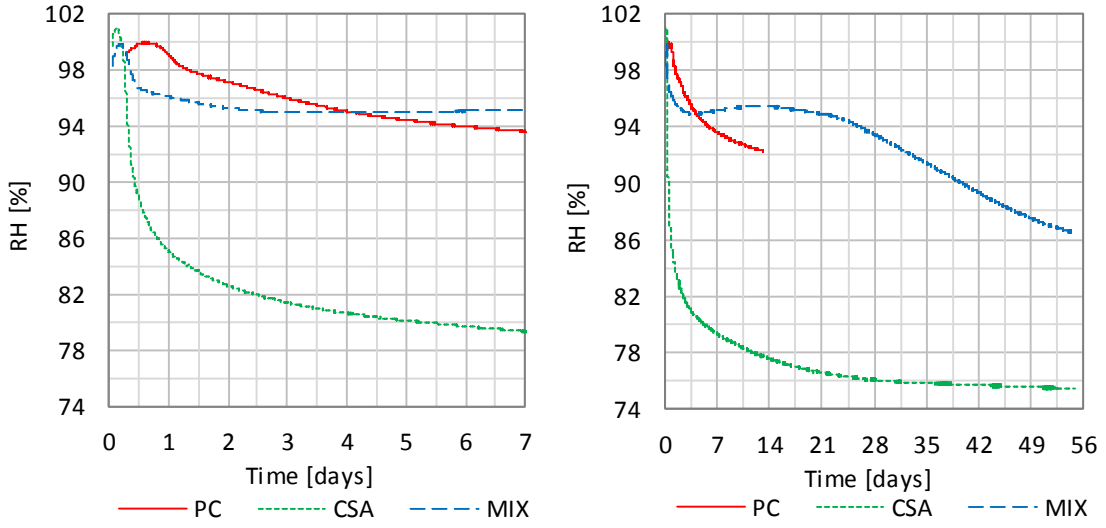

Figure 26 – Relative humidity evolution in autogenous condition in both early (a) and later age (b) for the three investigated mortars

4.1.2.2 *Autogenous shrinkage*

Figure 27 shows the autogenous deformation results for the three mortars until 24 hours. The reference PC mixture showed rapid shrinkage for the first two hours after final set, followed by slight expansion and a substantial plateau (at a total shrinkage value of about 100 µm/m) up to 24 hours. On the other hand, the CSA mortar showed even faster shrinkage after final set, reaching values around 800 µm/m in the first 30 minutes. After a discontinuity, the curve slope started to decrease constantly but at lower late, reaching 1200 µm/m at 24 hours. The blended mortar had an intermediate behavior, with final set close to that of the CSA mortar but reaching a plateau just one hour after set at a strain value around 600 µm/m.

From 24 hours forward, strain measurements were taken with the manual set-up. Figure 27b shows the overall strain development in autogenous conditions, from the time of set to 182 days. The pure CSA mortar continues to shrink until 28 days at a higher rate compared to the other two mortars, reaching a value about 1600 µm/m. The strain rate then decreases, adding only 150 µm/m in the next 5 months. The reference Portland mortar showed the smallest shrinkage, 350 µm/m at 28 days and only additional 50 µm/m in the next 5 months. The blended mortar had intermediate shrinkage, with a complex evolution in time. During the first week, shrinkage of 650 µm/m was measured, followed

by phase with slight expansion until 28 days. Unlike the other mixes, at this stage the blended mortar started a second shrinkage phase with higher shrinkage rate until 70 days, when the rate started to decrease. From 28 days to 6 months, the blended mortar showed the highest autogenous strain, about 250 µm/m.

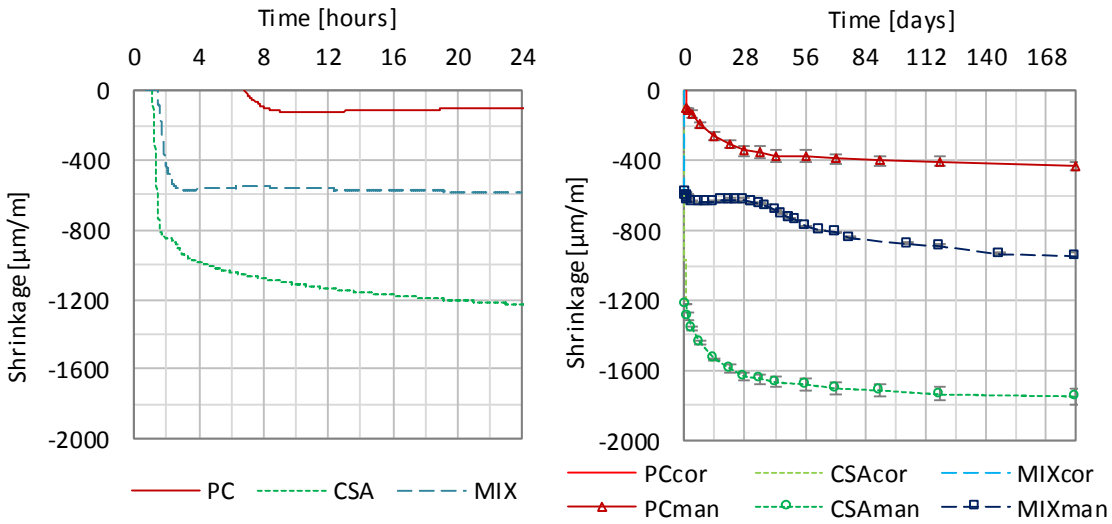

Figure 27 – Autogenous shrinkage evolution; (a) automatic measurements until 24 hours; (b) combination of automatic and manual measurements until 182 days

Autogenous shrinkage results follow the same trend showed by RH. Indeed, the most important aspect which influences autogenous shrinkage is the mixture self-desiccation which, itself, depends on the internal RH. These results confirm the multiphase evolution of MIX compared to CSA and PC (which showed a single curve trend) extending the investigated period from 56 until 182 days, time in which the evolution is stable and slows down gradually. If drying shrinkage become an issue just after demolding, autogenous shrinkage could be a problem even before (from the moment in which a solid skeleton is formed). At high deformation values, crack patterns could form even inside the mold. Thus, autogenous shrinkage should be limited. In this sense, MIX represents a good compromise; faster than PC with a lower autogenous shrinkage than CSA. Particular attention should be put on the later age, where the blend showed the highest evolution between 28 and 182 days.

4.1.2.3 *Mass change*

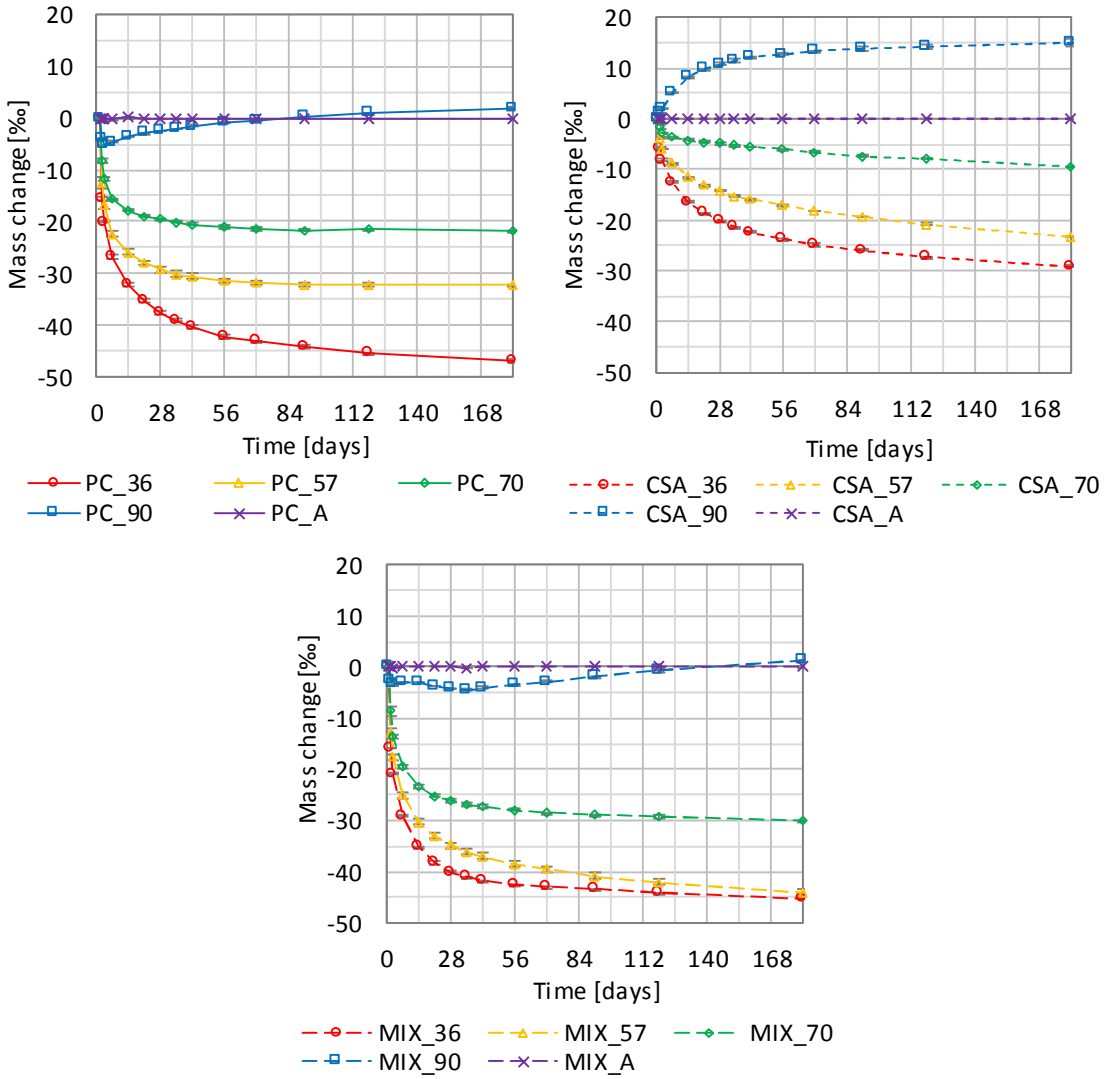

Figure 28 – Mass change until 182 days for the three investigated mortars

Figure 28 shows the mass change in time of samples stored at different RH. For all mortars, samples stored at 90% RH had different evolution than in the other environments. After an initial loss of mass during the first days, the Portland cement mortar started to slowly adsorb water from the external environment, recovering over time the mass loss. On the contrary, the CSA mortar showed a constant mass gain when exposed to 90% RH. Similarly, the blended mortar lost a small amount of water at early age followed by a small gain until 14 days, then moderate loss until 35 days and finally continuous gain until 6 months of age. In other RH conditions (36, 57 and 70% RH), the Portland and the blended mortars showed higher mass loss than the CSA mortar. The

blended mortar exhibited the highest mass losses at 70 and 57% RH, while the Portland cement mortar had slightly higher mass loss at 36% RH.

These trends are strongly connected with the internal RH evolution investigated in paragraph 4.1.2.1. The mass change curve at 90% RH environment is representative of the situation. The fast CSA self-desiccation led to an internal RH of 86% at 24 hours. Thus, in a 90% RH environment in which the sample is exposed after 24 hours to drying, the matrix absorb immediately water from the outside.

The mass change is also connected with the pore structure of the matrix. A porous structure characterized by small pores not well connected hinder the evaporation of water to the outer environment. On the contrary, big pores well connected help water to get outside from the microstructure easily.

4.1.2.4 *Shrinkage evolution after demolding*

Figure 29 shows the shrinkage evolution of the sealed specimens and the one exposed to drying at different RH from 1day. As expected, for all mortars, the lower the RH the higher the shrinkage. The blended mortar shrinks much less than the others. For the harshest drying condition (36% RH), the blended mortar reached shrinkage of about 450 μm/m after 180 days, while the CSA mortar and the Portland cement mortar shrunk 880 μm/m and 1330 μm/m, respectively.

Both the CSA and the blended mortars cured at 90% RH started to expand at 7 days from water addition. While the CSA mortars continued to swell over time, the blended mortars cured at 90% RH soon reached a plateau.

Considering the autogenous condition, in PC the evolution was close to the 90% RH curve while in CSA it follows the 70% RH trend. The blended mixture shows a particular situation in which the first thirty days are characterized by a trend similar to the 90% RH curve with less amount of shrinkage, followed by a strong drop of the curve which tends to follow the 70% RH evolution.

As said in paragraph 4.1.2.2, shrinkage in both autogenous and drying condition is governed by the RH. In autogenous condition this parameter evolves with the hydration, while in drying condition is imposed from the external environment. An hypothetical environment in which the RH evolution follows the internal condition, autogenous and drying shrinkage would be the same. Thus, from the comparison between drying

shrinkage curves at different RH and autogenous shrinkage curve is possible to derive an hypothetical internal RH since the temperature for both conditions are stable at 20°C.

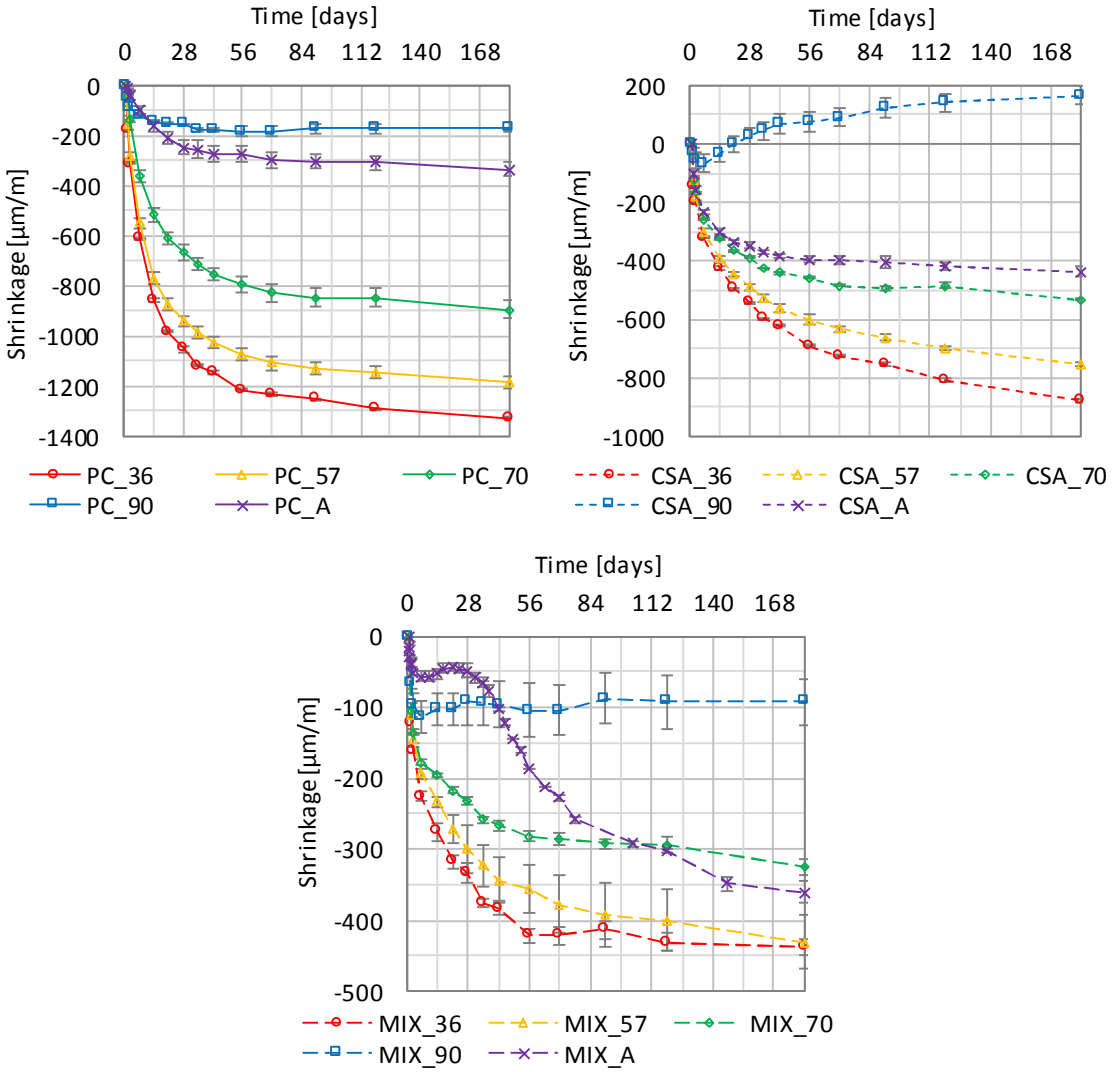

Figure 29 – Shrinkage evolution until 182 days for the three investigated mortars

4.1.2.5 *Relation between shrinkage, mass change and microstructure*

In autogenous conditions, no mass change was recorded during the investigated period. On the contrary, in drying conditions the lower is the environmental RH the higher the mass loss in time. More precisely, it is not important the environmental RH but the difference between it and the RH inside the sample (under autogenous conditions). The mass change evolution shown in Figure 28 underlines the internal RH of the samples. When the environmental RH is lower than the inner, some water evaporates and a mass loss is recorded. On the contrary, the reaction of the sample at an outside RH higher than

the one inside is an adsorption of water, increasing the mass of the sample. When an inversion of trend is recorded in the mass change graph of a particular RH condition, that evidence the moment in which the internal RH (in autogenous condition) decrease under the environmental RH level in which the samples are stored. Considering that, it is interesting the fact that all three mortars at 70% RH condition did not show any mass loss for the whole investigated period, underlining that until 182 days the inner RH was higher than 70%. The same trend was followed at 57 and 36% RH. A particular situation was recorded at 90% RH where all the mortars started to adsorb water from the external environment in different moments. While PC mortar started to gain mass after 7 days, CSA did it already after the demolding operation, evidencing its fast self-desiccation (decreasing of the internal RH in autogenous condition) compare to PC. In the blend mixture this inversion took place later on, at the sample age of 42 days; however, another small inversion was recorded before that deadline, after 7 days, like in the PC. In this case the adsorption was really small and last after one week, thus probably related with a reaction between Portland and calcium sulfoaluminate cement.

While the drying shrinkage depends on the environmental RH, which in our case is constant, the autogenous shrinkage depends on the sample inner RH, which is typical of the mortar and varies over time. Considering that at lower RH the shrinkage increases, we can estimate the moment in which the inner RH of a sample drops down certain levels by looking at the shrinkage curves in both autogenous and environmental condition. When the deformation curve of the sealed sample crosses another of a drying sample we can assume that the RH inside the sample is lower than in the compared environment, which means a higher shrinkage. This is a simplification of the real evolution because, as underlined before, the samples in autogenous condition have a story in which the RH changes over time, so the RH is not constant as the sample in drying condition. Data collected in this campaign are in good accordance with this assumption, showing for PC mortar an inversion in the mass change at 90% RH after 7 days and a cross between autogenous and drying shrinkage at 90% RH between 7 and 14 days. In CSA mortar the drying shrinkage at 90% RH is always lower than the curve in autogenous condition whilst the blend system begins to gain mass in 90% RH at 42 days and the autogenous shrinkage crosses the drying curve of 90% RH between 35 and 42 days. Moreover, the

closer is the autogenous shrinkage curve to another of drying condition, the more similar is the sample inner RH to the one which characterizes that environment.

4.1.2.6 *Complete shrinkage evolution*

All the shrinkage investigations done on the mixtures are summarized in Figure 30. These global graphs represent the shrinkage evolution in a real element which is casted in the molds, covered by plastic sheets to assure wet maturation, demolded after 24 hours and exposed to environments with different RH conditions. Moreover, considering an element cross section of big dimensions, two parts are created: an outer layer which is influenced by the external environment condition and undergo drying shrinkage and an inner part in which the external air can't get inside, remaining under autogenous condition. Each of these real situations are simulated by the previous test and summarized in the figures below.

The lowest shrinkage amount was showed by MIX, which has a higher autogenous shrinkage in the first 24 hours compared to PC but a smaller evolution hereafter which compensates the initial deformation. CSA expressed the highest global shrinkage, especially thanks to its autogenous deformation before demolding, which is by itself higher than the deformation expressed from 1 to 182 days.

If, on one hand, the total shrinkage evolution from the setting on is important to evaluate the total deformation in a particular condition, on the other hand also the relation between autogenous and drying shrinkage is fundamental to evaluate the stress level inside the matrix. While the autogenous condition before demolding involves the whole specimen volume, redistributing this deformation equally all over the microstructure (unless some constrain is present), the autogenous deformation expressed after demolding represents only the inner part of the specimen. On the specimen surface the conditions are defined by the external environment, thus there will be two different situations in the same specimen and the final stress state will be defined by a correlation between them.

Considering what is said above, CSA can be problematic especially for the total amount of shrinkage expressed until 182 days (over 1600 μm/m for RH condition below 70%) while PC can have strong internal stress conditions due to the difference between deformation on the outer layer and the inner part of the sample (from 1000 to 600 μm/m for 36 and 70 RH respectively). The blend system MIX showed the best compromise

between initial shrinkage and difference between inner and outer layer deformation, leading to the lowest expected stress situation.

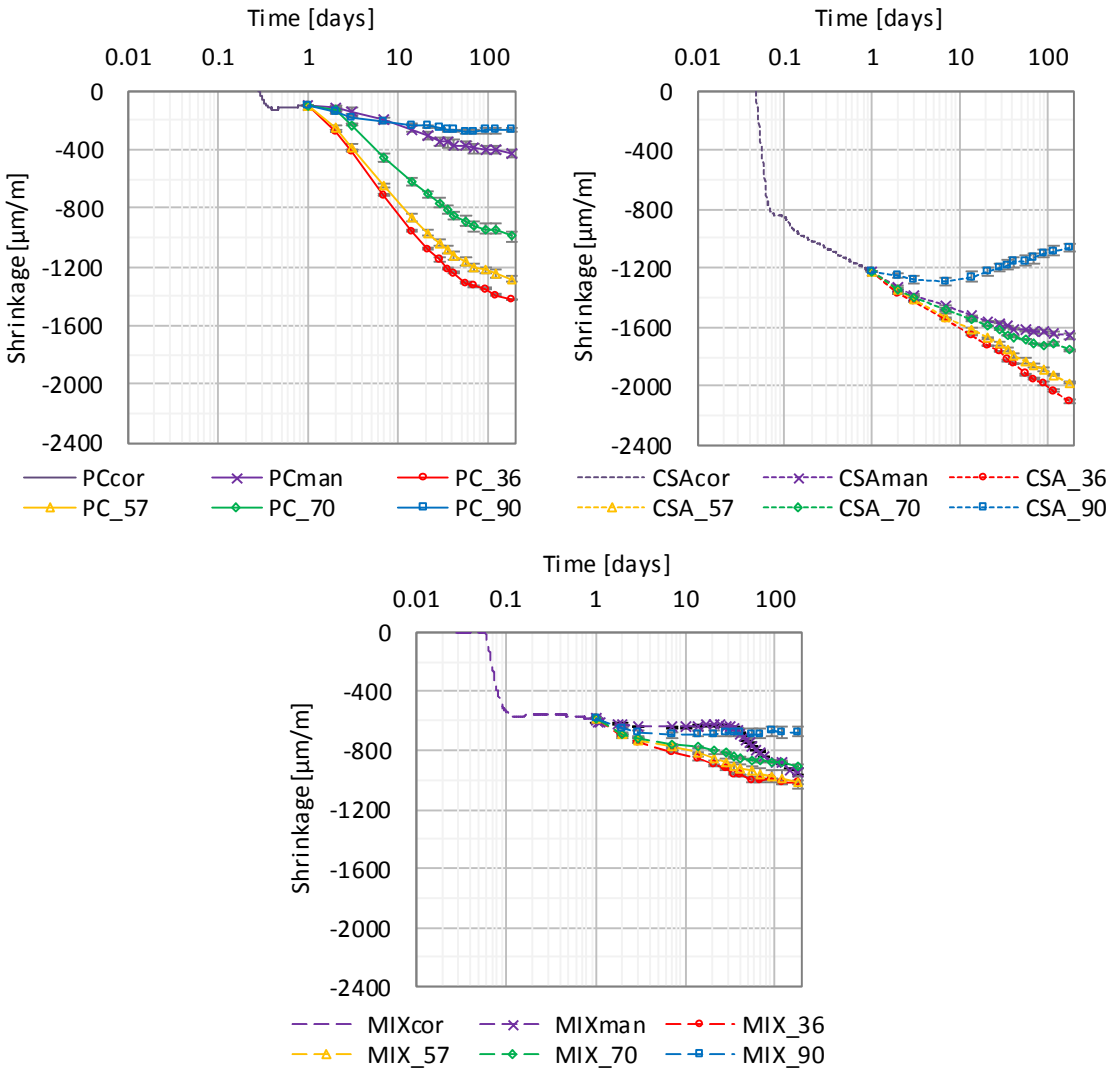

Figure 30 – Composition of autogenous and drying shrinkage at different RH after setting, considering a demolding time of 24 hours for the three investigated mortars

4.1.2.7 *Basic creep*

Figure 31 shows the evolution of the basic creep of the three mixtures. Results are reported in terms of the creep coefficient (a) and compliance function (b), with the latter taking into account the different compressive strength of the mixtures through the different stress levels to which they are loaded. In this way, the collected deformations are comparable with each other. Even though they represent the results in terms of different aspects, the mixtures trend in both graphs are similar. CSA showed higher values

for its investigated time. Compared to PC and MIX it expressed around five and two times their values respectively after 28 days. Considering MIX, it showed the smaller creep deformation. After 182 days it expressed a creep deformation that was nearly equal to the elastic deformation (φ=1.07). Moreover, for each MPa loaded on the sample, MIX deformed 46.4 με compared to PC which deformed 84.9 με after 182 days.

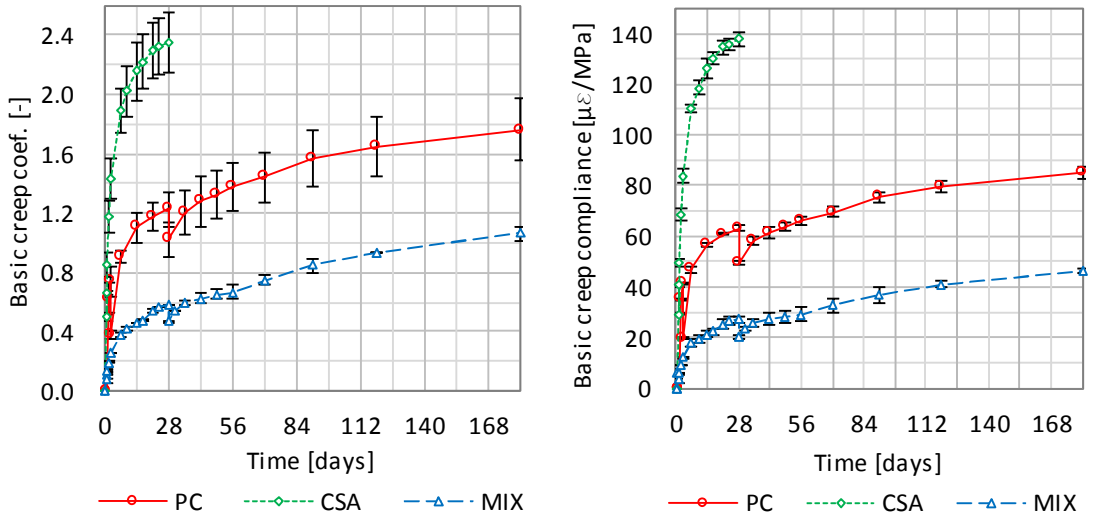

Figure 31 – Basic creep coefficient (a) and basic creep compliance (b) for the three investigated mortars

These results could be seen as the summary of the investigations described above since they combine a strain due to a stress. The pure CSA mixture showed a strong tendency to deform under load, while MIX did not. Probably the stress imposed by the load change the water redistribution inside the matrix, influencing all the deformation processes based on it [79]. High creep values are suitable for reinforced elements because they lead to a relaxation effect which decrease the stress accumulated around the reinforcement due to the shrinkage. A good example in this way is represented by CSA, where the initial high autogenous shrinkage lead to the formation of high stress areas around the steel bars, where the deformation is hindered. Even if the tensile strength is fast developed in CSA, it may be not enough to stand such stress. However, the strong tendency to deform under load creates a relaxation effect which decrease the stress, lowering the probability of cracks formation. However, high deformative elements could be detrimental for the linearity of a structure. In this case, MIX represents a dimensionally stable material,

suitable for structure in which the deflection must be limited, like bridges sections or beams of particular aesthetical importance.

4.2 Concrete

4.2.1 STRENGTH CHARACTERIZATION

For the strength characterization campaign on concrete a complete investigation was organized for the compressive strength definition. All the six mixtures were considered from the very early age (first moment after setting in which the test could be done) until one year. For the other tests, only two deadlines were considered, one for the early age properties characterization (24 hours) and one for the later age properties (28 days, the usual reference used in the main technical documents). The stress-strain diagram test in compression was investigated for the three main mixtures PC, CSA and MIX for the only 28 days deadline.

4.2.1.1 *Compressive strength*

The compressive strength development is reported in Figure 32 for the general trend until 360 days. The same results are reported in Table 5 in terms of percentages evolution compared to the 24^{th} hours and 28^{th} days values. In general, the systems based on pure CSA react faster, showing the first results already after 4 hours, while the blended systems followed at 8 hours with a mixture (MIX I) which delayed until 16 hours, time at which also PC started to show the first strength evolution. In terms of early age strength development, after 24 hours mixtures had 71.86, 78.91, 68.68, 58.21, 68.42 and 51.40% of the 28^{th} days values for CSA, CSA I, MIX, MIX I, MIX II and PC respectively. After 28 days pure CSA mixtures showed the highest compressive strength values, followed by MIX and PC which recovered the initial gap and, at lower level, MIX I and MIX II. However, in later age the blended mixtures showed an interesting feature. Compared to the other mixtures, blends evolved more compressive strength, improving the 28^{th} days values of 35.1, 46.48 and 28.35 % at 360 days, compared to the 10.24, 19.71 and 21.86% of CSA, CSA I and PC. After one year, MIX reached the highest compressive strength value.

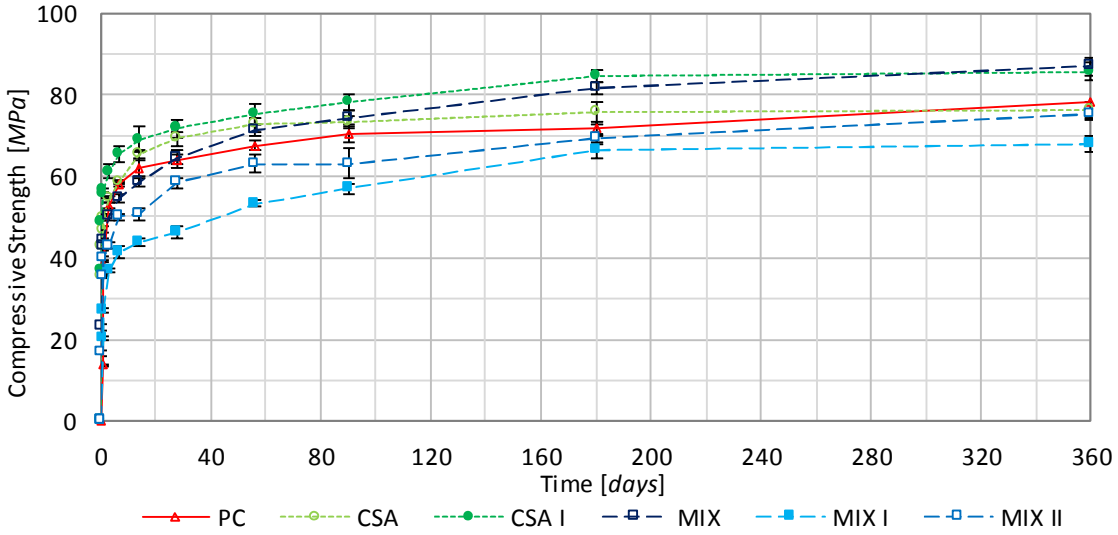

Figure 32 – Compressive strength evolution until 360 days

Table 5 – Compressive strength results

Deadlines		4	8	16	24	7	28	56	90	180	360
		[hours]				[days]					
MIX	MPa	0	23.12	43.08	44.20	54.72	64.36	71.28	74.45	81.74	86.95
	%*	0	52.3	97.5	**100**	123.8	145.6	161.3	168.4	184.9	196.7
	%**	0	35.9	66.9	68.7	85.0	**100**	110.7	115.7	127	135.1
MIX I	MPa	0	0	20.13	27.06	41.37	46.49	53.33	56.94	66.27	68.1
	%*	0	0	74.39	**100**	152.9	171.8	197.1	210.4	244.9	251.7
	%**	0	0	43.3	58.21	88.99	**100**	114.7	122.5	142.5	146.5
MIX II	MPa	0	16.7	35.75	40.02	50.13	58.49	63.25	63.18	69.27	75.07
	%*	0	41.73	89.33	**100**	125.3	146.1	158.0	157.9	173.1	187.6
	%**	0	28.55	61.12	68.42	85.71	**100**	108.1	108.0	118.4	128.3
CSA	MPa	35.42	43.07	47.05	49.77	58.55	69.26	72.59	73.18	75.57	76.35
	%*	71.2	86.5	94.5	**100**	117.6	139.2	145.8	147.0	151.8	153.4
	%**	51.1	62.2	67.9	71.8	84.5	**100**	104.8	105.7	109.1	110.2
CSA I	MPa	36.88	48.61	55.44	56.54	65.43	71.65	75.29	78.19	84.69	85.77
	%*	65.23	85.98	98.06	**100**	115.7	126.7	133.2	138.3	149.8	151.7
	%**	51.47	67.84	77.38	78.91	91.32	**100**	105.1	109.1	118.2	119.7
OPC	MPa	0	0	13.73	33.00	58.27	64.20	67.5	70.3	71.6	78.23
	%*	0	0	41.62	**100**	176.6	194.5	204.5	213.0	217.0	237.1
	%**	0	0	21.39	51.40	90.76	**100**	105.1	109.5	111.5	121.9

%* represent the relative percentage of compressive strength compared to 24 hours value

%** represent the relative percentage of compressive strength compared to 28 days value

Blend systems demonstrate to be suitable for structural application in terms of compressive strength. Compared to PC, they react faster, reaching good performance in less than 24 hours and, compared to CSA, they continue to evolve at a higher ratio after 28 days. In both early and later ages they expressed good performance; thus, they are suitable for several different structural applications. Alaoui [45] studied a binary concrete

system of sulfoaluminate clinker and gypsum in terms of compressive strength. The obtained results confirmed their very good strength at early ages, which made it possible to consider them in applications like prefabrication or quick demolding. It attests a general high strength for all classical applications and good long term resistances. Su et al. worked on CSA long term performance [100]; their investigation analyzed the compressive strength evolution until 6 years. They found that strength develops rapidly and continues to improve with age. Effective is the fact that in concrete structures built in China since 1970's no accidents are attributed to decrease in strength or other instabilities.

4.2.1.2 *Flexural strength, splitting tensile strength and modulus of elasticity*

The results in terms of flexural and splitting tensile strength are reported in Figure 33 (a-b). As reported in the literature [89], results coming from the splitting test have a closer correlation to the tensile strength of the material compared to flexural data, giving an initial idea of the behavior in tension of those materials. Mixtures based on pure CSA showed higher values after 24 hours and a good evolution until 28 days in both tests. PC showed similar results to MIX after 24 hours but it expressed a much higher evolution until 28 days. The two remaining blended mixtures are lower in performance compared to the other mixtures. Concrete blend systems results are in agreement with the assumption done on mortars of the stable period between 24 hours and 28 days for the flexural strength. However, as reported by Zhang [100], there is a strong relation between compressive strength evolution and the elastic modulus, splitting strength and flexural strength; thus, improvements are expected on later ages for these aspects.

In terms of modulus of elasticity, results are reported in Figure 33 (c). PC showed the highest values in terms of dynamic modulus of elasticity while CSA was the more performant in the static set-up. Blends showed less values in both early and later ages, in particularly in the static set-up. Considering the evolution in time of these aspects, a general increase of 6% was recorded in the dynamic values, with the exception of PC which increases of 10% between 24 hours and 28 days. In the static set-up the situation is different, with PC, CSA and MIX that improved of around 10% and the other less than 5%. Another interesting aspect is the difference between static and dynamic values reported in Figure 34. Blends and PC behaved similarly, with a difference of about 10%, while pure CSA mixtures expressed a much lower difference of about 5%.

As the modulus of elasticity represents the capacity of the material to deform under a unit load in the elastic field, MIX showed the highest elastic deformation while CSA the highest stiffness. One of the situation in which this parameter become important is with composed materials. The one with higher modulus of elasticity will deform less, thus, it will adsorb more load than the other with low modulus of elasticity. These materials require a specific design which takes into account their different stiffness in order to control the stress redistribution, like in reinforced concrete elements. Moreover, the material modulus of elasticity composes the element stiffness in the dynamic structural analysis (flexural stiffness "EJ"), defining the entire structure force redistribution.

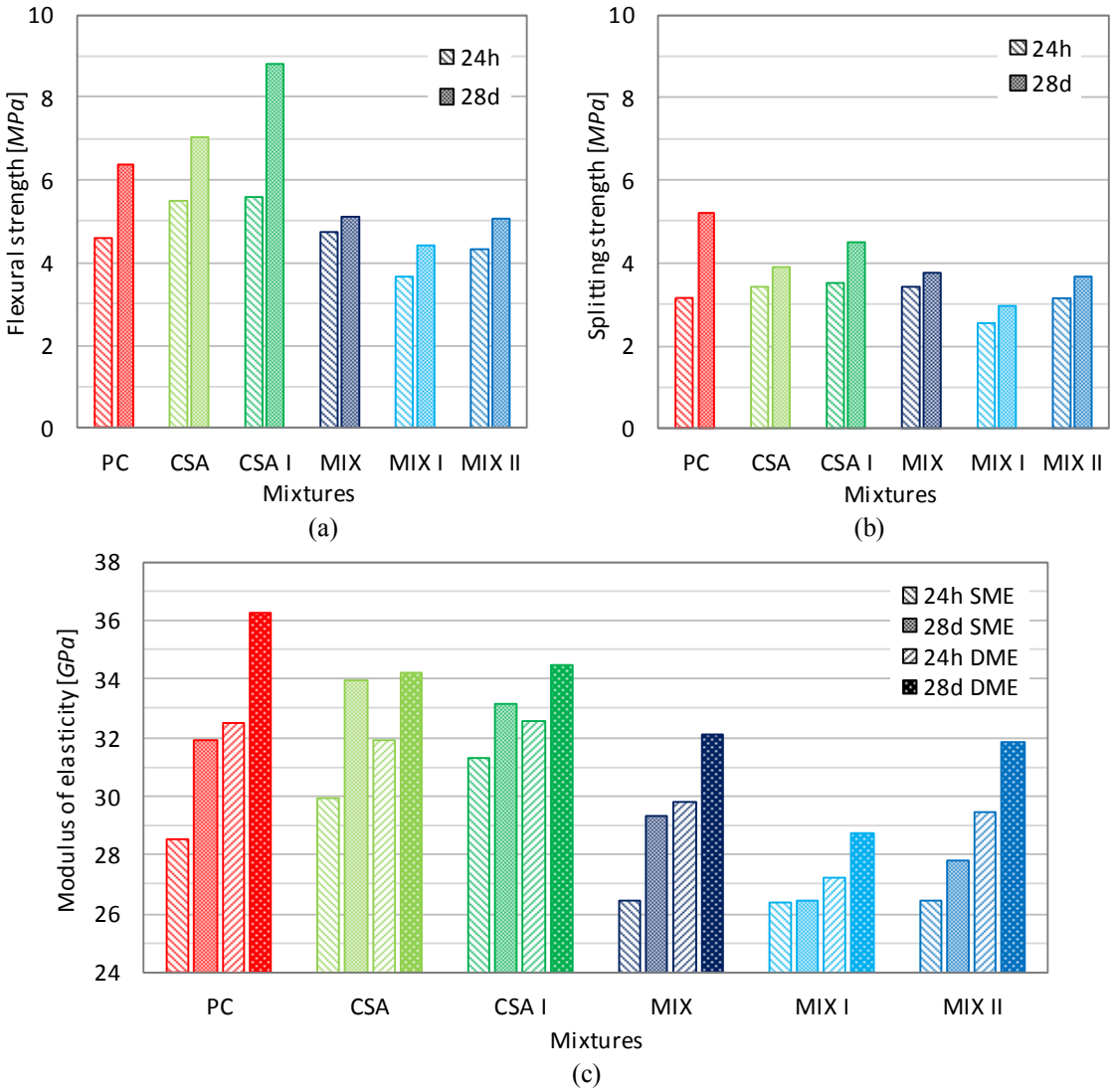

Figure 33 – Results in terms of flexural strength (a), splitting tensile strength (b) and modulus of elasticity in both static (SME) and dynamic (DME) condition (c)

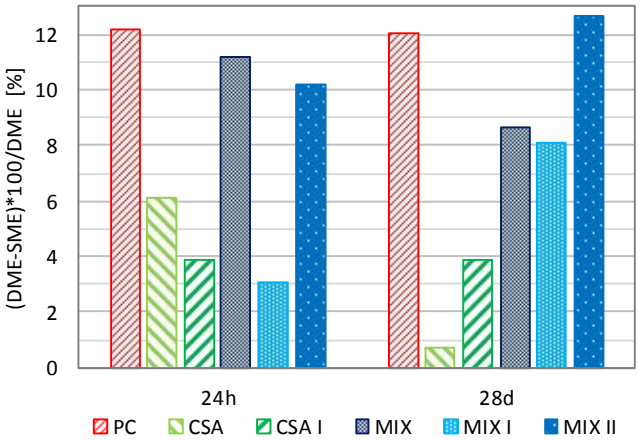

Figure 34 – Percentages difference between dynamic and static modulus of elasticity using the former as base of calculation

4.2.1.3 *Stress-strain diagrams in compression*

The stress-strain behavior (in compression) was determined according to an internal procedure at 28 days; the results are shown in Figure 35. Due to the different compressive strength reached for each mixture at the peak point (a), the data were represented even after normalization (b). This procedure consists in drawing the stress data in terms of f*c/fc where f*c and fc represent the peak and the general stress respectively. The same procedure was followed for the strain normalization. By the resulted graph, it is easier to compare different mixtures, especially in terms of dissipated energy (area enclosed under the curve).

While PC and MIX showed a similar initial branch evolution, CSA shifted apart because of its higher stiffness. The stress peaks were reached at a deformation level of 2.48, 2.69 and 2.73‰ for MIX, CSA and PC respectively. By the post-peak analysis, CSA and MIX showed a fragile behavior, losing quickly their capacity to bear the stress. On the contrary, PC showed a flat peak with a gradual decrease of the stress. This is underlined in (b) where PC represents the curve related with the higher dissipative capacity, identified by the higher area beneath its curve.

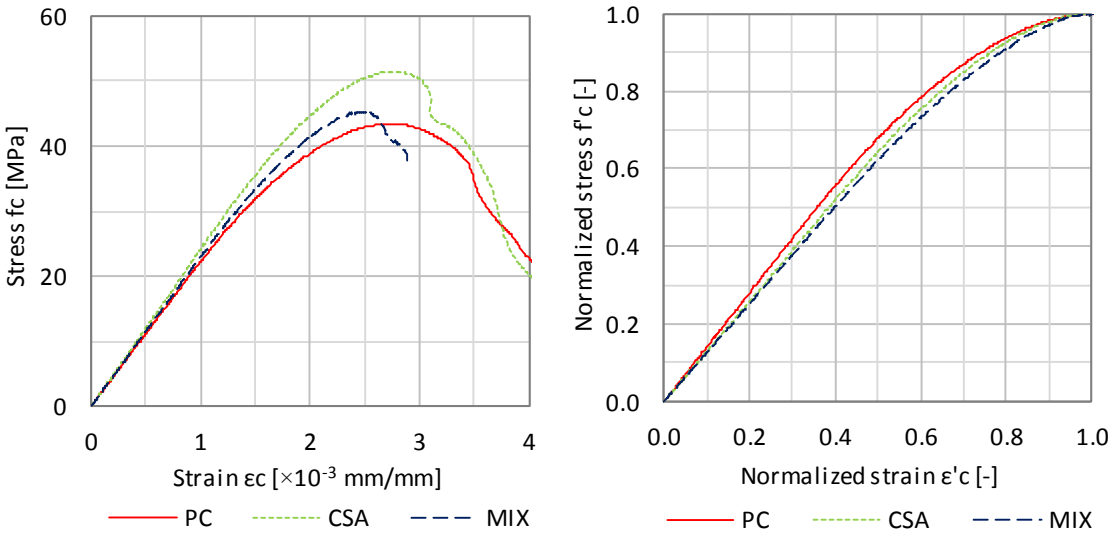

(a) (b)

Figure 35 – Stress strain diagrams in compression for the three main mixtures (a) and their normalized representation (b).

4.2.2 DIMENSIONAL STABILITY

As seen in paragraph 4.1.2, the deformative characterization is not immediate. Several aspects are involved in its description and even more different conditions can vary its global trend. Moreover, the higher aggregates dimensions used to produce concrete can vary the expectations built on the mortar results. Considering these complications, three different campaigns were organized to investigate the deformative features of the studied mixtures. The first is identified by the simple name of the considered mixtures, the second by one apex and the third by two (MIX, MIX', MIX''). One was organized to define the drying shrinkage of all the 6 mixtures, in order to have a first idea on their deformation and their relation. Only one environmental condition was considered with a higher number of samples in order to have a statistical reference. Another campaign was organized to study the relation between autogenous and drying shrinkage. The two most representative mixtures were chosen and the same drying condition were followed as in the first campaign, in order to have a comparison between the two campaigns. Last but not least, the third campaign was organized to study the creep evolution of the three main mixtures. In order to obtain the creep deformation, the shrinkage evolution is required. Hence, in the final campaign drying and autogenous shrinkage were described again and the creep under sealed and drying conditions defined. Even if this last campaign was built on the creep definition, it can be seen as a summary of the previous deformative investigations.

4.2.2.1 *Autogenous shrinkage*

Figure 36 reports the autogenous shrinkage evolution for the CSA based concrete mixtures studied in the second and third campaign. The two campaigns differ by the initial time at which the test started. In the first campaign the investigation started after 8 hours for both CSA' and MIX' while in the third campaign the two mixtures were firstly measured after 24 hours. MIX evolution was not influenced by this initial gap, showing similar evolution in both campaigns. On the contrary, CSA' shrunk around 350 μm/m more when demolded just after 8 hours. Considering the general trend, as seen in the mortar campaign, also the concrete mixture MIX in sealed condition showed the same initial instable evolution. It initially shrunk until 14 days, time at which it started to expand, reaching a plateau after 28 days and restarting to shrink at 44 days. CSA was

characterized by an initial fast shrink phase which slowed down after 28 days, continuing shrinking hereafter at a slower ratio. Results after 364 days for the second campaign were quite the same for both mixtures, reaching around 200-250 µm/m. For the first campaign was not the same, underlining the huge importance in CSA systems of the demolding time for a complete autogenous shrinkage investigation. These results are in agreement with the one collected with automatic set-up in the mortar campaign, reported in paragraph 4.1.2.2. Unlike the drying shrinkage, which happens just after demolding, autogenous shrinkage become at the moment of setting The closer is the initial investigation to that moment, the higher the considered portion of the autogenous shrinkage evolution. Thus, low autogenous shrinkage does not mean a correspondent low probability of cracks appearance. It depends on the time at which the measurements start, especially with rapid hardening systems as CSA.

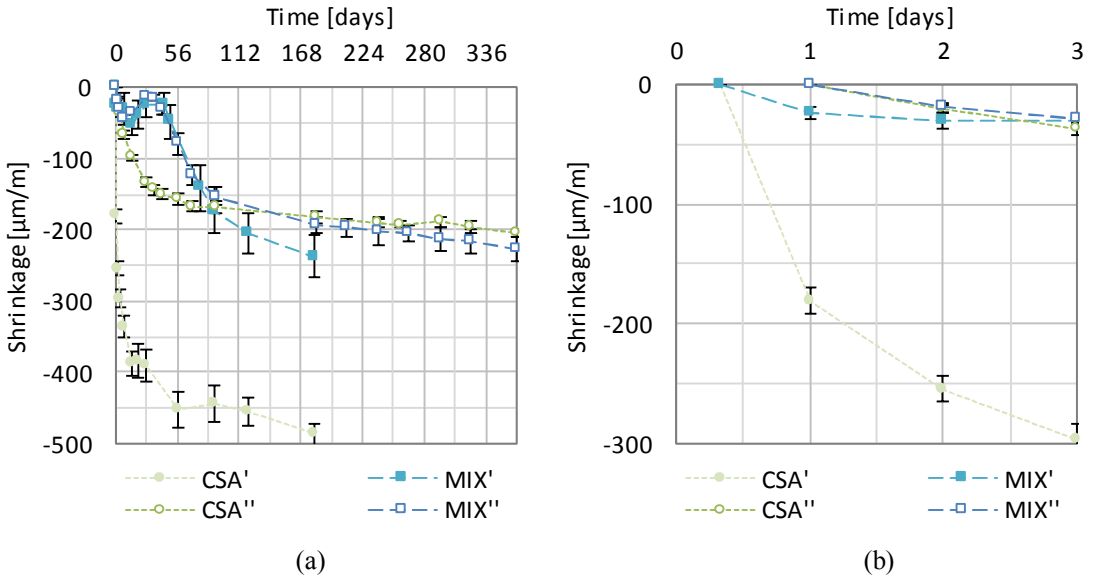

Figure 36 – Autogenous shrinkage comparison between results from the second and the third campaign in both early (b) and later age (a)

4.2.2.2 *Mass change*

The mass change in time for the first campaign is reported in Figure 37, while a comparison between the two chosen mixtures of the campaign two and the same mixtures of campaign one is reported in Figure 38. Blends lost much more water compared to the other mixtures, reaching around -33, -30 and -25‰ of their weight until 364 days. PC lost more water than CSA mixtures, though is closer to them than to MIX. Comparing the

results of the two campaigns, no particular differences are evidenced. Considering MIX, even though the demolding time had a difference of 8 hours between the two campaigns, just a difference of 3‰ was recorded after 182 days.

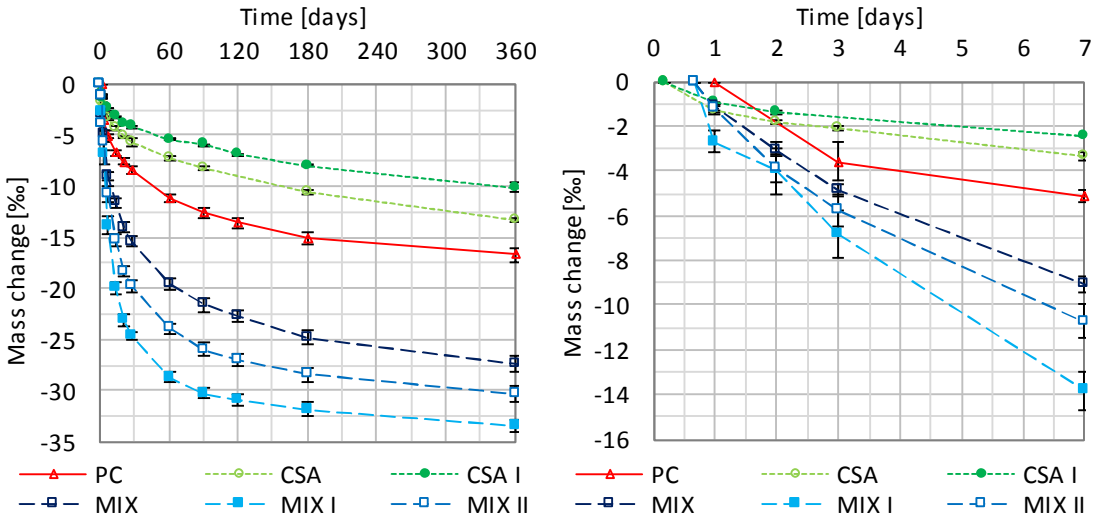

Figure 37 – Mass change until 1 year in the early (b) and later age (a) for the first campaign

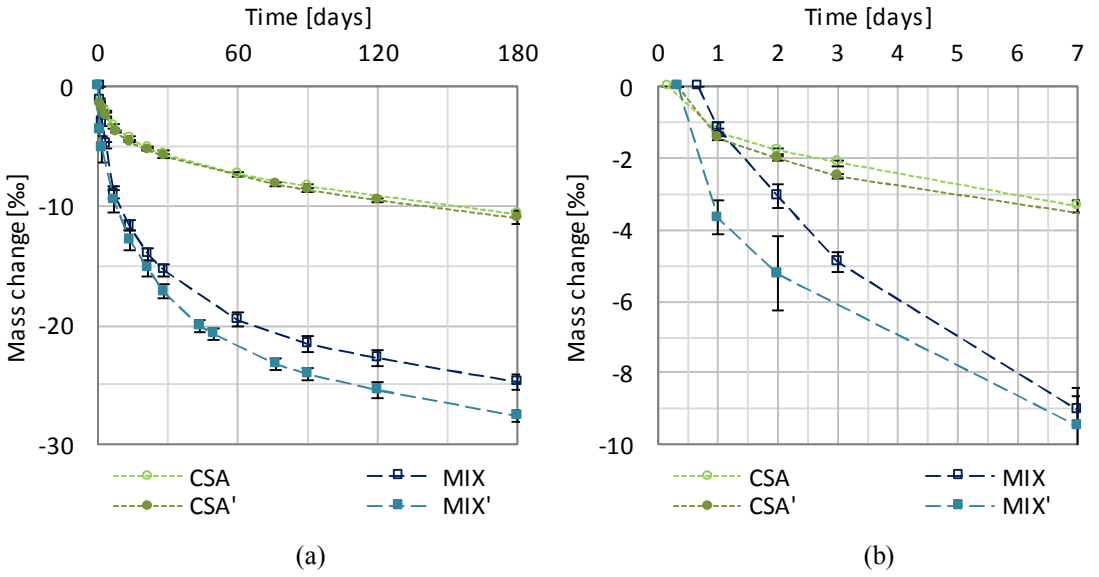

Figure 38 – Mass change comparison between results from the first and second campaign in both early (b) and later age (b)

These results are in good accordance with the one collected in the mortar campaign; then, the previous assumptions are valid even for these results. Blend systems are probably characterized by a well-connected microstructure with pores of big dimensions, which

allow water to evaporate to the external environment. On the contrary, pure CSA systems seem to be characterized by a dense microstructure with hindered areas where water is not allowed to get outside easily.

4.2.2.3 *Drying shrinkage*

This aspect was the most studied, being investigated three times. Results for the first campaign are shown in Figure 39, while a comparison between results of the three campaigns is reported in Figure 40. CSA and PC followed the same evolution for the first 28 days, reaching around 380 μm/m while blends were around 110 μm/m at that deadline. Hereafter, CSA slowed down similarly to blends but more than PC, expressing until 360 days other 120 μm/m compared to the 70 and 250 μm/m of blends and PC respectively. After 180 days each mixture reached a trend which was close to a plateau.

In the comparison graph proposed in Figure 40 only the three main mixtures are showed. A clarification is required: the third campaign was developed in similar but not equal environmental conditions with RH of 57% instead of 50%. Considering that, MIX followed the same trend in each campaign, with a slightly lower shrinkage for MIX'' probably due to the higher RH condition. On the contrary, CSA of the first and second campaign followed the same trend and showed similar results while CSA of the third campaign expressed much lower results compared to them. In this system, the effect of the demolding time is strong and it is perfectly explained by the smaller results of CSA'' demolded after 24 hours compared to the 4 and 8 hours of the first and second campaign respectively. This difference in demolding time do not influence the part due to drying, but the autogenous one. As the concrete samples have a big cross section, they are characterized by an external layer which is under drying conditions and an internal under autogenous condition. Thus, there is always a part which is governed by autogenous condition even in drying shrinkage test, especially for samples with big cross section dimensions. As the CSA autogenous shrinkage is high, especially in the very early age, this delay in demolding led to a smaller autogenous part involved in the measurement, then, in a smaller global shrinkage. PC samples in both campaign followed the same evolution, with a small difference of 50 μm/m after 360 days, probably due to the slightly higher RH condition.

In cementitious systems characterized by an important self-desiccation, drying shrinkage curves cannot be considered without an evaluation of the correspondent evolution in autogenous condition. As reported in Figure 40, CSA and PC have a similar drying shrinkage evolution; however, anticipating the demolding time would strongly enhance CSA, because of the high contribution of autogenous shrinkage, while PC would be just slightly influenced.

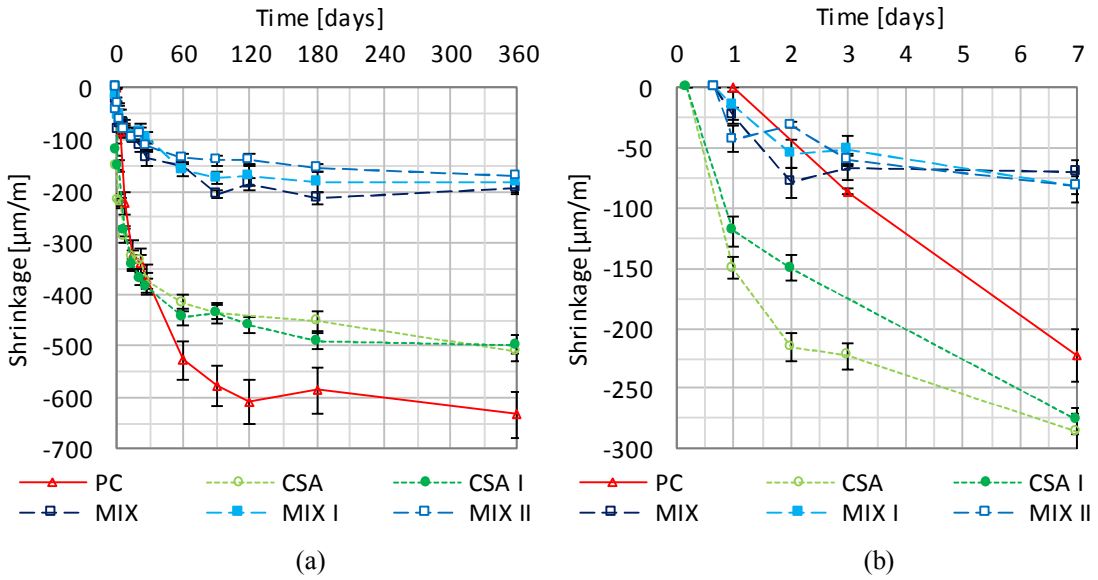

Figure 39 – Drying shrinkage evolution at early age (b) until 1 year (a) for the first campaign mixtures

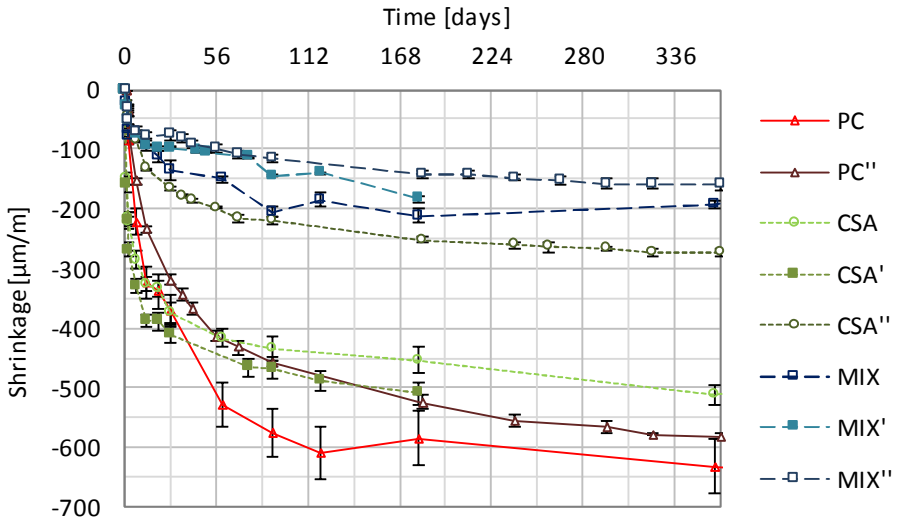

Figure 40 – Drying shrinkage evolution until 1 year for all the three campaign mixtures

4.2.2.4 *Comparison between autogenous and drying condition*

Results of shrinkage under both autogenous and drying conditions are reported in Figure 41, for the second (a) and third campaign (b). The relation between autogenous and drying evolution underlines the difference between the investigated systems.

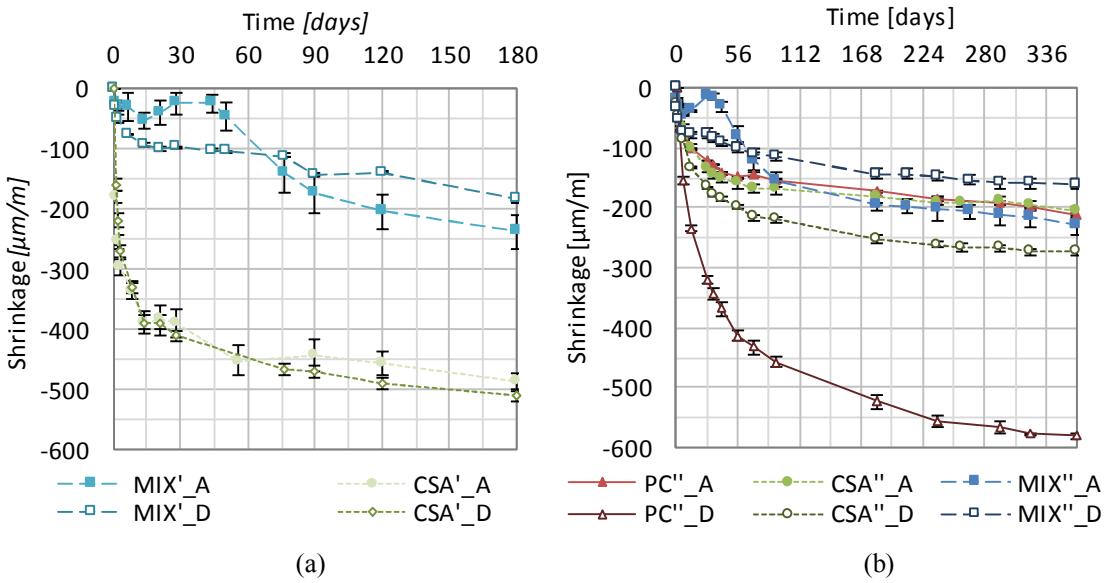

Figure 41 – Relation between autogenous and drying shrinkage in the second (a) and third campaign (b)

Considering PC'' evolution, in drying condition it showed the highest value while in autogenous condition it shrunk similarly to the other mixtures. The most important aspect to be highlighted here is the difference between these two conditions, which in case of PC'' was the highest. After 364 days was 360, 70 and -70 µm/m for PC'', CSA'' and MIX'' respectively. While PC'' had the highest difference from drying to autogenous condition, CSA'' showed the lowest, underlining its sensibility to autogenous deformation instead of losing water from the outer layer. A particular case was recorded in MIX'' where, after 60 days, the sealed samples shrunk more than the drying. It was not an error reports in negative the difference between the two conditions. This inverse tendency represents a strong modification in the microstructure which occurs during hydration. This change in the inner structure can be attributed to the water availability thanks to the sealed condition. This water can be used by the cement to create different hydration products than in drying condition, where the mass change investigation also attested a huge loss of water during time for blends. This particular trend was confirmed by the other campaigns, which developed the same crossing trend for MIX'. In the case

of CSA', the values are higher due to the earlier demolding time, but the trend respects what said before on the small difference between drying and autogenous evolutions.

4.2.2.5 *Creep*

Figure 42 shows the creep compliance evolution of the three investigated mixtures. Results for both autogenous and drying conditions are reported in terms of the compliance function, which took into account the different compressive strength of the mixtures through the different stress levels to which they were loaded. In this way, the collected deformations are comparable with each other. PC showed higher drying creep compliance compared to CSA and MIX. After 182 days, the compliance was 78, 54 and 36 $\mu\varepsilon/MPa$ for PC, CSA and MIX respectively, with PC still growing while the others were close to a plateau. A different situation was shown in basic creep, where the samples were sealed. Compared to the drying creep, PC and CSA showed similar trends with lower values. On the contrary, in MIX the creep compliance in sealed conditions became higher than under drying conditions already at the second but especially after the third loading step at 28 days, becoming the highest compared to the other mixtures after 90 days. Values of the coefficient at 182 days were 49, 41 and 55 $\mu\varepsilon/MPa$ for PC, CSA and MIX, respectively. While PC and CSA evolved at a slow ratio after 182 days, MIX continues to increase at a high ratio, giving the idea of a microstructure strongly influenced by sealed condition.

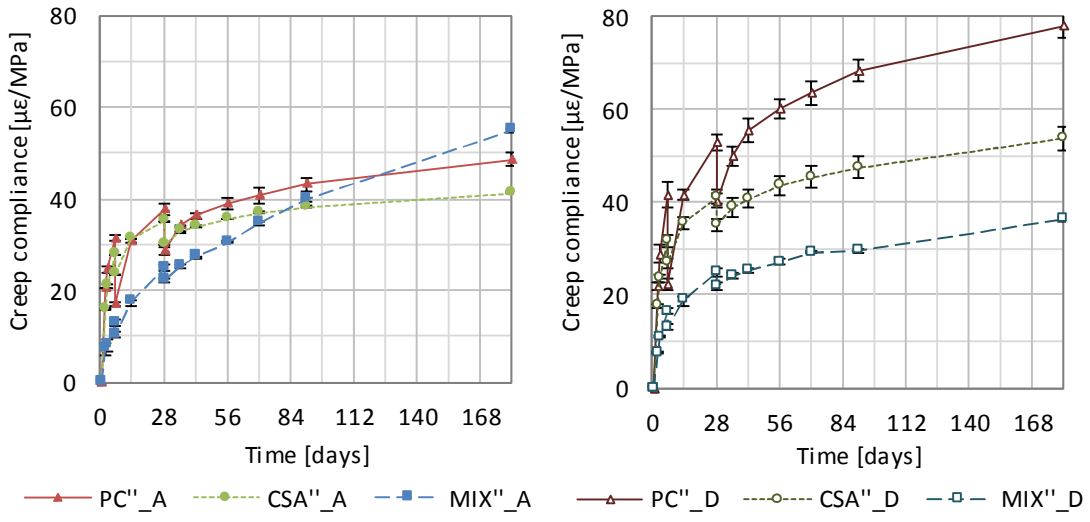

Figure 42 – Third campaign basic (a) and drying creep compliance (b) for the three investigated mixtures

The considerations on the relation between the evolution in drying and autogenous condition taken in paragraph 4.2.2.4 are suitable even for creep test. In this case, inversion between autogenous and drying curve for MIX seems to be enhanced by the applied load. Unlike base creep results on mortar, CSA concrete deform similarly to PC. This is probably due to the different initial demolding time, which was 8 hours for CSA mortar and 24 hours for concrete mixtures. As said before, for CSA autogenous condition the demolding time is fundamental in the definition of the total strain amount expressed. Another aspect which is different form the mortar campaign is the MIX evolution. In concrete scale the trend is completely different from PC, while in mortar campaign was the same just with a lower entity. While in mortar the plateau from 1 to 28 days evidenced by MIX seems to be completely adsorbed from the matrix at later age, in concrete scale this plateau leaves an effect which remain visible in the performance. However, this effect did not affect the compressive strength in later age (which even increase in time) and did not show any particular results in later age shrinkage evolution. Thus, this effect is assumed to be not detrimental for the inner structure of the material.

4.2.3 CONSTITUTIVE LAWS EVALUATION

The mechanical characterization carried out in the present research was aimed at describing the most important constitutive laws on which the studied mixtures are based and evaluating their correspondence to the already known Portland laws. This passage is fundamental for designers because a good accordance between the behaviour of the new systems based on CSA with systems based on Portland can lead to the use of the already known design formulas with, at most, the addition of some corrective coefficient. These formulas are usually defined by the characteristic or mean compressive strength, thus, by one parameter the most representative material properties would be defined. Since the comparison is based on standard formulas, the test values are considered at 28 days.

4.2.3.1 *Tensile strength*

In this paragraph, the results obtained during the investigation of flexural strength and splitting tensile strength are transformed into mean tensile strength values by literature Portland equations and evaluated with the describing function of the Portland tensile strength, obtained by mean of compressive strength values. This relation can be helpful in defining a first range of accuracy between the new systems and Portland.

Data are reported in Figure 43; blends and pure CSA systems gave results which are in good accordance with the tensile strength constitutive law. Moreover, the only point that felt outside the reliability range was the splitting tensile strength of Portland, underlining that this range is not absolute but mostly an indication.

In blend systems, the tensile strength derived by the flexural test was always lower than that derived by splitting. On the contrary, in pure CSA systems is equal or even higher. PC followed the same trend of the blends with a higher difference between the two aspects.

As the splitting results were transformed into tensile strength by a coefficient "$\alpha_{sp} = 2.08 \cdot (f_{cm})^{-0.16}$" which was function of the mean compressive strength, another comparison study was proposed. The function which describes this coefficient was compared to its singular values which were obtained as the ratio between mean tensile strength, resulted from the standard formula using the compressive strength obtained by the test, and splitting tensile strength collected by the test. Results showed a good

accordance between the function and the results, especially for the blends and the pure CSA systems. Again, the farthest point was the one describing the PC results.

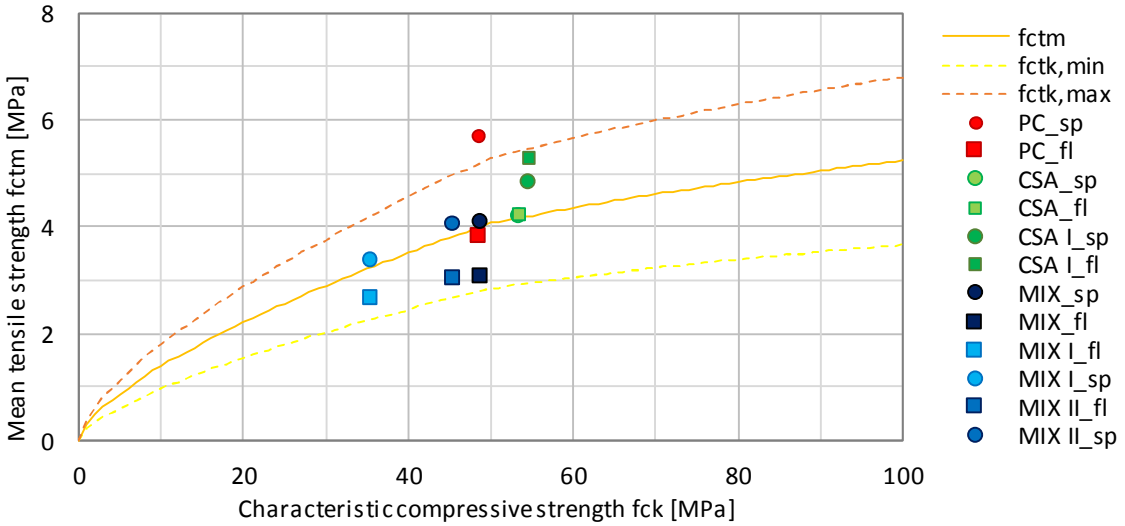

Figure 43 – Comparison between tensile strength directly calculated from standards and indirectly obtained from test.

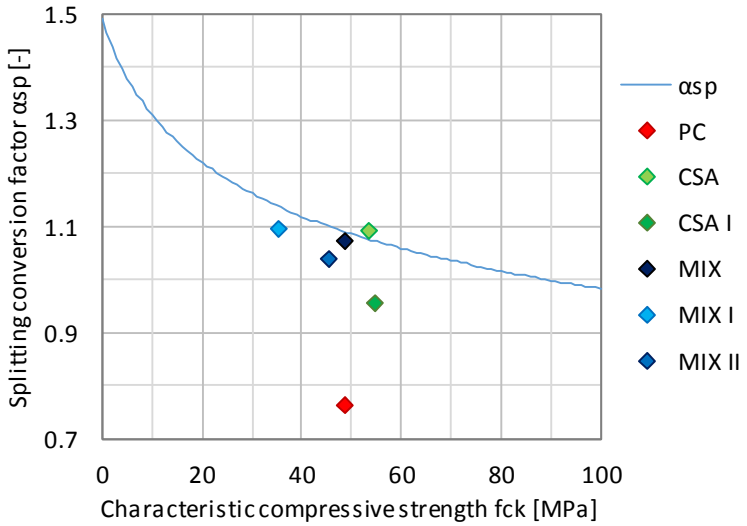

Figure 44 – Splitting conversion factor of the investigated mixtures.

4.2.3.2 *Modulus of elasticity*

Like in paragraph 4.2.3.1, another comparison is proposed here, based in this case on the modulus of elasticity calculation. Figure 45 reports the standard function of the static and dynamic modulus of elasticity compared with the test values. In this case no modification was applied to the test values, thus the comparison is direct. Despite test results were

lower than the functions of about 5 GPa, their trend was rational. Static results were always lower than the dynamic ones and their evolution followed the function.

Standards report a coefficient to obtain the static modulus of elasticity from the dynamic one, which means that there is a relation between their values. This relation was considered and plotted in Figure 46, where the function and the results coming from the tests are reported. This relation turned out to be more precise than the one proposed in Figure 45. Values are close to the function and the farthest was again PC's.

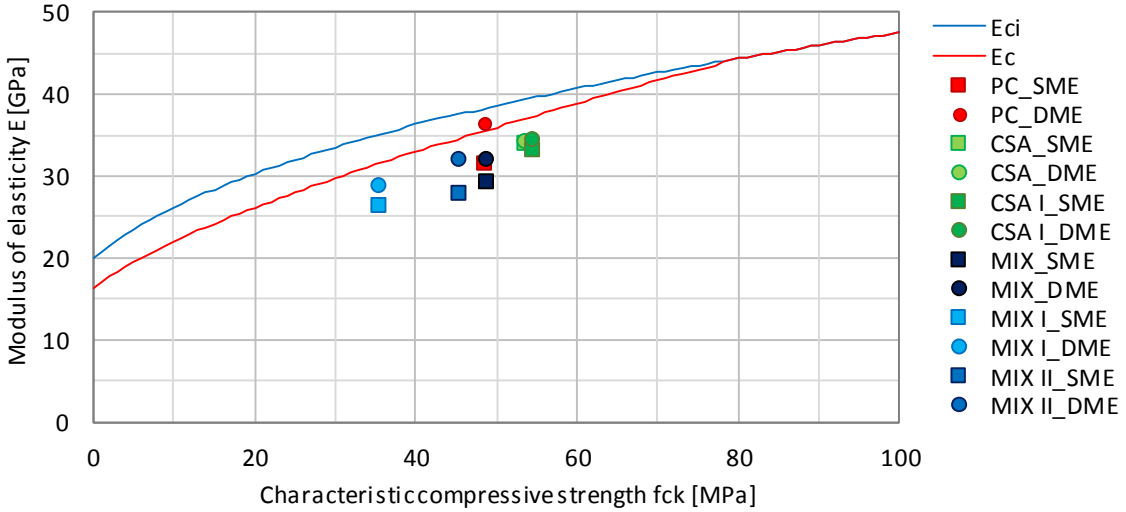

Figure 45 – Comparison between modulus of elasticity calculated from the standards and obtained from the test in both static and dynamic conditions

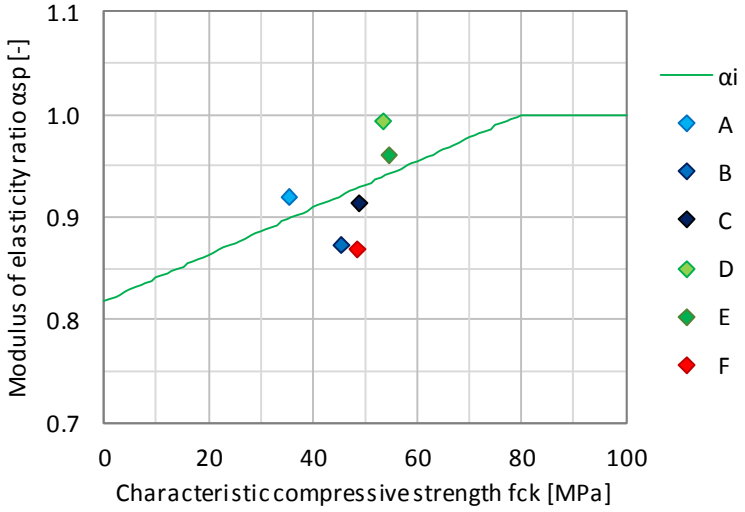

Figure 46 – Real and calculated ratio between static and dynamic modulus of elasticity

4.2.3.3 *Stress-strain diagram in compression*

The stress-strain diagram of the three main mixtures was used to study their compatibility with the most used stress-strain constitutive laws present in literature. The considered models were Kent & Park [91], Thorenfeldt (similar to the Mander model) [94], Carreira & Chu [95] and the one proposed by Model Code 2010 [89]. Their relation is reported in Figure 47. The stress was normalized in order to compare the different mixtures strength while the strain was not modified. By the results shown in the graphs, models like Thorenfeldt's and Carreira & Chu's are the best in fitting the curves. Considering the first branch, Carreira & Chu simulated the evolution of all the three mixtures quite perfectly while Thorenfeldt fitted PC but slightly shifted away in CSA and MIX. However, in the post-peak trend the model proposed by Thorenfeldt was more accurate than Carreira's, even though the post-peak was not the main aim of the research.

These results attest that the literature models for stress-strain diagrams are suitable not only for Portland but also for CSA based mixtures. The difference evidenced in some constitutive laws are the same in each considered mixture, confirming the good accordance between Portland and calcium sulfoaluminate constitutive laws.

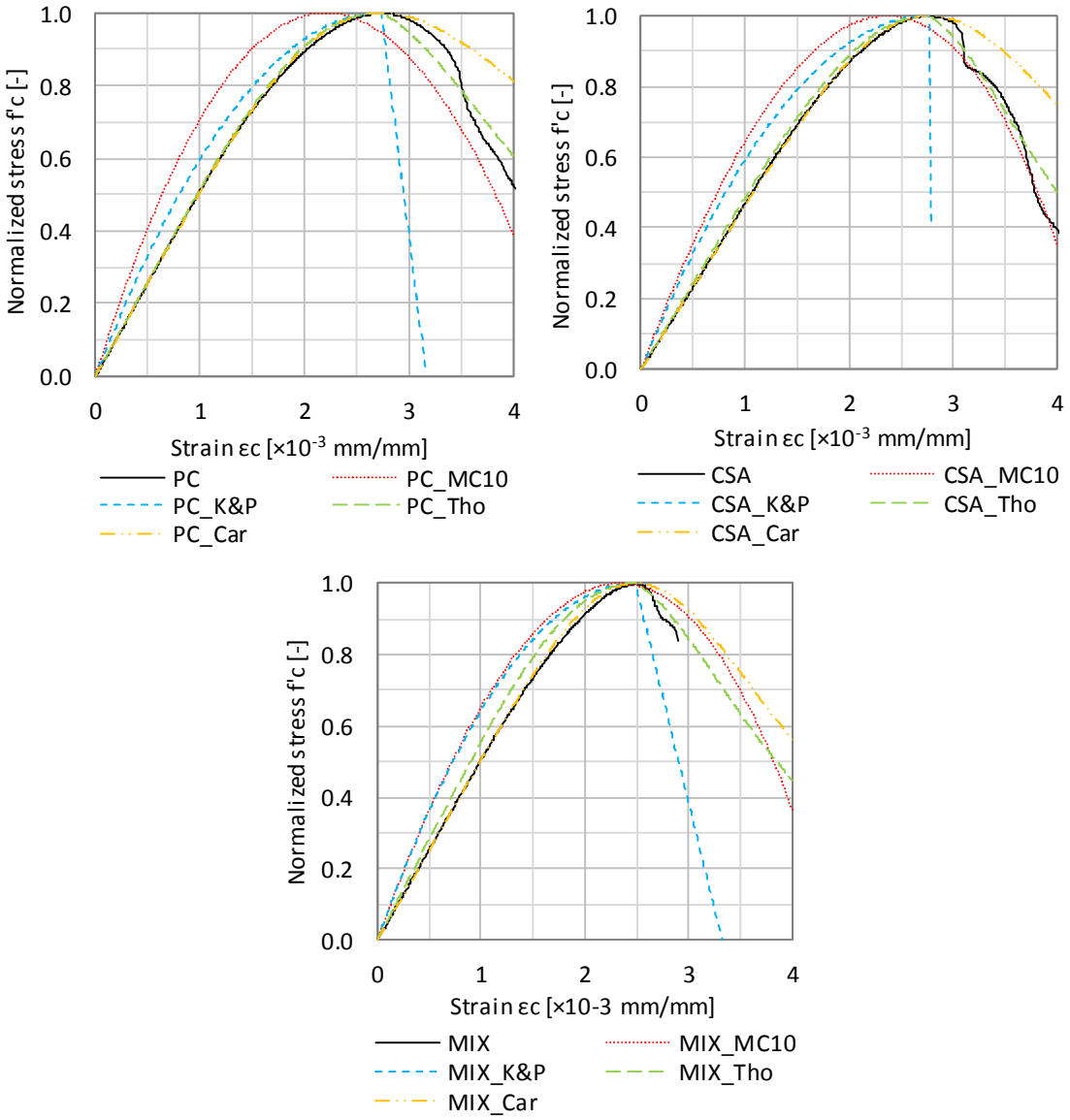

Figure 47 – Comparison between stress-strain diagrams as obtained from the test and their most common used literature description

5 CONCLUSIONS

In this research the mechanical performance of CSA based concrete mixtures was studied in order to evaluate their compatibility with the well-known Portland's constitutive laws. This evaluation was aimed at defining a first reference on which rely for the use of these new formulations in real structures, in particular for PC/CSA blends. These systems represented the most interesting solution for an industrial production and widespread distribution thanks to the combination of a lower cost compared to pure CSA systems, maintaining, nevertheless, a lower carbon footprint compared to Portland systems.

Three mixtures were initially defined in terms of performances; one representing the pure CSA system, one the Portland (CEM II-LL 42.5R) and one the blend of the two cement, mixed at a PC/CSA ratio of 50/50. These systems were initially studied on mortar scale in order to define their main aspects. Two major characteristics came out from this campaign. Compared to PC, CSA based mixtures were faster, showing higher performance at early age, and expressed lower shrinkage in time. However, even though the shrinkage of blends was smaller, a particular evolution was recorded in autogenous condition. From these considerations, the concrete campaign was defined. Three CSA based mixtures were added: one pure CSA and two blends at a PC/CSA ratio of 50/50 and 60/40. In this way, six concrete with different 24 hours strength class were defined.

In terms of mechanical performance, pure CSA systems showed the fastest reaction and the highest strength values in the early age, while PC reacted later but expressed the highest evolution between 24 hours and 28 days. Even though blends showed a faster reaction than PC, they evolved slightly smaller performance before 28 days. However, the long term results in the compressive strength test attested the highest evolution in blends, underlining the good collaboration between CSA and Portland cement. Results in terms of dimensional stability evidenced the different microstructures developed by the studied systems. While PC showed the highest difference in shrinkage between drying and autogenous condition, CSA evolved similar trend between them. The highly reactive CSA cement strongly self-desiccated, quickly consuming the available mixing water which, together with its dense pore structure developed during hydration, led to a nearly absence of evaporated water from the outer layer during drying. On the contrary, PC reacts slowly evolving, in the early age, a continuous, well connected pore network [52][37], providing a big amount of water available for evaporation in drying condition.

The combination of the two cements in the blended system created a totally different microstructure compared to them. This microstructure was assumed to be characterized by bigger pores than PC and more connected than CSA as the shrinkage was the lowest (related with the impossibility to create capillary pressure in big pores) and the mass change the highest (as the big pores allowed more water to evaporate). Despite blend initial complex shrinkage evolution in autogenous condition, the strength improvement in long term test confirmed the development of a good microstructure quality, attesting the collaboration between the two different cements, discarding the possibility of a detrimental relation. The results mentioned above were respected also under load, evidencing the stability of the investigated aspect in more realistic conditions.

Once defined the mechanical properties of CSA based concrete mixtures, a comparison with the PC constitutive laws reported in the major widespread technical documents was done. Results coming from the tests were in good agreement with the chosen standards. CSA based mixtures showed small difference between the test results and these constitutive laws, less than that showed by PC. In the case in which this difference was higher, the PC results were always similar to their trend, confirming the good correspondence of the standards with these new systems. This accordance was eventually confirmed by the stress-strain diagram in compression. Trends were similar between the three investigated mixtures (PC, CSA and MIX) and correctly simulated by models taken from the literature.

In conclusion, concrete systems based on blends of calcium sulfoaluminate cement and limestone Portland represent a possible alternative to simple Portland systems for structural application, thanks to their rapid hardening behavior and the development of a stable microstructure in a system which slightly deforms, even under load. The mechanical properties developed by pure CSA and blended systems evidenced an evolution which is close enough to the PC constitutive laws described in the most important technical documents in order to consider for these new systems the same constitutive laws mentioned above, eventually with some specific coefficient to be defined.

6 FUTURE RESEARCH

This research represents the first step of a bigger program which has the aim to extend the use of calcium sulfoaluminate cement to concrete scale for structural applications. The present research studied some particular mixtures which were defined in order to represent each a particular concrete category. The mechanical characterization campaign defined their properties and the comparison with the most used technical documents evidenced their relation with ordinary Portland systems. Thus, three are the field on which focus in the next steps, each of them representing a particular characteristic: the quality, the extension and the practical utility of CSA based concrete.

In order to improve the quality of the present research, a more detailed investigation is required on the base processes which characterize CSA based mixtures so as to confirm certain assumption and extend the conclusions. For instance, MIX shrinkage and creep evolution in autogenous condition requires explanations of their different stages. Hydration experiments to determine the composition of solid and liquid phases at various ages could explain it; thus, thermogravimetric analysis, X-ray diffraction and scanning electron microscopy tests are required. Moreover, the study of the evolution of the microstructure by mercury intrusion porosimetry (MIP) in the different mixtures can be related with the hydration study, improving the quality of the assumptions.

To improve the extension, a higher number of investigated mixtures is required. These mixtures could be divided in macro-categories (blends or pure systems) and should cover as much as possible strength classes. They should be defined, at least, for the main mechanical aspects of the compressive strength, the indirect tensile strength and the modulus of elasticity.

Eventually, the most important phase is the application of the investigated mixtures in a real structure, in order to evaluate the correspondence between mechanical aspects under controlled and real conditions. A possible investigation could be represented by the restoration of a bridge beam using MIX. A three-point bending test could be organized on two beams 15-20m length. Both beams would be realized with ordinary Portland concrete; however, one of the two would be damaged (simulating time degradation) and, then, restored with MIX. In this way, comparing the un-damaged beam with the restored, the test should give the idea of the quality of the restoration.

7 ACKOWLEDGEMENT

This research was conducted in i.lab, research and innovation centre of Italcementi, Heidelbergcement group in Bergamo and in EMPA, Swiss federal laboratories for materials science and technology in Zurich. Italcementi, Heidelbergcement group founded this study.

I would like to thank my supervisor Prof. P. Riva for supporting me during these years. Thanks also to my whole research group at the Università degli studi di Bergamo for the support, the critical review and the collaboration during this period. Thanks Alessandra, Andrea, Consuelo, Chiara, Fabrizio, Simone, Marco and Michele. A special thanks to the technical staff in the university laboratories for their hospitality, Daniele and Luca.

I would also like to thank Maurizio and Sergio from Italcementi, Heidelbergcement group for their scientific contribution and collaboration in the concrete campaign definition. Thanks also to the whole i.lab technical staff, for their hospitality and friendly collaboration.

The whole mortar campaign was conducted in Zurich during a one-year internship at EMPA. I would like to thank Prof. P. Lura for this opportunity. His friendly attitude and vast scientific knowledge was really helpful during my permanence. I would also like to thank W. Mateusz, for his scientific and practical contribution to my results, and to the whole EMPA technical staff, for their hospitality, their collaboration and their friendship. A special thanks to Nikolaj and Janis.

8 BIBLIOGRAPHY

[1] M. C. G. Juenger, F. Winnefeld, J. L. Provis, and J. H. Ideker, "Advances in alternative cementitious binders," *Cem. Concr. Res.*, vol. 41, no. 12, pp. 1232–1243, 2011.

[2] B. Lothenbach, K. Scrivener, and R. D. Hooton, "Supplementary cementitious materials," *Cem. Concr. Res.*, vol. 41, no. 12, pp. 1244–1256, 2011.

[3] E. Mokrzycki and A. Uliasz-Bocheńczyk, "Alternative fuels for the cement industry," *Appl. Energy*, vol. 74, no. 1–2, pp. 95–100, Jan. 2003.

[4] P. Mehta, "Investigations on energy-saving cements," *World Cem. Technol.*, no. may, pp. 166–177, 1980.

[5] W. Lan and F. P. Glasser, "Hydration of calcium sulphoaluminate cements," *Adv. Cem. Res.*, vol. 8, no. 31, pp. 127–134, 1996.

[6] L. Zhang and F. P. Glasser, "Hydration of calcium sulfoaluminate cement at less than 24 h," *Adv. Cem. Res.*, vol. 14, no. 4, pp. 141–155, 2002.

[7] L. Zhang, M. Su, and Y. Wang, "Development of the use of sulfo- and ferroaluminate cements in China," *Adv. Cem. Res.*, vol. 11, no. 1, pp. 15–21, 1999.

[8] M. S. Meddah, M. Suzuki, and R. Sato, "Influence of a combination of expansive and shrinkage-reducing admixture on autogenous deformation and self-stress of silica fume high-performance concrete," *Constr. Build. Mater.*, vol. 25, no. 1, pp. 239–250, 2011.

[9] S. Slatnick, K. A. Riding, K. J. Folliard, M. C. G. Juenger, and A. K. Schindler, "Evaluation of autogenous deformation of concrete at early ages," *ACI Mater. J.*, vol. 108, no. 1, pp. 21–28, 2011.

[10] T. Noguchi, P. Sun-Gyu, and I. Maruyama, "Mechanical properties of high-performance concrete with expansive additive and shrinkage reducing admixtures under simulated completely-restrained condition at early age," in *Self-Desiccation and Its Importance in Concrete Technology: Proceedings of the 4th International Seminar*, 2005.

[11] T. Le-Bihan, J. F. Georgin, M. Michel, J. Ambroise, and F. Morestin, "Measurements and modeling of cement base materials deformation at early age: The case of sulfo-aluminous cement," *Cem. Concr. Res.*, vol. 42, no. 8, pp. 1055–1065, 2012.

[12] J. Péra and J. Ambroise, “New applications of calcium sulfoaluminate cement,” *Cem. Concr. Res.*, vol. 34, no. 4, pp. 671–676, 2004.

[13] J. F. Georgin, J. Ambroise, J. Péra, and J. M. Reynouard, “Development of self-leveling screed based on calcium sulfoaluminate cement: Modelling of curling due to drying,” *Cem. Concr. Compos.*, vol. 30, no. 9, pp. 769–778, 2008.

[14] J. Ambroise and J. Péra, “Use of calcium sulfoaluminate cement to improve strength of mortars at low temperature,” *Concr. Repair, Rehabil. Retroffiting II*, pp. 881–886, 2009.

[15] E. UNI, “197-1: 2011 Cement–Part 1: Composition, specifications and conformity criteria for common cement,” *UNI Ente Naz. Ital. di unificazione*, 2011.

[16] A. Klein, “Calcium aluminosulfate and expansive cements containing same.” Google Patents, 03-Nov-1964.

[17] Y. Wang and M. Su, “The third cement series in China,” *World Cem*, vol. 25, no. 8, pp. 6–10, 1994.

[18] Q. Zhou, N. B. Milestone, and M. Hayes, “An alternative to Portland cement for waste encapsulation—the calcium sulfoaluminate cement system,” *J. Hazard. Mater.*, vol. 136, no. 1, pp. 120–129, 2006.

[19] C. C. D. Coumes, S. Courtois, S. Peysson, J. Ambroise, and J. Pera, “Calcium sulfoaluminate cement blended with OPC: a potential binder to encapsulate low-level radioactive slurries of complex chemistry,” *Cem. Concr. Res.*, vol. 39, no. 9, pp. 740–747, 2009.

[20] E. Gartner, “Industrially interesting approaches to ‘low-CO2’ cements,” *Cem. Concr. Res.*, vol. 34, no. 9, pp. 1489–1498, 2004.

[21] F. P. Glasser and L. Zhang, “High-performance cement matrices based on calcium sulfoaluminate-belite compositions,” *Cem. Concr. Res.*, vol. 31, no. 12, pp. 1881–1886, 2001.

[22] K. Quillin, “Performance of belite-sulfoaluminate cements,” *Cem. Concr. Res.*, vol. 31, no. 9, pp. 1341–1349, 2001.

[23] L. Zhang, “Microstructure and performance of calcium sulfoaluminate cements,” University of Aberdeen, 2000.

[24] J. Beretka, B. De Vito, L. Santoro, N. Sherman, and G. L. Valenti, “Hydraulic behaviour of calcium sulfoaluminate-based cements derived from industrial

process wastes," *Cem. Concr. Res.*, vol. 23, no. 5, pp. 1205–1214, 1993.

[25] P. Arjunan, M. R. Silsbee, and D. M. Roy, "Sulfoaluminate-belite cement from low-calcium fly ash and sulfur-rich and other industrial by-products," *Cem. Concr. Res.*, vol. 29, no. 8, pp. 1305–1311, 1999.

[26] M. Su, D. Junan, W. Zongdao, and L. Xiaoxin, "Research on the chemical composition and microstructures of sulpho-aluminate cement clinker," in *9th International Congress on the Chemistry of Cements, New Delhi, India*, 1992, vol. 2, pp. 94–100.

[27] F. Winnefeld and S. Barlag, "Influence of calcium sulfate and calcium hydroxide on the hydration of calcium sulfoaluminate clinker," *ZKG Int.*, vol. 62, no. 12, pp. 42–53, 2009.

[28] M. Marchi and U. Costa, "Influence of the Calcium Sulphate and W/C Ratio on the Hydration of Calcium Sulfoaluminate Cement," *13th Int. Congr. Chem. Cem.*, pp. 1–7, 2011.

[29] I. Janotka and L. Krajči, "An experimental study on the upgrade of sulfoaluminate—belite cement systems by blending with Portland cement," *Adv. Cem. Res.*, vol. 11, no. 1, pp. 35–41, Jan. 1999.

[30] L. Pelletier, F. Winnefeld, and B. Lothenbach, "The ternary system Portland cement-calcium sulphoaluminate clinker-anhydrite: Hydration mechanism and mortar properties," *Cem. Concr. Compos.*, vol. 32, no. 7, pp. 497–507, 2010.

[31] I. Janotka, A. Ray, and S. C. Mojumdar, "The hydration phase and pore structure formation in the blends of sulfoaluminate-belite cement with Portland cement," *Cem. Concr. Res.*, vol. 33, no. 4, pp. 489–497, 2003.

[32] F. Winnefeld and S. Barlag, "Calorimetric and thermogravimetric study on the influence of calcium sulfate on the hydration of ye'elimite," *J. Therm. Anal. Calorim.*, vol. 101, no. 3, pp. 949–957, 2010.

[33] D. Gastaldi, E. Boccaleri, F. Canonico, and M. Bianchi, "The use of Raman spectroscopy as a versatile characterization tool for calcium sulphoaluminate cements: A compositional and hydration study," *J. Mater. Sci.*, vol. 42, no. 20, pp. 8426–8432, 2007.

[34] F. Winnefeld and B. Lothenbach, "Hydration of calcium sulfoaluminate cements - Experimental findings and thermodynamic modelling," *Cem. Concr. Res.*, vol. 40,

no. 8, pp. 1239–1247, 2010.

[35] E. Smrčková, M. Palou, and V. Tomková, “Application of conduction calorimetry for study of the reactivity of C2S in the system C2S-C4A3¯ SC¯ SH,” *J. Therm. Anal. Calorim.*, vol. 46, no. 2, pp. 597–605, 1996.

[36] P. Lura, F. Winnefeld, and S. Klemm, “Simultaneous measurements of heat of hydration and chemical shrinkage on hardening cement pastes,” *J. Therm. Anal. Calorim.*, vol. 101, no. 3, pp. 925–932, 2010.

[37] G. Bernardo, A. Telesca, and G. L. Valenti, “A porosimetric study of calcium sulfoaluminate cement pastes cured at early ages,” *Cem. Concr. Res.*, vol. 36, no. 6, pp. 1042–1047, 2006.

[38] G. Le Saoût, B. Lothenbach, A. Hori, T. Higuchi, and F. Winnefeld, “Hydration of Portland cement with additions of calcium sulfoaluminates,” *Cem. Concr. Res.*, vol. 43, no. 1, pp. 81–94, 2013.

[39] I. A. Chen, C. W. Hargis, and M. C. G. Juenger, “Understanding expansion in calcium sulfoaluminate-belite cements,” *Cem. Concr. Res.*, vol. 42, no. 1, pp. 51–60, 2012.

[40] S. Irico, D. Gastaldi, F. Canonico, and G. Magnacca, “Investigation of the microstructural evolution of calcium sulfoaluminate cements by thermoporometry,” *Cem. Concr. Res.*, vol. 53, pp. 239–247, 2013.

[41] I. Janotka, L. Krajči, and S. C. Mojumdar, “Performance of sulphoaluminate-belite cement with high C4A 3S̄ content,” *Ceram. - Silikaty*, vol. 51, no. 2, pp. 74–81, 2007.

[42] M. García-Maté, I. Santacruz, Á. G. De La Torre, L. León-Reina, and M. A. G. Aranda, “Rheological and hydration characterization of calcium sulfoaluminate cement pastes,” *Cem. Concr. Compos.*, vol. 34, no. 5, pp. 684–691, 2012.

[43] M. Michel, J. F. Georgin, J. Ambroise, and J. Péra, “The influence of gypsum ratio on the mechanical performance of slag cement accelerated by calcium sulfoaluminate cement,” *Constr. Build. Mater.*, vol. 25, no. 3, pp. 1298–1304, 2011.

[44] J. Beretka, M. Marroccoli, N. Sherman, and G. L. Valenti, “The influence of C4A3S̄ content and W/S ratio on the performance of calcium sulfoaluminate-based cements,” *Cem. Concr. Res.*, vol. 26, no. 11, pp. 1673–1681, 1996.

[45] A. Alaoui, A. Ferraille, A. Dimassi, V. H. Nguyen, R. Le Roy, and L. Divet, "Experimental Study of Sulfoaluminate Concrete Based Materials," *Concr. under Sev. Cond. Environ. Load.*, pp. 909–916, 2007.

[46] V. Kasselouri, P. Tsakiridis, C. Malami, B. Georgali, and C. Alexandridou, "A study on the hydration products of a non-expansive sulfoaluminate cement," *Cem. Concr. Res.*, vol. 25, no. 8, pp. 1726–1736, 1995.

[47] R. Khoshnazar, J. Beaudoin, R. Alizadeh, and L. Raki, "Volume stability of calcium sulfoaluminate phases," *J. Am. Ceram. Soc.*, vol. 95, no. 12, pp. 3979–3984, 2012.

[48] J. Bizzozero, C. Gosselin, and K. L. Scrivener, "Expansion mechanisms in calcium aluminate and sulfoaluminate systems with calcium sulfate," *Cem. Concr. Res.*, vol. 56, pp. 190–202, 2014.

[49] G. L. Valenti, M. Marroccoli, M. L. Pace, and A. Telesca, "Discussion of the paper 'Understanding expansion in calcium sulfoaluminate-belite cements' by I.A. Chen et al., Cem. Concr. Res. 42 (2012) 51-60," *Cem. Concr. Res.*, vol. 42, no. 11, pp. 1555–1559, 2012.

[50] I. A. Chen, C. W. Hargis, and M. C. G. Juenger, "Reply to the discussion of the paper Understanding expansion in calcium sulfoaluminate-belite cements by G.L. Valenti, M. Marroccoli, M.L. Pace, A. Telesca," *Cem. Concr. Res.*, vol. 42, no. 11, pp. 1560–1562, 2012.

[51] M. D. Cohen, "Theories of expansion in sulfoaluminate - type expansive cements: Schools of thought," *Cem. Concr. Res.*, vol. 13, no. 6, pp. 809–818, 1983.

[52] A. Telesca, M. Marroccoli, M. L. Pace, M. Tomasulo, G. L. Valenti, and T. R. Naik, "Expansive and non-expansive calcium sulfoaluminate-based cements," *3rd Int. Conf. Sustain. Constr. Mater. Technol.*, vol. 3, no. 1, 2013.

[53] P. K. Mehta, "Mechanism of expansion associated with ettringite formation," *Cem. Concr. Res.*, vol. 3, no. 1, pp. 1–6, 1973.

[54] H. F. W. Taylor, C. Famy, and K. L. Scrivener, "Delayed ettringite formation," *Cement and Concrete Research*, vol. 31, no. 5. pp. 683–693, 2001.

[55] K. Ogawa and D. M. Roy, "C4A3S hydration ettringite formation, and its expansion mechanism: I. expansion; Ettringite stability," *Cem. Concr. Res.*, vol. 11, no. 5–6, pp. 741–750, 1981.

[56] P.-C. Aïtcin, *High performance concrete*. CRC press, 2011.

[57] M. Schmidt and E. Fehling, "Ultra-high-performance concrete: research, development and application in Europe," *ACI Spec. Publ.*, vol. 228, pp. 51–78, 2005.

[58] I. Vlahinić, H. M. Jennings, and J. J. Thomas, "A constitutive model for drying of a partially saturated porous material," *Mech. Mater.*, vol. 41, no. 3, pp. 319–328, 2009.

[59] N. Neithalath, B. Pease, J. H. Moon, F. Rajabipour, J. Weiss, and E. Attiogbe, "Considering moisture gradient and time-dependent crack growth in restrained concrete elements subjected to drying," *NSF Work. High Perform. Concr.*, pp. 279–290, 2005.

[60] V. Gribniak, G. Kaklauskas, R. Kliukas, and R. Jakubovskis, "Shrinkage effect on short-term deformation behavior of reinforced concrete – When it should not be neglected," *Mater. Des.*, vol. 51, no. July 2015, pp. 1060–1070, 2013.

[61] A. Bentur, "Evaluation of early age cracking characteristics in cementitious systems," *Mater. Struct.*, vol. 36, no. 257, pp. 183–190, 2003.

[62] F. R. and J. W. P.Lura, B. Pease, Guy Mazzotta, "Influence of Shrinkage-Reducing Admixtures on Development of Plastic Shrinkage Cracks," *ACI Mater. J.*, vol. 104, no. 2, pp. 187–194, 2008.

[63] P. Lura, O. M. Jensen, and K. Van Breugel, "Autogenous shrinkage in high-performance cement paste: An evaluation of basic mechanisms," *Cem. Concr. Res.*, vol. 33, no. 2, pp. 223–232, 2003.

[64] O. Mejlhede Jensen and P. Freiesleben Hansen, "Autogenous deformation and change of the relative humidity in silica fume-modified cement paste," *ACI Mater. J.*, vol. 93, no. 6, pp. 539–543, 1996.

[65] G. Sant, P. Lura, and J. Weiss, "Measurement of Volume Change in Cementitious Materials at Early Ages: Review of Testing Protocols and Interpretation of Results," *Transp. Res. Rec.*, vol. 1979, no. 1, pp. 21–29, 2006.

[66] G. Sant *et al.*, "Detecting the fluid-to-solid transition in cement pastes," *Concr. Int.*, vol. 31, no. 6, pp. 53–58, 2009.

[67] G. Ye, P. Lura, K. Van Breugel, and A. L. A. Fraaij, "Study on the development of the microstructure in cement-based materials by means of numerical simulation

and ultrasonic pulse velocity measurement," *Cem. Concr. Compos.*, vol. 26, no. 5, pp. 491–497, 2004.

[68] S. I. Igarashi, A. Bentur, and K. Kovler, "Autogenous shrinkage and induced restraining stresses in high-strength concretes," *Cem. Concr. Res.*, vol. 30, no. 11, pp. 1701–1707, 2000.

[69] D. Sirtoli, S. Tortelli, P. Riva, M. Marchi, R. Cucitore, and M. N. Rose, "Mechanical and durability performances of sulpho-based rapid hardening concrete," *ACI Spec. Publ.*, vol. 305, pp. 1–8, 2015.

[70] C. Di Bella, M. Wyrzykowski, and P. Lura, "Evaluation of the ultimate drying shrinkage of cement-based mortars with poroelastic models," *Mater. Struct.*, no. January, 2017.

[71] P. Lura, K. Van Breugel, and I. Maruyama, "Effect of curing temperature and type of cement on early-age shrinkage of high-performance concrete," *Cem. Concr. Res.*, vol. 31, no. 12, pp. 1867–1872, 2001.

[72] J. Weiss, P. Lura, F. Rajabipour, and G. Sant, "Performance of Shrinkage-Reducing Admixtures at Different Humidities and at Early Ages," *ACI Mater. J.*, vol. 105, no. 5, 2008.

[73] O. M. Jensen and P. Lura, "Techniques and materials for internal water curing of concrete," *Mater. Struct.*, vol. 39, no. 9, pp. 817–825, 2006.

[74] A. Bentur, S. I. Igarashi, and K. Kovler, "Prevention of autogenous shrinkage in high-strength concrete by internal curing using wet lightweight aggregates," *Cem. Concr. Res.*, vol. 31, no. 11, pp. 1587–1591, 2001.

[75] Y. M. Luosun, J. Zhang, and Y. Gao, "Evaluation of Shrinkage Resulted Cracking of High Strength Calcium Sulfoaluminate Cement Concrete with Impact of Internal Curing," *Key Eng. Mater.*, vol. 629–630, pp. 144–149, 2014.

[76] H. Ito, I. Maruyama, M. Tanimura, and R. Sato, "Early age deformation and resultant induced stress in expansive high strength concrete," *J. Adv. Concr. ...*, vol. 2, no. June, pp. 155–174, 2004.

[77] Z. P. Bažant, "Prediction of concrete creep and shrinkage: Past, present and future," *Nucl. Eng. Des.*, vol. 203, no. 1, pp. 27–38, 2001.

[78] Z. P. Bazant, "Mathematical modelling of creep and shrinkage of concrete.pdf," *Matheatical Modeling of Creep and Shrinkage of Concrete*. pp. 99–215, 1988.

[79] M. Wyrzykowski and P. Lura, “The effect of external load on internal relative humidity in concrete,” *Cem. Concr. Res.*, vol. 65, pp. 58–63, 2014.

[80] ASTM Standard, “C215-08 Standard Test Method for Fundamental Transverse, Longitudinal, and Torsional Frequencies of Concrete Specimens,” 2008.

[81] C. Di Bella, M. Griffa, T. J. Ulrich, and P. Lura, “Early-age elastic properties of cement-based materials as a function of decreasing moisture content,” *Cem. Concr. Res.*, vol. 89, pp. 87–96, 2016.

[82] A. Spinner and W. E. Teft, “A method for determining mechanical resonance frequencies and for calculating elastic moduli from these frequencies,” *Proc. Am. Soc. Test. Matrials, 61*, vol. 61, pp. 1221–1239, 1961.

[83] M. Azenha, R. Faria, F. Magalhães, L. Ramos, and Á. Cunha, “Measurement of the E-modulus of cement pastes and mortars since casting, using a vibration based technique,” *Mater. Struct.*, vol. 45, pp. 81–92, 2012.

[84] ASTM Standard, “C1698–09 Test Method for Autogenous Strain of Cement Paste and Mortar,” 2009.

[85] M. Wyrzykowski, Z. Hu, S. Ghourchian, K. Scrivener, and P. Lura, “Corrugated tube protocol for autogenous shrinkage measurements: review and statistical assessment,” *Mater. Struct.*, vol. 50, no. 1, p. 57, 2017.

[86] D. Gawin, F. Pesavento, and B. A. Schrefler, “Modelling creep and shrinkage of concrete by means of effective stresses,” *Mater. Struct.*, vol. 40, no. 6, pp. 579–591, 2007.

[87] British standards institution, *Eurocode 2: Design of Concrete Structures: Part 1-1: General Rules and Rules for Buildings*. British Standards Institution, 2004.

[88] Consiglio Superiore dei Lavori Pubblici, “Norme tecniche per le costruzioni,” *Gazz. Uff. della Repubb. Ital.*, 2008.

[89] J. Walvaren, “Model Code 2010, final drafts,” *FIB Bull.*, vol. 1 & 2, no. 65 & 56, p. 105, 2012.

[90] H. S. Müller, I. Anders, R. Breiner, and M. Vogel, “Concrete: Treatment of types and properties in fib Model Code 2010,” *Struct. Concr.*, vol. 14, no. 4, pp. 320–334, 2013.

[91] D. C. Kent and R. Park, “Flexural Members with Confined Concrete,” *Journal of the Structural Division*, vol. 97, no. 7. pp. 1969–1990, 1971.

[92] S. Popovics, “A numerical approach to the complete stress-strain curve of concrete,” *Cem. Concr. Res.*, vol. 3, no. 5, pp. 583–599, 1973.

[93] P. Mander, J. B.;Priestley, M. J. N.; Park, “Theoretical Stress-Srain Model for Confined Concrete,” *J. Struct. Eng.*, vol. 114, no. 8, pp. 1804–1826, 1989.

[94] A. Thorenfeldt, E., Tomaszewicz and J. Jensen, “Mechanical properties of high-strength concrete and application in design,” in *Proceedings of the symposium utilization of high strength concrete*, 1987, pp. 149–159.

[95] D. J. Carreira and K.-H. Chu, “Stress-Strain Relationship for Plain Concrete in Compression,” *ACI J.*, vol. 82, no. 6, pp. 797–804, 1985.

[96] L. Pelletier-Chaignat, F. Winnefeld, B. Lothenbach, and C. J. Müller, “Beneficial use of limestone filler with calcium sulphoaluminate cement,” *Constr. Build. Mater.*, vol. 26, no. 1, pp. 619–627, 2012.

[97] J. C. Simmons, “Dynamic and Static Measurements,” *Mag. Concr. Res.*, no. July, pp. 61–68, 1955.

[98] J. L. Granja *et al.*, “Comparison between different experimental techniques for stiffness monitoring of cement pastes,” *J. Adv. Concr. Technol. J. Adv. Concr. Technol.*, vol. 12, no. 7, pp. 261–271, 2014.

[99] M. Wyrzykowski and P. Lura, “Effect of relative humidity decrease due to self-desiccation on the hydration kinetics of cement,” *Cem. Concr. Res.*, vol. 85, pp. 75–81, 2016.

[100] M. Su, Y. Wang, L. Zhang, and D. Li, “Preliminary study on the durability of sulfo/ferro-aluminate cements,” *Proc. 10th Int. Congr. Chem. Cem., Goteborg, Sweden*, vol. 4, p. 4iv029-12, 1997.